Spatio-Temporal Analysis of Landslide Hazard in Southern Kyrgyzstan Using GIS and Remote Sensing Data

vorgelegt von

M.Sc. Geoinformatik

Darya Golovko

Von der Fakultät VI – Planen Bauen Umwelt

der Technischen Universität Berlin

zur Erlangung des akademischen Grades

Doktor der Naturwissenschaften

Dr. rer. nat.

genehmigte Dissertation

Promotionsausschuss:

Vorsitzender:	Prof. Dr. Martin Kada
Gutachterin:	Prof. Dr. Birgit Kleinschmit
Gutachter:	Prof. Dr. Tomás Fernandez-Steeger
Gutachter:	Prof. Dr. Mahdi Motagh

Tag der wissenschaftlichen Aussprache: 24. Mai 2018

Berlin 2019

Acknowledgements

I thank Professor Dr. Birgit Kleinschmit from the Technical University of Berlin for the supervision and review of this thesis as well as insightful comments on the manuscript drafts.

I thank Professor Dr. Tomás Fernández-Steeger from the Technical University of Berlin for the review of this thesis.

I thank Professor Dr. Mahdi Motagh from the Leibniz Universität Hannover and GFZ for the review of the thesis and interesting discussions about the study area.

I thank my direct supervisor Dr. Sigrid Roessner from the GFZ for the great amounts of time invested into this project, countless valuable ideas, participation in the manuscript revisions and the encouragement to bring it all to an end.

I thank my colleagues at the GFZ: Dr. Robert Behling for being there to answer my questions and the memorable field work experience, and Dr. Carsten Neumann for the proofreading.

I thank Khaibula Valiyevich Ibatulin and Aman Kurgomisovich Sarnagoyev from the Ministry of Emergency Situations of Kyrgyzstan, Dr. Zoya Arslanovna Kalmetyeva from the CAIAG in Bishkek and Isakbek Asangaliyevich Torgoev from the "Geopribor" center in Bishkek for their valuable help during the field work, the materials on the study area they provided and inspiring discussions.

I thank Christian Schröder from the Technical University of Berlin for the flexible working hours that allowed me to meet the deadlines for the manuscript submission and revisions.

I thank the anonymous reviewers of the three papers that are part of this dissertation.

I thank developers of open-source software and contributors to open geodata whose work was used to prepare this thesis.

Last but not least, I thank my partner Rafaela Wahl Herrera for the countless proofreading sessions and discussions, the encouragement, sanity, and anything else I might not even know that led me to finish this.

List of Publications

Pages 35-52:

Golovko, D., Roessner, S., Behling, R., Wetzel, H.-U. and Kleinschmit, B. (2015). Development of Multi-Temporal Landslide Inventory Information System for Southern Kyrgyzstan Using GIS and Satellite Remote Sensing. PFG Photogrammetrie, Fernerkundung, Geoinformation, 2:157-172. (Postprint)
https://doi.org/10.1127/pfg/2015/0261

Pages 53-80:

Golovko, D., Roessner, S., Behling, R. and Kleinschmit, B. (2017). Automated derivation and spatio-temporal analysis of landslide properties in southern Kyrgyzstan. Natural Hazards, 85:1461-1488. (Postprint)
https://doi.org/10.1007/s11069-016-2636-y

Pages 81-106:

Golovko, D., Roessner, S., Behling, R., Wetzel, H.-U. and Kleinschmit, B. (2017). Evaluation of of Remote-Sensing-Based Landslide Inventories for Hazard Assessment in Southern Kyrgyzstan. Remote Sensing, 9(9):943. (Postprint)
https://doi.org/10.3390/rs9090943

Abstract

Large areas in southern Kyrgyzstan are affected by intensive landsliding, which results in the loss of human life and damages to the housing and infrastructure. A quantitative landslide hazard assessment based on a systematic landslide record is needed to better understand landslide processes in the region and to implement more effective hazard mitigation measures. Landslide investigations have been carried out by the local authorities since the 1950s; however, such a hazard assessment has not been performed so far. The large size of the study area, the high number of landslide-prone slopes, a complex spatio-temporal pattern of landsliding and limited funding designated to landslide investigations in the region create additional challenges.

The objective of this study is the development of an approach to perform such a quantitative hazard assessment. Due to the limited data availability in the study area and its large size, remote sensing was utilized at every stage of the investigation. Optical satellite images were used to derive information on the landslides or prepare it for the use in the hazard assessment. A further methodological objective of this thesis is an analysis of how the properties of the landslide data influence the results of the hazard assessment.

A multi-source landslide inventory was prepared that included results of manual landslide mapping based on verbal archive descriptions, manual geomorphological mapping based on mono-temporal satellite images, and automated landslide detection from multi-temporal satellite images. This inventory was extended to include landslide attributes derived in an automated manner. The landslide data sources were found to differ substantially in their spatial and temporal resolution, completeness, and the time period covered, which was also visible in the attribute values. Finally, a susceptibility assessment was performed using the results of automated landslide detection and visual expert mapping. The resulting susceptibility maps revealed that different aspects of the landslide susceptibility can be emphasized by the choice of the landslide inventory data. E.g. the analysis can focus on the recent landsliding or a longer time period, landslide initiation zones or locations of the displaced masses, etc. The automatically detected landslides with their failure dates were used to evaluate the temporal aspect of landslide hazard.

The findings emphasize that the properties of the underlying landslide data should be evaluated when interpreting the results of the hazard assessment. Especially for large and data-scarce regions, the automated landslide mapping based on satellite images is capable of producing a more precise, complete and systematic landslide inventory and hazard assessment. The prerequisite is the availability of suitable satellite imagery.

Zusammenfassung

Große Gebiete in Südkirgisistan sind von der intensiven Hangrutschungsdynamik beeinflusst, welche zum Verlust von Menschenleben und Schäden an Häusern und Infrastruktur führt. Eine quantitative Einschätzung der Hangrutschungsgefährdung, die auf einem systematischen Hangrutschungskatalog basiert, ist notwendig für ein besseres Verständnis von Hangrutschungsprozessen in der Region und für die Implementierung effizienterer Vorbeugungsmaßnahmen. Hangrutschungsuntersuchungen werden von den Behörden vor Ort bereits seit den 1950er Jahren durchgeführt. Jedoch wurde eine solche systematische Analyse noch nicht realisiert. Die weite Ausdehnung des Untersuchungsgebietes, die hohe Anzahl an Hangrutschungen, komplexe raumzeitliche Aktivierungsmuster und die unzureichende Finanzierung der Hangrutschungsuntersuchungen in der Region sind zusätzliche Herausforderungen.

Diese Arbeit hat zum Ziel, einen Ansatz für eine solche quantitative Gefährdungseinschätzung zu entwickeln. Aufgrund der begrenzten Datenverfügbarkeit und der weiten Ausdehnung des Untersuchungsgebietes wurden Fernerkundungsdaten in jeder Phase der Untersuchung verwendet. Optische Satellitenbilder wurden genutzt, um Hangrutschungsinformationen abzuleiten oder sie für die Gefährdungseinschätzung aufzubereiten. Ein weiteres methodisches Ziel dieser Arbeit ist eine Analyse, wie die Eigenschaften der Hangrutschungsdaten die Ergebnisse der darauf basierten Gefährdungseinschätzung beeinflussen.

Ein Hangrutschungskatalog wurde aus mehreren Datenquellen erstellt. Dazu gehören Ergebnisse einer manuellen Hangrutschungskartiereung aus verbalen Beschreibungen, einer manuellen geomorphologischen Kartierung unter Verwendung von monotemporalen Satellitenbildern und einer automatisierten Hangrutschungsidentifizierung aus multitemporalen Satellitenbildern. Dieser Katalog wurde um Hangrutschungsattribute erweitert, die mit einem automatischen Ansatz abgeleitet wurden. Es wurde festgestellt, dass die Quellen der Hangrutschungsinformationen sich erheblich in ihrer räumlichen und zeitlichen Auflösung, Vollständigkeit und der abgedeckten Zeitperiode unterscheiden, was sich auch in den Attributwerten zeigte. Schließlich wurde eine Anfälligkeitsanalyse durchgeführt: zum einen mit Ergebnissen der automatischen Hangrutschungsidentifizierung und zum anderen mit den Ergebnissen der visuellen Expertenkartierung. Die dabei entstandenen Anfälligkeitskarten zeigten, dass verschiedene Aspekte der Hangrutschungsgefährdung durch die Wahl der Hangrutschungsdaten hervorgehoben werden können. So kann sich die Analyse auf die jüngste oder auch ältere Hangrutschungsaktivität fokussieren, die Gebiete der Hangrutschungsinitiierung oder die verlagerten Massen berücksichtigen.

Diese Erkenntnisse zeigen, dass bei der Interpretation der Gefährdungseinschätzung die Eigenschaften der verwendeten Hangrutschungsdaten einbezogen werden

müssen. Insbesondere bei großen Gebieten mit eingeschränkter Datenverfügbarkeit eignet sich die automatische Hangrutschungsidentifizierung aus Satellitenbildern, um einen genaueren, vollständigen und systematischen Hangrutschungskatalog zu erhalten. Die Voraussetzung ist die Verfügbarkeit passender Satellitendaten.

Contents

List of Figures

List of Tables

List of Abbreviations

AGU	American Geophysical Union
ALOS	Advanced Land Observation Satellite
a.s.l.	Above sea level
ASTER	Advanced Spaceborn Thermal Emission and Reflection Radiometer
AUROC	Area under under the receiver operating characteristic (curve)
BMBF	Bundesministerium für Bildung und Forschung, Federal Ministry of Education and Research of Germany
CAIAG	Central-Asian Institute for Applied Geosciences
CR, Cr	Cretaceous
DEM	Digital elevation model
DLR	Deutsches Zentrum für Luft- und Raumfahrt, German Aerospace Center
(E)TM	(Enhanced) Thematic Mapper
FR	Frequency ratio
GDEM	Global digital elevation model
GFZ	GeoForschungsZentrum, German Research Centre for Geosciences
GIS	Geographic information system
GPS	Global Positioning System
ID	Identifier
InSAR	Interferometric synthetic aperture radar
IRS	Indian Remote Sensing (satellite)
J	Jurassic
LiDAR	Light detection and ranging
LISS	Linear Imaging Self-Scanning Sensor
LSI	Landslide susceptibility index
MES	Ministry of Emergency Situations
MODIS	Moderate Resolution Imaging Spectroradiometer
N	Neogene
NDVI	Normalized difference vegetation index
PG, Pg	Paleogene
PROGRESS	Potsdam Research Cluster for Georisk Analysis, Environmental Change and Sustainability
Q	Quaternary
RMSE	Root-mean-square error
SAGA	System for Automated Geoscientific Analyses
SPOT	Satellite Pour l'Observation de la Terre, Satellite for Observation of Earth
SRTM	Shuttle Radar Topography Mission
SPI	Stream power index
TIPTIMON	Tien Shan - Pamir Monitoring Program

TM	Trademark
UNESCO	United Nations Educational, Scientific and Cultural Organization
USGS	United States Geological Survey
UTM	Universal Transverse Mercator
WGS	World Geodetic System

Chapter 1

Introduction

1.1 Motivation

Landslides are a natural phenomenon that endangers and affects millions of people worldwide. Several thousand people each year lose their lives due to landslides (Perkins, 2017). In 2017 alone, large landslide disasters were in the international news, e.g. the mudslide in Freetown, Sierra Leone on the 14th of August with an estimated death toll of over 1 000 people (Petley, 2017c), the debris flow near Mocoa, Columbia on the 1st of April with 301 fatalities (Li et al., 2017), the period of heavy rain, flooding and landslides in Sri-Lanka in May with over 200 victims (Petley, 2017b) or the Xinmo landslide in China on the 24th of June that killed at least 83 people (Ouyang et al., 2017). The year 2017 has seen an above-average number of landslide catastrophes. However, as extreme weather events become more frequent and more severe due to climate change, developing precise and reliable methods to monitor landslides and assess the landslide hazard is becoming increasingly important.

Lower-income countries experience most of the casualties due to landsliding (Petley, 2012). One reason is certainly that this is where vast mountainous regions with steep slopes and areas of monsoon climate with high population density are located. However, the limitations and shortcomings in landslide monitoring and mitigation measures as well as insufficient knowledge of the landslide processes also play a substantial role in increasing the death toll and damages to the housing and infractructure.

Southern Kyrgyzstan is one of the regions with frequent and dangerous landslide activity, which is distributed over a large area. Landslide investigations are undertaken by local scientists and the Ministry of Emergency Situations of Kyrgyzstan, but, considering the landslide number and the size of the area, their capabilities are limited. In this thesis, this issue is addressed by proposing an approach that relies on the use of remote sensing data and GIS in order to gain a deeper understanding of the landslide processes in the region and, where possible, automate the process of landslide hazard assessment.

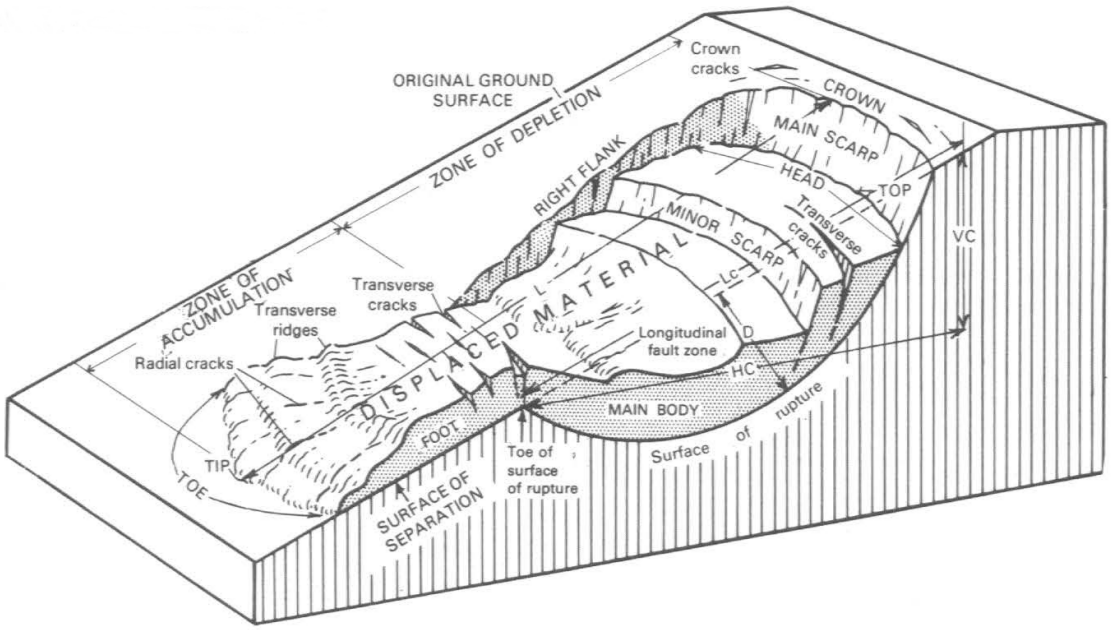

Figure 1.1: Model of a slump–earth flow (after Varnes (1978)).

1.2 Research Background

1.2.1 Landslides: Gravitational Mass Movements

Landslides are gravitational mass movements. The term 'landslide' is used for a variety of processes and includes many movement types, e.g. rotational, translational and block slides, debris flows, debris avalanches, earthflows, rockfalls, topples, lateral spread, and creep (USGS, 2004). Often, complex slope failures occur that combine elements of two or more types, e.g. landslides that start as a rotational slide but turn into a flow in their lower part. While gravitation remains the main reason for the mass movements, other factors influence the slopes and play a role in their offset, e.g. saturation of slopes with water, earthquakes, slope undercutting due to erosion or human activity, loading of the slopes or their crests, etc.

More strictly, the term 'landslide' is used only to refer to rotational, translational and block slides. In these landslide types, a sliding surface develops, typically along a lithological boundary, and separates the material that slides from the more stable underlying rock. These slides have following morphological elements: the main scarp that is located at the top of the affected area and exposes the upper part of the sliding surface, the landslide body that is made up of the displaced material, the toe of the landslide that is the furthest point away from the scarp that was reached by the displaced mass (Fig. 1.1). Furthermore, the depletion and accumulation zones of the landslide can be distinguished. Often, cracks are visible on the slope next to the main scarpe. Their growth indicates that the landslide-prone slope is likely to produce another failure.

Landslides are typically visible in aerial and satellite images due to their lower vegetation levels, hummocky terrain, ponds and wet areas that form because of the disruption of water circulation in the landslide mass, cracks at the crown and the body of the landslide, a river channel shift at the landslide toe, etc.

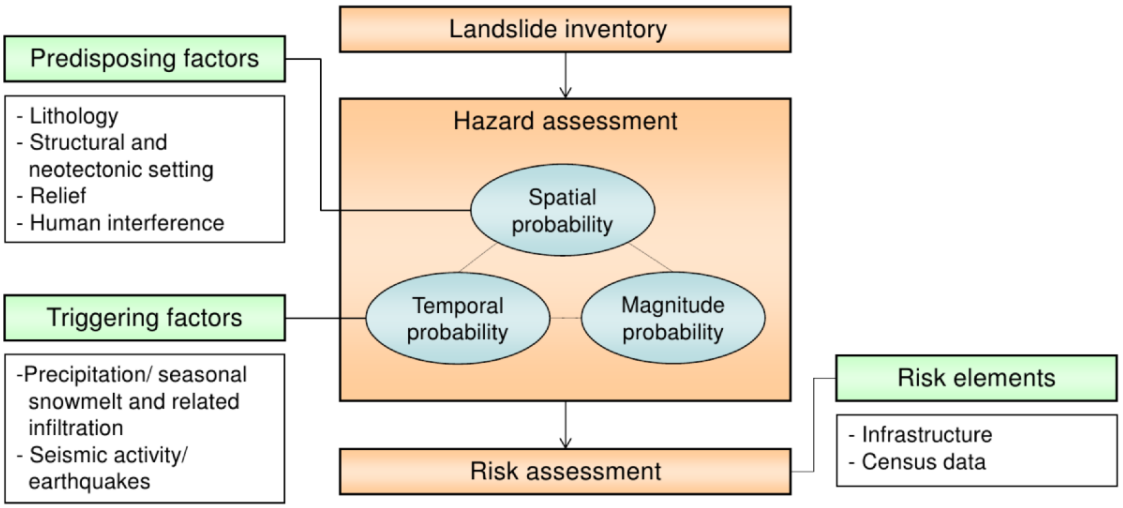

Figure 1.2: Conceptual scheme of landslide hazard assessment (after Guzzetti et al. (2005)).

1.2.2 Landslide Hazard Assessment: an Overview

Landslide hazard assessment is conducted with the aim to mitigate possible effects of landslides on people and infractructure. It is based on the assumption that the conditions that led to slope failures in the past are the same ones that are responsible for possible landsliding in the future. Landslide hazard assessment includes an evaluation of the spatial ("Where can landslides occur?"), temporal ("When / how often can landslides occur?") and magnitude ("How large can the landslides be?") probability of landslide occurrence (Fig. 1.2, Guzzetti et al. (2005)).

The analysis of the spatial component of landslide hazard is referred to as landslide susceptibility. Landslide susceptibility seeks to establish a relationship between the distribution of landslides in the study area and that of predisposing factors (equivalent to the International Geotechnical Societies' term 'preparatory factors' (Popescu, 1994)), i.e. factors that are modeled as invariable in time. Typical examples are geological and structural characteristics of the area, lithology and soils, land use (if persistence of land use classes is assumed), aspect, slope, curvature, distance from streams, etc. This is the most common stage of the landslide hazard assessment to be carried out, and its methodology has been researched extensively. In the quantitative landslide research, two groups of methods can be distinguished: data-driven statistical methods and physically based methods. The former seek to estimate the likelihood of the different factor combinations to initiate a landslide based on the past landslide occurrence. The goal is usually to predict the probability of future failures in areas with no previous landslide record. Physically based models rely on detailed data describing the conditions and physical processes that affect the slopes. They are only suitable for susceptibility analysis at specific sites or at the local scale in areas with homogeneous geological and geomorphological conditions. Susceptibility assessments can concentrate on the landslide initiation zones or include runout modeling as well (Corominas et al., 2014).

The temporal probability of landsliding is estimated either by calculating the landslide frequency based on the past failures or by establishing a link between the temporal changes in the triggering factors (e.g. precipitation, seismicity, changes in

the land use, volcanic erruptions, etc.) and the slope failures. Only some studies that focus on landslide hazard assessment include the temporal component, usually due to difficulties in obtaining reliable temporal data on landslides and triggering factors with sufficient detail.

The magnitude component is typically evaluated in the magnitude-frequency analysis. The resulting magnitude-frequency curves show the distribution of landslide numbers by landslide size classes. These curves are helpful to evaluate the completeness of the underlying inventory and determine for which landslide sizes the results of the hazard analysis are applicable. Such curves are typically plotted on the logarithmic scale and display the so-called roll-over effect (Havenith et al., 2015), i.e. a decrease in landslide numbers (compared to the power-law distribution) for smaller landslides.

The results of landslide hazard assessment can be combined with data on settlements and infrastructure (so-called 'elements at risk') to evaluate the landslide risk and vulnerability.

At every step of landslide hazard assessment, mapping units (i.e. spatial units to which the input data and the results of the analyses are attributed) play a role. They can be of different types, e.g. pixels, unique-condition units that result from an overlay of vector layers or terrain-based units that model slopes. Their choice depends on the scale and the objectives of the analysis.

1.2.3 Landslide Inventories

A landslide inventory is the prerequisite for each stage of landslide hazard assessment and largely determines the quality of its outcome and how the results are to be interpreted. Depending on the time frame of the recorded landslide activity and the information source, landslide inventories are classified by Guzzetti et al. (2012) as follows:

- Archive inventories contain landslide information obtained from archive sources, e.g. newspapers, reports of the authorities, fire brigade records, etc.
- Geomorphological inventories contain landslides that were mapped using geomorphological evidence obtained in the field, aerial or satellite images. They are subdivided into:
  - Historical inventories include all landslides that can be observed at a certain point in time without a differentiation of their age.
  - Event-based invenventories are composed of landslides that failed as a result of a triggering event, e.g. an earthquake or a rainstorm.
  - Seasonal inventories contain landslides that occurred during a particular season or several seasons.
  - Multi-temporal inventories contain landslide events that occurred over a prolonged period of time with a differentiation of the failure dates. Multiple failures at the same location can be recorded in this inventory type.

A landslide inventory will typically include attributes that characterize the properties of the landslides. The set of the attributes depends on the purpose of the inventory and data availability.

Historically, landslide inventories have been prepared manually in the field or in the process of visual analysis of aerial images. These methods require a trained geomorphologist (Guzzetti et al., 2012). Due to the development of remote sensing techniques in the last two decades, new methods of landslide mapping have emerged. The spatial and temporal resolution of the available optical satellite data has improved significantly in the last two decades. Landslide detection from optical images can be performed visually or (semi)-automatically using algorithms for change detection, clustering, object-oriented image analysis, etc. Pre-processing is very important in (semi)-automatic analyses in order to ensure comparability of the images. The surface morphology can be analyzed using the LiDAR (light detection and ranging) and InSAR (synthetic aperture radar) techniques for the acquisition of detailed elevation data (Van Westen et al., 2008).

1.3 Study Area

1.3.1 Landslide Situation in Southern Kyrgyzstan

Landslides in southern Kyrgyzstan are abundant at the eastern rim of the Fergana basin (Fig. 1.3). Most of these landslides are complex failures caused by a combination of predisposing and triggering factors. They mainly develop in weakly consolidated folded Mesozoic and Cenozoic sediments and are spatially controlled by the structural and tectonic setting of the region (Roessner et al., 2005; Wetzel et al., 2000). Due to water accumulation in these folds, these areas are especially susceptible to landsliding. Furthermore, they are covered by loess of varying thickness. The loess is often deposited in an irregular manner in the folds in form of pockets, which makes its identification difficult based only on the information about the ground surface.

Locations with a loess layer of substantial thickness produce very rapid and therefore very dangerous landslides, which often turn into flows with long runout zones in their lower part. These landslides are the main cause of the fatalities in the region because the whole landslide mass can be displaced literally within a few minutes. The other widespread landslide type are deep-seated landslides in more clay-rich deposits. They usually move more slowly but can affect large areas. On gentle slopes, they can develop into very large slow-moving structures that can be observed with InSAR methods (Teshebaeva et al., 2015).

Most of the slope failures in the region occur in the months March to May during and after the snowmelt when the ground is saturated with water. The intensity of landsliding is very different between the years; the differences can be tenfold and more. The variations are related to the amount of snow accumulated during the winter and the amount of rainfall in the spring months (Torgoev et al., 2010; Ibatulin, 2011).

Southern Kyrgyzstan is a seismically active region. According to the existing

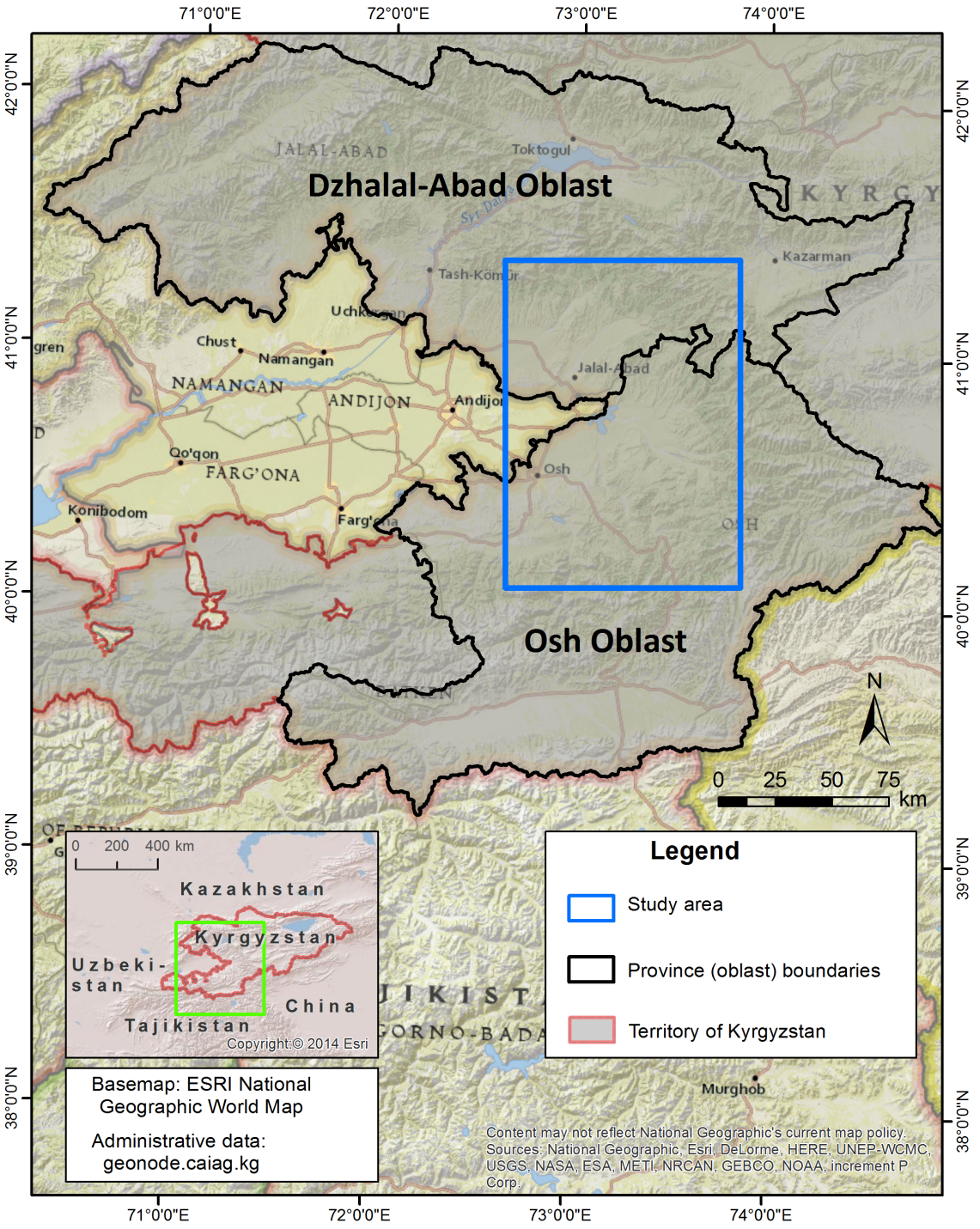

Figure 1.3: Study area in southern Kyrgyzstan

earthquake record, the seismicity in the study area is characterized by frequent earthquakes of light and modeate magnitudes (USGS, 2017). The earthquakes in the region play a preparatory role in the landsliding process because they destabilize the slopes and make them more susceptibile to landsliding in the next period when the ground becomes saturated with water (Danneels et al., 2008). Thus, the association between the landslide occurrence and the landslide triggering factors in the study area is a complex one. In contrast to regions with clearly pronounced triggering events, such as a major earthquake or a prolonged rainstorm, the triggering factors in southern Kyrgyzstan exert their influence on the landslide-prone slopes

over prolonged periods of time. Seismicity and accumulation of water in the ground destabilize the slopes in such a way that even a small fluctuation in the conditions can initiate a slope failure. Thus the concrete failure dates of the landslide events may be difficult to link to single triggering events.

However, there is evidence that the Fergana basin can experience major earthquakes with a return period that is longer than the time period covered by the available earthquake catalogs (Korzhenkov et al., 2014). In that case, earthquakes can act as a classical triggering factor with a direct temporal link to the landslide events, which could cause great damage in this scenario.

Landslide observations have been conducted in the region by local authorities since the 1950s with the goal in mind of protecting the local residents. I.e. the data collected by the local authorities focus on the areas in the vicinity of settlements and possibly disregard remote or uninhabited parts of the region. Due to a history of underfunding of the landslide and other geoscientific invenstigations since the beginning of the 1990s, the data of the local authorities on the landslides as well as on the landslide predisposing factors in the study area remain incomplete. Assessments of landslide susceptibily, hazard and risk have been performed by the local experts and have been of qualitative nature (CAIAG Geonode, 2017).

1.3.2 Remotely Sensed Data for Landslide Hazard Assessment

Because of the limited spatial and temporal data availability in Kyrgyzstan and the large size of the study area (over 12,000 km^2), multi-temporal satellite remote sensing is the only consistent, reliable and up-to-date source of spatial information for the region. It plays a central role for the acquisition and preparation of data on all of the components of the landslide hazard assessment. Satellite remote sensing data are characterized by high spatial accuracy. They can be used as the common spatial reference for the heterogeneous data that have been collected from various sources in order to characterize landslide hazard in southern Kyrgyzstan as fully as possible.

Since landslides are a phenomenon that in most cases significantly changes surface characteristics, they are usually well detectable with optical imagery, which has already been archived for several decades and thus enables a long-term analysis of landslide activity in the region. The presence of a period with green vegetation in Kyrgyzstan (spring and early summer) is the basis to differentiate the slope failure extents from the surrounding unaffected areas with intact vegetation.

The resolution of the imagery used for landslide mapping must be chosen in accordance with the typical landslide sizes in the study area. In southern Kyrgyzstan, landslides can reach large sizes, which implies that even Landsat images with the spatial resolution of 30 m can deliver useful information for the period when no data with higher resolution are available. Nevertheless, higher image resolution is necessary to obtain a more comprehensive landslide inventory.

Due to the development of the techniques for the acquisition and processing of optical satellite images in the last two decades, the amount of archive data acquired by different sensors and suitable for landslide mapping is growing. For southern

Kyrgyzstan, a database of optical satellite images with the spatial resolutions between 30 m and 5 m has been created by Behling et al. (2014b). This database contains over 700 co-registered images acquired by different satellites that cover the period from 1986 to 2016.

In the future, the amount and quality of the satellite data suitable for the landslide mapping will be increasing. The Sentinel-2A and -2B missions have recently started data acquisition, and the resulting L1C products will be made available to the public (ESA Sentinel Online, 2017). This is especially important for regions like southern Kyrgyzstan where limited funding is available to carry out landslide investigations.

With such amounts of data available, efficient methods for automated landslide detection become essential. This thesis builds up on the dissertation by Behling (2016). The automated approach he developed detects landslides from optical satellite imagery using temporal NDVI trajectories. This approach will be referred to in this thesis as 'automated landslide detection'. The present thesis makes the next step to evaluate what effect the use of an inventory acquired by automated landslide detection has on the landslide hazard assessment, particularly on its spatial component.

Apart from the landslide mapping, remote sensing can be used to support the spatially differentiated characterization of landslide predisposing and triggering factors. Digital elevation modes (DEM), e.g. the ones obtained by the SRTM, ASTER and ALOS missions, are suitable for the derivation of landslide-related relief parameters. Optical images in a combination with a DEM can be used to delineate geological units and fault zones based on existing geological map information and field investigations. Hydrometeorological parameters can be analyzed in their spatio-temporal dynamics using MODIS land cover and surface temperature data.

1.4 Research Objectives and Structure

To gain a better spatio-temporal understanding of landslide processes in the region and to reduce the landslide risk, there is a big need for new methods for an objective, systematic and spatially differentiated landslide hazard assessment at a regional scale. However, such an assessment has not been conducted yet. The objective of this study is the development of an approach based on the use of remote sensing and GIS to accomplish this task. In the context of the study area, there is all the more reason to rely on satellite remote sensing because of the large size of the area and limited availability of other data sources.

The availability of an automated method for landslie detection from satellite images implies that large inventories can be produced efficiently. Moreover, the inventories can be updated when new images are acquired with much less effort than was needed before. Therefore, efficient methods are necessary to derive landslide attributes and, if desired, carry out repeated analyses of the landslide hazard after the inventory updates. GIS tools for spatial analysis are required to accomplish this task.

On the methodological level, the detailed multi-temporal landslide data obtained

by Behling et al. (2016) with over 1,500 objects presents the oportunity to examine the possible direction of future landslide hazard investigations, especially for data-scarce regions. With the growing accessibility of satellite images and a further increase in their resolution, the automated methods for landslide detection like the one suggested in the above publication will be used more widely. Therefore, the effect of the application of such techniques needs to be evaluated and compared to conventional methods, e.g. to the visual landslide mapping (Van Westen et al., 2008). Because data-driven methods commonly applied in landslide hazard assessment strongly depend on the type and quality of the input data, the second objective of this study is to evaluate how the characteristics of the landslide data influence the results of the various stages of the hazard assessment.

This study was conceived as a cumulative dissertation and includes three papers that have been published in international journals. Each of these papers forms a chapter of the thesis focusing on the preparation of the multi-source landslide inventory, the derivation of landslide attributes for the inventory and performing an assessment of the landslide hazard in the study area, respectively. The research questions of each paper are outlined below.

1.4.1 Chapter 2: Landslide Inventory

published as:

Golovko, D., Roessner, S., Behling, R., Wetzel, H.-U. and Kleinschmit, B. (2015). Development of Multi-Temporal Landslide Inventory Information System for Southern Kyrgyzstan Using GIS and Satellite Remote Sensing. PFG Photogrammetrie, Fernerkundung, Geoinformation, 2, 157–172, doi:10.1127/pfg/2015/0261. With permission of Schweizerbart Science Publishers.

The objective of the first paper is to summarize the information on landslides that is available for the region, evaluate it and prepare it in a way that can be used for the subsequent analyses of landslide hazard. Research questions posed in this chapter are:

- What sources of data on landslide activity can be used and what are their characteristics?
- What types of landslide inventories are suitable in the context of the present research and which of them can be produced for the study area?
- What is the role of remote sensing and GIS in the compilation of a landslide inventory for southern Kyrgyzstan?
- What is the spatial and temporal precision of the available landslide data and how can they be accommodated in a single inventory?

1.4.2 Chapter 3: Landslide Attributes

published as:

Golovko, D., Roessner, S., Behling, R. and Kleinschmit, B. (2017). Automated derivation and spatio-temporal analysis of landslide properties in southern Kyrgyzstan. Natural Hazards, 85(3), 1461–1488, 10.1007/s11069-016-2636-y. With permission of Springer.

A landslide inventory typically includes not only the information on landslide locations and failure dates but also a number of further attributes. The objective of chapter 3 is to complement the multi-source inventory prepared in the previous step by deriving the landslide attributes in an automated way. In this process, the following research questions have to be answered:

- Which landslides attributes are often included into landslide inventories and which ones of them can be derived automatically for large inventories?
- Which values of landslide attributes are particularly frequent in the study area?
- How do the values of landslide attributes differ for landslides documented from different sources?
- Are there differences in landslide properties between different parts of the study area?
- What is the size (maximal and minimal area) of landslides that are sufficiently represented in the database (e.g. in order to estimate their frequency / return period)?

1.4.3 Chapter 4: Susceptibility Assessment

published as:

Golovko, D., Roessner, S., Behling, R., Wetzel, H.-U. and Kleinschmit, B. (2017). Evaluation of Remote-Sensing-Based Landslide Inventories for Hazard Assessment in Southern Kyrgyzstan. Remote Sensing, 9(9), 943, doi:10.3390/rs9090943.

A landslide susceptibility assessment establishes an association between the distribution of landslides and of the predisposing factors. It is the most frequently performed element of the landslide hazard assessment. However, many studies perform the susceptibility assessment based on the landslide inventory that is available, whereas the influence of the properties of the inventory on the results of the susceptibility assessment is rarely analyzed in detail. In this chapter, this influence is investigated by comparing susceptibility maps produced with a historical inventory (results of expert interpretation of landslide complexes) and a multi-temporal inventory (results of automated landslide detection). An overview of the chapter 4 is shown in Fig. 1.4. The following research questions are posed:

- How do the properties of the underlying landslide inventory influence the results of landslide susceptibility mapping?

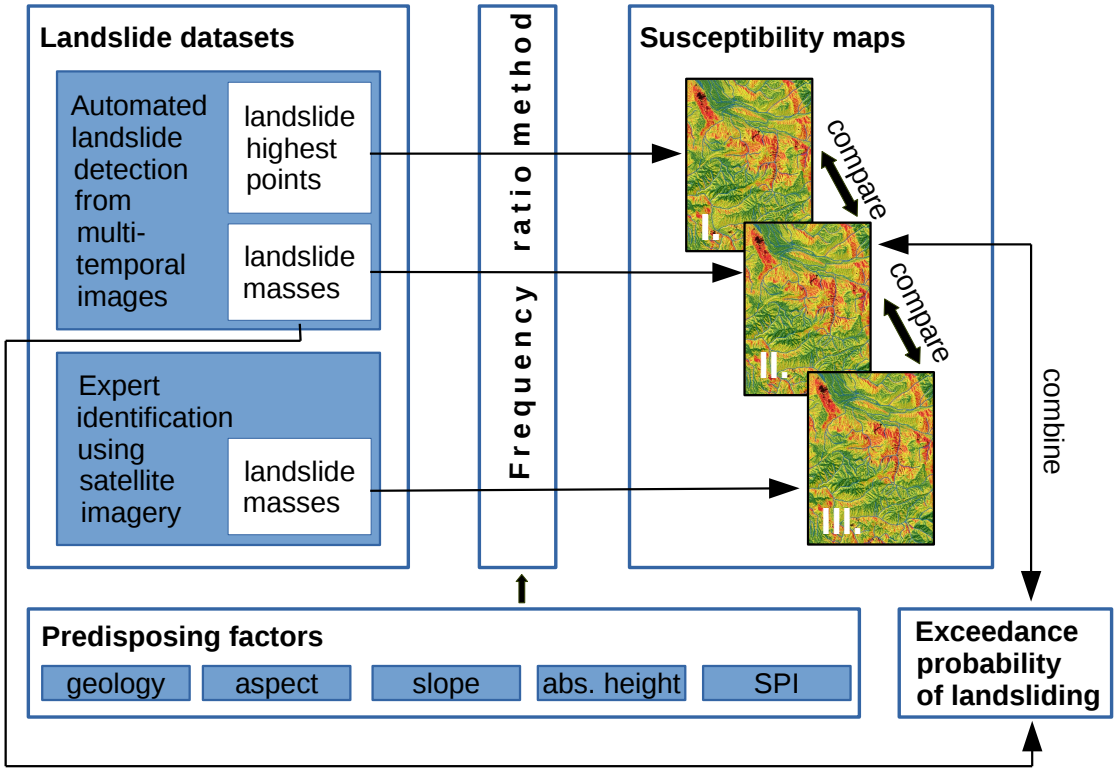

Figure 1.4: Overview of chapter 4. This figure was used as the graphical abstract for the publication Golovko et al. (2017b).

- What are the most important landslide predisposing factors in the study area?
- How can remote sensing and GIS contribute to the acquisition and clarification of information on landslide predisposing factors in the study area?
- How can the susceptibility assessment be supplemented to include the temporal aspect of landslide hazard?

Chapter 2

Multi-Source Landslide Inventory

Development of Multi-Temporal Landslide Inventory Information System for Southern Kyrgyzstan Using GIS and Satellite Remote Sensing

Darya Golovko, Sigrid Roessner, Robert Behling, Hans-Ulricht Wetzel, Birgit Kleinschmit

Originally published in PFG Photogrammetrie, Fernerkundung, Geoinformation (2015), 2, 157-172
https://doi.org/10.1127/pfg/2015/0261

Summary

In Southern Kyrgyzstan, landslides regularly endanger human lives and infrastructure. They are a very dynamic phenomenon with significant variations of the process activity in different years. This creates a need for the development of new methods of dynamic and spatially differentiated landslide hazard assessment at a regional scale. Because of the large size of the study area (over 12,000 km^2), remote sensing data are a valuable and reliable source of detailed and consistent spatial information for landslide investigations in Southern Kyrgyzstan. The paper demonstrates how GIS and remote sensing techniques are used for the acquisition, verification and homogenization of heterogeneous multi-source landslide data with the goal of generating a multi-temporal landslide inventory. Special emphasis is placed on the spatial data consistency, the documentation of temporal information and the possibility to document repeated slope failures within the same slope. The multi-temporal landslide inventory is an integral part of a landslide inventory information system, which is implemented in the QGIS environment and provides self-customized functionality for data queries and spatial analysis including the derivation of landslide attributes. The information system contains additional spatial base data such as a spatially consistent multi-temporal archive of satellite images and topographic maps.

Zusammenfassung

Entwicklung eines Informationssystems zur multitemporalen Inventarisierung von Hangrutschungen für Südkirgistan unter Verwendung von GIS und Satellitenfernerkundung. In Südkirgistan werden durch Hangrutschungsereignisse regelmäßig Menschenleben sowie technische und soziale Infrastruktur gefährdet. Da die Hangrutschungsaktivität in dieser Region zwischen den Jahren sehr variiert, besteht der dringende Bedarf, Methoden zu entwickeln, welche eine dynamische und räumlich differenzierte Einschätzung der Hangrutschungsgefährdung auf regionaler Ebene erlauben. Aufgrund der Größe des Untersuchungsgebietes von über 12.000 km^2 sind für die Entwicklung dieser Methoden satellitengestützte Fernerkundungsdaten besonders geeignet, da sie die einzige räumlich kontinuierliche und zeitlich wiederholbare Informationsbasis für die gesamte Region darstellen. In diesem Paper wird gezeigt, wie GIS- und Fernerkundungsverfahren fÃijr die Erfassung, Überprüfung und Homogenisierung heterogener Hangrutschungsdaten aus mehreren Quellen verwendet werden, um eine multitemporale Inventarisierung von Hangrutschungen zu ermögli-chen. Besonderer Wert wird dabei auf die räumliche Konsistenz der Daten, die Dokumentation des zeitlichen Auftretens und die Erfassung von wiederholten Hang-rutschungsereignissen innerhalb desselben Hangs gelegt. Um die multitemporale Hangru-tschungsinventarisierung zu unterstützen, ist ein QGIS-basiertes Informationssystem entwickelt worden, welches mit angepassten Datenabfragen und räumli-chen Analysen zur Ableitung von Hangrutschungsattributen beiträgt. Das Informationssystem beinhaltet zusätzliche Geobasisdaten wie ein räumlich konsistentes multitemporales Archiv von Satellitenbildern und topographische Karten.

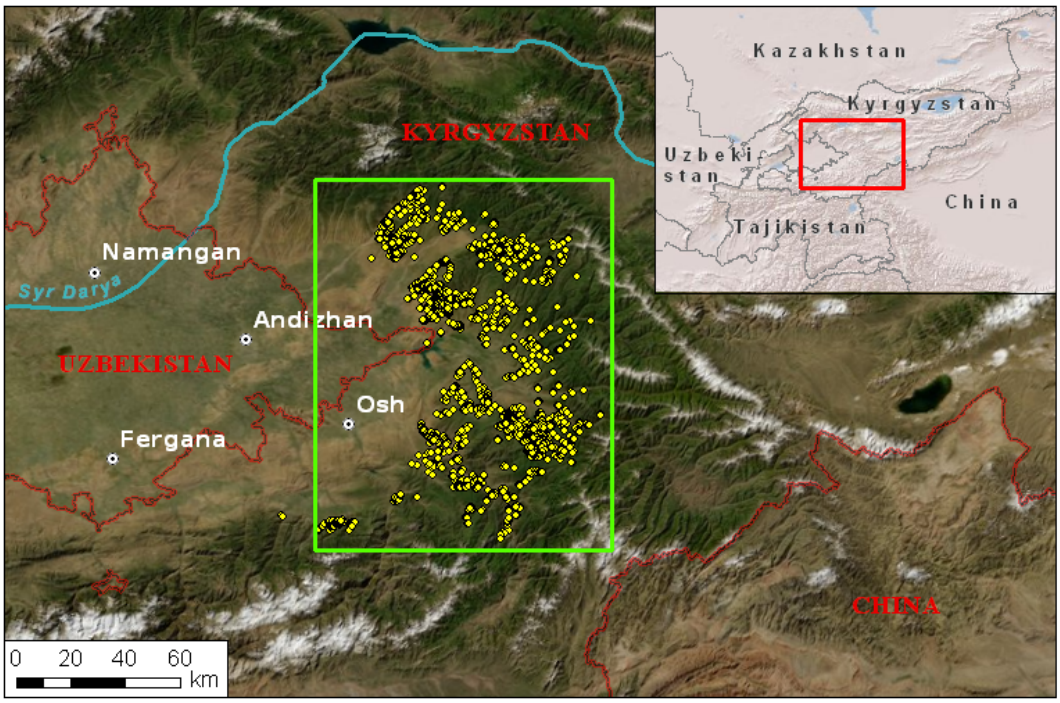

Figure 2.1: Study area in Southern Kyrgyzstan (green) with landslide locations (yellow) according to data obtained from Yerokhin (1999). Spatial base data from Esri.

2.1 Introduction

The foothills of the Tien Shan mountain ranges along the eastern rim of the Fergana basin in Southern Kyrgyzstan are subject to high landslide activity as a result of pronounced relief and ongoing tectonic activity. Furthermore, the topographically rising eastern rim of the Fergana basin represents a barrier to the prevailing westerlies leading to increased precipitation levels in comparison to areas that are situated further east (Kalmetyeva et al., 2009). All of these factors create favourable conditions for the intense and frequent occurrence of landslides in this area of about 12,000 km^2 administratively covering the Osh and Dzhalal-Abad provinces (oblasts), presenting an important human living space in this mountainous country (Fig. 2.1). Large landslides occur mostly within weakly consolidated Mesozoic and Cenozoic sediments at elevations between 800 m and 2,000 m a.s.l. Slope failures in massive Quaternary loess sediments are especially dangerous due to their very rapid and destructive avalanche-like movement. Another type of landslides develops in more clay-rich sediments and is characterized by lower movement rates but can nevertheless affect large areas (Roessner et al., 2014, 2005; Wetzel et al., 2000). Since landslides represent a major threat to the local population frequently causing fatalities and severe economic losses, observations of landslide activity in Southern Kyrgyzstan have been carried out by local organizations since the 1950s. Between 1969 and 2010, approximately 4,500 landslides were recorded in Southern Kyrgyzstan (Ibatulin, 2011). Since 1993, over 250 persons have died as a result of catastrophic slope failures in Kyrgyzstan (Torgoev et al., 2010). Landslide activity in this region is characterized by frequent and at the same time sporadic occurrence of events. This creates a strong need for a spatially differentiated assessment of landslide hazard and risk.

A landslide inventory is one of the main prerequisites for an objective landslide hazard assessment, which includes both the spatial and the temporal aspects of the probability of landslide occurrence (Guzzetti et al., 2005). A landslide inventory is a register of the distribution of landslides and their characteristics (Hervas, 2013; Guzzetti et al., 2012). The latter usually include the landslide id, location, dates of first occurrence and reactivations, type, state of activity, area and volume. Additionally, information on landslide geometry, geo-environmental characteristics at landslide site, triggering factors, landslide impact, monitoring data, etc. can be incorporated. The set of recorded characteristics may differ depending on the scale and method used to create the inventory, on properties of the study area as well as on the project goals. An overview of the most common landslide attributes is presented in Tab. 2.1.

Table 2.1: Overview of landslide attributes: '++' = 'very suitable', '+' = 'suitable', '-' = 'unsuitable'. (after Van Den Eeckhaut and Hervás (2012); International Geotechnical Societies' UNESCO Working Party for World Landslide Inventory (1993); USGS (2004); Hervas (2013); Wieczorek (1984)).

Attribute Group	**Selected Attributes**	**Methods for Derivation**		
		Terrestrial	*Map / GIS*	*Remote Sensing*
General information	ID, reporter, photographs, bibliography	-	-	-
Landslide location	Coordinates, reference to river valley or settlements, administrative units	++	++	+
Landslide dimensions	Length / width / depth at head / middle / toe part	+	++	++
	Volume	++	-	-
	Area, perimeter / area ratio	+	++	+
	Elevation drop	+	+	++
Landslide classification	Type of movement (e.g. flow, rotational or translational slide), slope material (e.g. rock / debris / mud flow)	++	+	+
Geo-environmental characteristics	Relief: slope, aspect, curvature and derivatives	+	-	++
	Lithology, tectonic structures, land use, distance to roads	++	++	+
Landslide history and activity	Known failure and reactivation dates, state of activity (e.g. active / dormant / relict landslide)	++	+	++
Causes	Hydrometeorological, seismic and other conditions preceeding the failure	++	-	+
Consequences and elements at risk	Fatalities and injuries	-	-	-
	Building damages, road closures, loss of arable land, number of people and buildings at risk	++	++	+

A wide range of methods have been developed in order to generate landslide inventories discussed in Van Westen et al. (2008) and Guzzetti et al. (2012). These methods include visual and (semi-) automated interpretation of optical, lidar and radar remote sensing data, geomorphological field mapping and archive studies. Geomorphological field mapping and visual interpretation allow integrating expert knowledge on the geological setting in the region into the mapping process but these methods are prone to subjectivity and are only suitable for mapping areas of limited size. Visual interpretation of optical aerial and satellite images, sometimes combined

with a DEM, remains a widely used technique for landslide mapping. In the recent years, approaches have been developed for automated and semi-automated landslide detection from high-resolution multi-spectral satellite images based on the classification of a single image or combined analysis of pre-event and post-event images. These approaches can be pixel-based or object-based. Whereas optical remote sensing enables the detection of slope failures that have already occurred, InSAR techniques allow detecting small surface deformations. In case of landslides, these deformations mainly indicate reactivations of previously active slopes that precede a new failure (Motagh et al., 2013; Wasowski and Bovenga, 2014). Overall, applications of satellite remote sensing for landslide mapping have become more important in the last decade due to the substantial increase in the satellite data availability, their spatial resolution and the development of hardware and software for image processing. The ongoing nature of satellite data acquisition permits going beyond producing a single landslide inventory map towards an information system with capabilities for future data updates as indicated by Van Westen et al. (2006). Such dynamic landslide inventories can serve as the basis for improved landslide hazard assessment that can incorporate input data updates and be carried out repeatedly, e.g. upon the availability of new data. GIS tools can be used for an efficient derivation of many of the landslide attributes from vector and raster data (Tab. 2.1).

Objective landslide hazard assessment for the study area requires a systematic landslide record in form of a multi-temporal landslide inventory, which documents slope failures over a long period of time including the dates or periods of their occurrence. The goal of this study is the establishment of a landslide inventory information system for Southern Kyrgyzstan enabling convenient data access and analysis and serving as the basis for subsequent landslide hazard assessment at a regional scale. Due to the highly dynamic nature of the landslide activity in this region and its complex interrelations with factors that cause its differentiation in space and time, we aim at establishing a GIS-based multi-temporal landslide inventory enabling efficient derivation of landslide attributes and subsequent hazard analysis. For this purpose, we develop a GIS and remote sensing based approach for the generation of the inventory from multiple information sources with the possibility of future data updates. The resulting inventory contains spatially explicit and consistent information about landslide activity with the best possible temporal resolution. This information includes single landslide events as well as complex landslide-prone slopes, which have been subject to several phases of reactivation. Such a comprehensive inventory has not yet been compiled for the area of high landslide activity in Southern Kyrgyzstan and, when completed, can serve as an example of multi-source landslide inventory mapping in a data-scarce environment.

The use of customized GIS tools makes it possible to develop a spatial information system for landslide hazard assessment accommodating the heterogeneous data on landslides, their predisposing and triggering factors and other supplementary information as well as functionality adapted to the procedures of landslide hazard assessment. Such a system has the potential to provide more consistent data storage, efficient data access, systematic data update procedures and customized tools for spatial and statistical analysis. Due to the advances in open-source GIS, it is possible to implement the system in the framework of already existing software packages. This allows using already available GIS functionality and taking advantage of the benefits of open-source software, such as the possibility of customization,

minimization of costs and flexibility. We implement the landslide inventory information system in the QGIS environment including self-customized functionality for efficient access to the landslide inventory data and derivation of additional landslide information.

2.2 Data Sources

The establishment of a multi-temporal landslide inventory for Southern Kyrgyzstan is a challenging task since the existing information on landslide failures is very heterogeneous. We consider all available sources of landslide data including information from local organizations, field work as well as results of multi-temporal satellite remote sensing analysis. The preparation of the landslide data from various sources for integration into the inventory and their verification requires the use of spatial base data of different kinds. In this section, we give an overview of the available sources of spatial base data and information on landslide occurrence.

2.2.1 Spatial Base Data

Spatial base data are needed for the derivation of the spatial location and extents of the landslides that originally did not have an explicit spatial reference and for the verification of existing spatio-temporal information on slope failures. They are an integral part of the data provided by the landslide inventory information system and are used to derive landslide attributes, e.g. landslide dimensions, the reference to the river valley, settlement and administrative unit where the landslide is located, etc.

In order to obtain a consistent archive of surface conditions over large areas with the best temporal resolution possible and to provide common spatial reference for multi-source landslide data, a multi-temporal database of optical remote sensing imagery has been created (Behling et al., 2014a). It contains 592 multi-spectral middle- and high-resolution remote sensing datasets. This database includes Landsat (E)TM, ASTER, SPOT and RapidEye images acquired in 1986 âĹŠ 2013 with the spatial resolution ranging between 5 m and 30 m. Standard orthorectified products from the providers were used to minimize the preprocessing effort. Even though the sensors record data in different channels, the combination of the green, red and near-infrared spectral bands is the least common spectral denominator which enables multi-sensor analysis of landslide-related surface changes. In order to ensure spatial consistency between the standard data products required for their automated analysis, they were co-registered to the Landsat reference using a fully automated approach. Overall accuracy has resulted in a high relative image-to-image accuracy of 17 m (RMSE) and a high absolute accuracy of 23 m (RMSE) for the whole co-registered database. Further details regarding the automated co-registration of the included 592 satellite images can be found in Behling et al. (2014a).

Derivation of landslide attributes, clarification of ambiguities related to landslide data and general orientation in the study area require the use of topographic data. We have used the 1:100 000 Soviet ordnance survey maps that were originally produced in the 1950s and 1960s and updated in the 1970s and 1980s. These

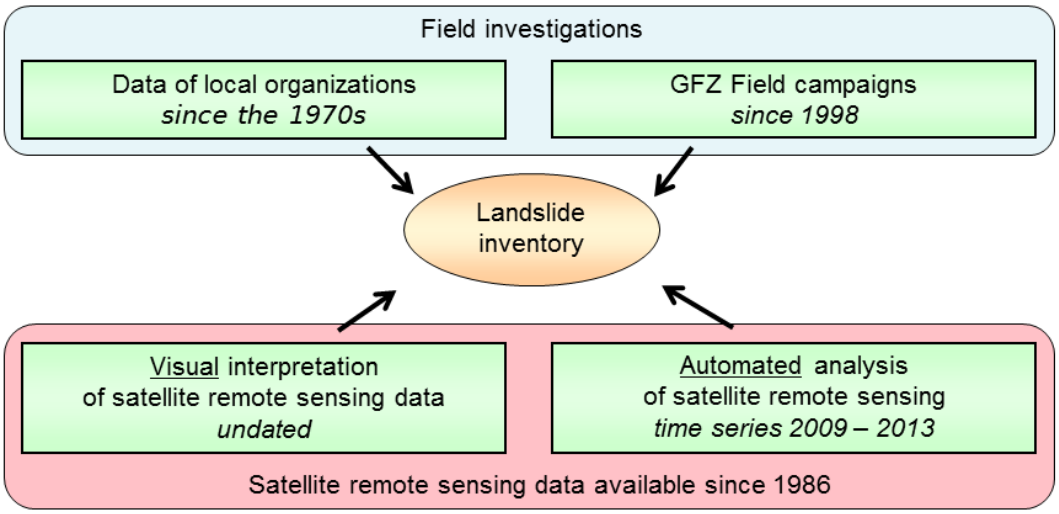

Figure 2.2: Overview of main sources of data on landslide occurrence in Southern Kyrgyzstan.

topographic maps are consistently based on a transverse Mercator projection and represent a high level of spatial detail. However, they are in part outdated and many of the settlement names have changed since the independence of Kyrgyzstan in 1991.

Furthermore, digital elevation data have been used in this study to derive relief-related landslide characteristics and for perspective visualization. These data include a SRTM X-band DEM (Rabus et al., 2003), which was obtained from the German Aerospace Center (DLR) in a spike-removed form, and the freely available ASTER GDEM Version 2 (2011). These digital surface models largely correspond to the Earth's surface topography due to the predominantly treeless character of the vegetation in the study area.

2.2.2 Landslide Information

Multiple sources of landslide data are available (Golovko et al., 2015). They include data obtained from local organizations, landslide mapping conducted during field campaigns, results of visual interpretation of mono- and multi-temporal satellite images as well as landslides which have been automatically detected from a multi-temporal satellite image database. However, these sources vary in their temporal coverage, their spatial and temporal completeness as well as their accuracy (Fig. 2.2). Furthermore, these landslide data are of analogue and digital origin. They have different formats, such as verbal description, tabular data, and vector information.

Information obtained from local organizations

From the 1960s until the breakup of the Soviet Union, regular landslide monitoring was conducted by local authorities for the most endangered areas in the region focusing on settlements and their surroundings (Roessner et al., 2005, 2014). After the independence of Kyrgyzstan, these activities have continued; however, they decreased due to shortage of funding. The landslide records of local organizations are

therefore a valuable source of landslide information covering the time period before regular satellite remote sensing data acquisition. One recent source of information on slope failures is the report by Ibatulin (2011) containing descriptions of selected landslide failures which have been documented mostly as the result of extensive field investigations carried out between the 1970s and 2004. The report comprises detailed verbal descriptions of the slope failures including results from geotechnical investigations of potentially endangered slopes. The report also contains precise temporal information on single landslide events whereby in most of the cases the exact day of the failure is known. However, it does not include explicit coordinate or map-based spatial information on the location of the slope failures. Instead, the landslide locations are described verbally in relation to significant topographic features. Overall, the report focuses on large landslides in the vicinity of inhabited areas. Thus, it contains episodic rather than systematic landslide inventory information.

A less recent but more extensive and systematic source of information on past landslide activity is the report by Yerokhin (1999) consisting of verbal descriptions accompanied by tabular and map-based information on landslides. It represents the cumulative assessment of the landslide situation by the end of the 1980s without specifying the dates of documented slope failures. Although this report contains spatially explicit information, the mapped landslides needed to be evaluated and spatially adjusted using satellite remote sensing data due to the coarse spatial resolution of the maps included into the report (Fig. 2.3). The report documents a number of landslide attributes including dimensions, position on the slope and activity stage making it the most comprehensive source of information on the properties of landslides in Southern Kyrgyzstan. Thus, the distribution of landslide attributes derived within a GIS can be validated against statistics calculated using this report.

Moreover, employees of the Ministry of Emergency Situations of Kyrgyzstan visited selected areas affected by landslides between the years 2002 and 2010 and recorded new landslides. The results of these surveys are available in form of tables. They represent only a small number of landslides which occurred in inhabited areas. Their location is represented in the table by a pair of x- and y-coordinates. However, their spatial extent is not documented. Temporal information is only contained in form of the date of field mapping whereas the time of the actual failure is mostly unknown.

GFZ field campaigns

The Remote Sensing Section of the German Research Centre for Geosciences (GFZ) has been conducting field work in Southern Kyrgyzstan since 1998 in cooperation with the Ministry of Emergency Situations of Kyrgyzstan with the purpose of selective landslide mapping and verification of data from other sources. Because of the large area affected by landslides, each of these field campaigns has covered selected parts of the study area. However, many of these areas have been visited multiple times. Field work has been extensively supported by satellite remote sensing analysis in order to efficiently cover large areas, especially for structural geological and landslide mapping. The findings were recorded in GPS-waypoint-oriented field documentation, satellite remote sensing based maps and field photographs. Furthermore, high-accuracy measurement with differential GPS were carried out for

selected topographic features and spatial reference points.

Satellite remote sensing analysis

Landslide mapping conducted during field investigations has been extended by expert interpretation of satellite remote sensing data in combination with digital elevation data and geological information using the perspective visualization capabilities of a GIS (Roessner et al., 2005). As a result, landslide scarps and bodies have been determined systematically for the whole area of interest. This method has proven to be especially suitable for mapping landslide-prone slopes which have experienced several phases of reactivation resulting in complex morphological structures.

However, visual mapping is labour-intensive and thus could only be carried out for subsets of the study area. In order to perform multi-temporal analysis for the whole study area, an approach for automated landslide detection has been developed based on the spatially aligned multi-temporal satellite remote sensing database (Behling et al., 2014a). This approach allows analysing large areas in multiple time steps. Applying this approach to the complete study area has resulted in automated detection of over 600 landslides that occurred between 2009 and 2013 (Behling et al., 2014a; Roessner et al., 2014). The obtained results, which were visually verified in the field, have revealed a constantly ongoing process activity in this region requiring regular and systematic landslide monitoring.

2.3 Methodology

The landslide inventory information system includes a landslide inventory and a spatial base as well as standard and customized functionalities for data querying and analysis as part of a GIS. We have implemented the landslide inventory information system in the QGIS environment because QGIS is a well-developed open-source software package with an easy interface for the incorporation of new plugins (QGIS Development Team, 2015). Furthermore, working in the framework of QGIS allows using its available core functionality and many already existing plugins, e.g. the OpenLayers plugin for convenient visualization of data served by a Web Map Service, such as Google Satellite and OpenStreetMap, or plugins that integrate R scripts for statistical analysis.

Fig. 2.3 gives an overview of the steps necessary for the generation of the multi-source landslide inventory for Southern Kyrgyzstan. Most of the input data underwent preparatory processing such as digitalization, data verification and other procedures necessary to bring them to a spatially consistent form. Spatial base data were required at this stage. After the multi-source landslide inventory has been generated, it can be used for further analyses, such as derivation of landslide attributes and data preparation for landslide hazard assessment. In the following, we discuss particular steps of this workflow in more detail. They include the creation of common spatial reference, derivation of spatial mapping units, preparation of the multi-source landslide data for GIS-based integration into the resulting landslide inventory and the development of a customized functionality in the QGIS environment for efficient data access and derivation of additional landslide information.

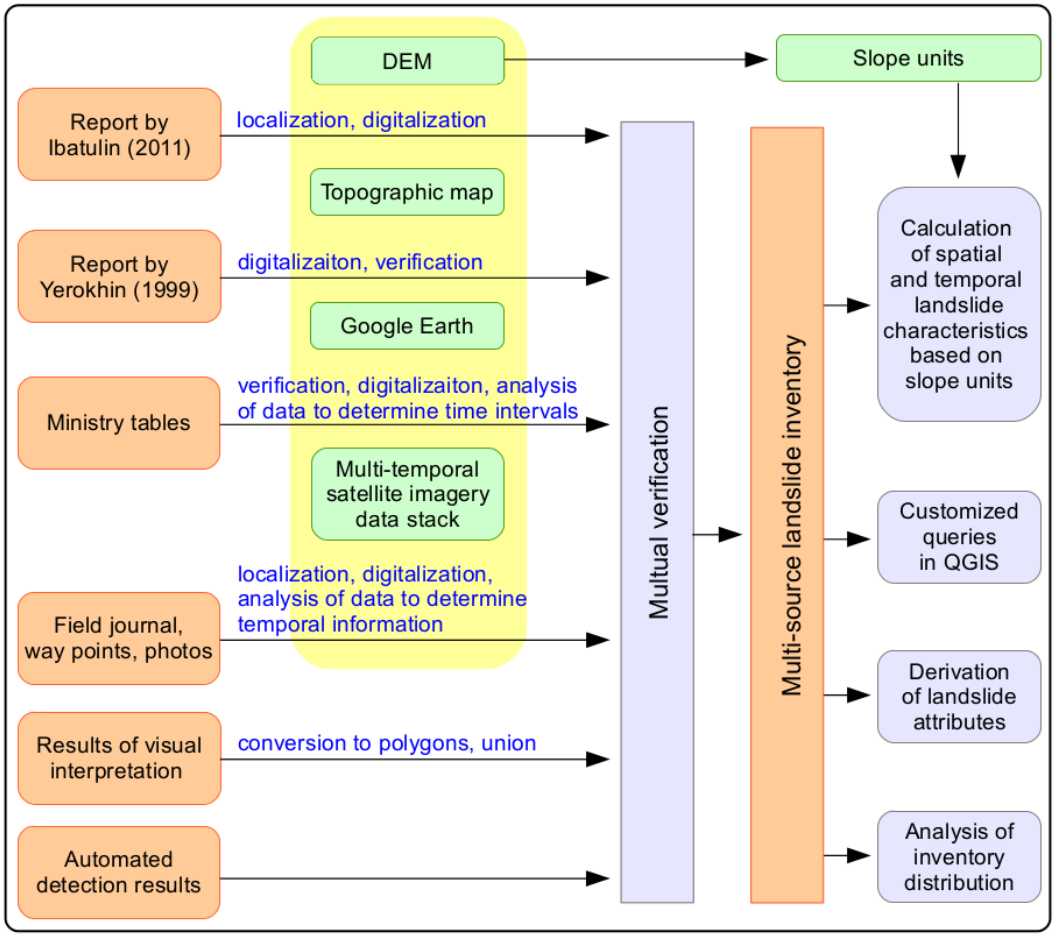

Figure 2.3: Overview of main sources of data on landslide occurrence in Southern Kyrgyzstan.

2.3.1 Creation of a Common Spatial Reference

The integration of all described landslide information sources into a single system requires the establishment of a common spatial reference. For this study, the multi-temporal satellite remote sensing database (section 2.2.2) represents the common spatial reference. UTM/WGS84 was used as the common map projection. The resulting spatially adjusted multi-temporal satellite remote sensing database is characterized by a high relative spatial accuracy between the image datasets amounting to less than the pixel size of the Landsat reference. Moreover, the absolute positional accuracy of this database has been assessed using high-accuracy differential GPS measurements. This investigation has revealed a systematic offset of the multi-temporal image database comprising 22 m in western and 5 m in northern direction (Behling et al., 2014a). Due to the use of orthorectified input imagery, this displacement can be regarded as a shift. The database was shifted accordingly in order to eliminate these systematic errors and ensure compatibility with spatial information originating from other sources. As a result, a consistent area-wide database of multi-temporal and multi-resolution images with a common spatial reference has been created. All other spatial data used for the generation of the multi-source landslide inventory information system have been checked in regard to their spatial fit to this common spatial reference system. The positional accuracy of the DEMs was checked using drainage network analysis and no systematic shifts could be iden-

tified. Thus, the DEMs can be used in their original form. The scanned topographic maps were georeferenced to the common UTM/WGS projection based on their corner coordinates. In a next step, the topographic maps were used to geocode the scanned paper maps contained in the report by Yerokhin (1999). Thus, conformity of all used spatial data with the common spatial reference has been achieved.

2.3.2 Derivation of Spatial Mapping Units

Some of the landslide data sources provide information on single landslide failures, whereas the others document complex landslide-prone slopes, which are a result of a large number of landslide events. Both types of data need to be analysed in a combined way in order to reconstruct the spatial and temporal evolution of landslide activity for distinct slopes. This requires the determination of adequate spatial mapping units, which also form the basis for subsequent hazard assessment. They can comprise cells of a regular grid, slope units, unique condition units, seed cells and other spatial units (Guzzetti et al., 1999; Van Den Eeckhaut et al., 2009; Erener and Düzgün, 2012; Süzen and Doyuran, 2004). For this study, morphologically-based slope units which can be derived from DEM-based watershed delineation have been chosen as the most suitable mapping units because they reflect the physical properties of the relief as the main landslide predisposing factor and have the potential for handling the remaining spatial uncertainties contained in the landslide data. Due to the fractal nature of these units, their size can be adjusted to the different mapping scales by varying the parameters for watershed delineation, e.g. the stream orders or the minimum basin size (Calvello et al., 2013). For the study area, they were derived from the SRTM DEM and the ASTER digital elevation data and are shown in an exemplary way in Figs. 2.5 and 2.6.

2.3.3 Landslide Data Preparation and Integration

Landslide data from each of the sources described above differ in their properties and had to undergo a plausibility check due to imprecision, uncertainty or errors in the data. Additional data preparation was necessary to transfer landslide data from the different sources to a consistent vector form. Fig. 2.4 illustrates the initial situation of the landslide information availability and the outcome of the multi-source data integration for landslide inventory mapping using the example of a complex landslide-prone slope in the Kara-Tuz river valley. Only slope failures detected automatically from multi-temporal satellite imagery in an object-based way were available in form of polygons that can be integrated into the inventory information system without further preprocessing (Fig. 2.4a). In case of this data source, the temporal information on the landslide occurrence was provided in form of a time interval between two image acquisition dates within which the slope failure occurred. This format was chosen for the resulting inventory to ensure comparability of data from the different sources. When the exact failure date was known, the start of the time interval was the same as its end.

Incorporating landslide information from verbal descriptions such as the report by Ibatulin (2011) required primary approximate localization of landslides using the topographic maps. Afterwards, the precise localization of the failures within the

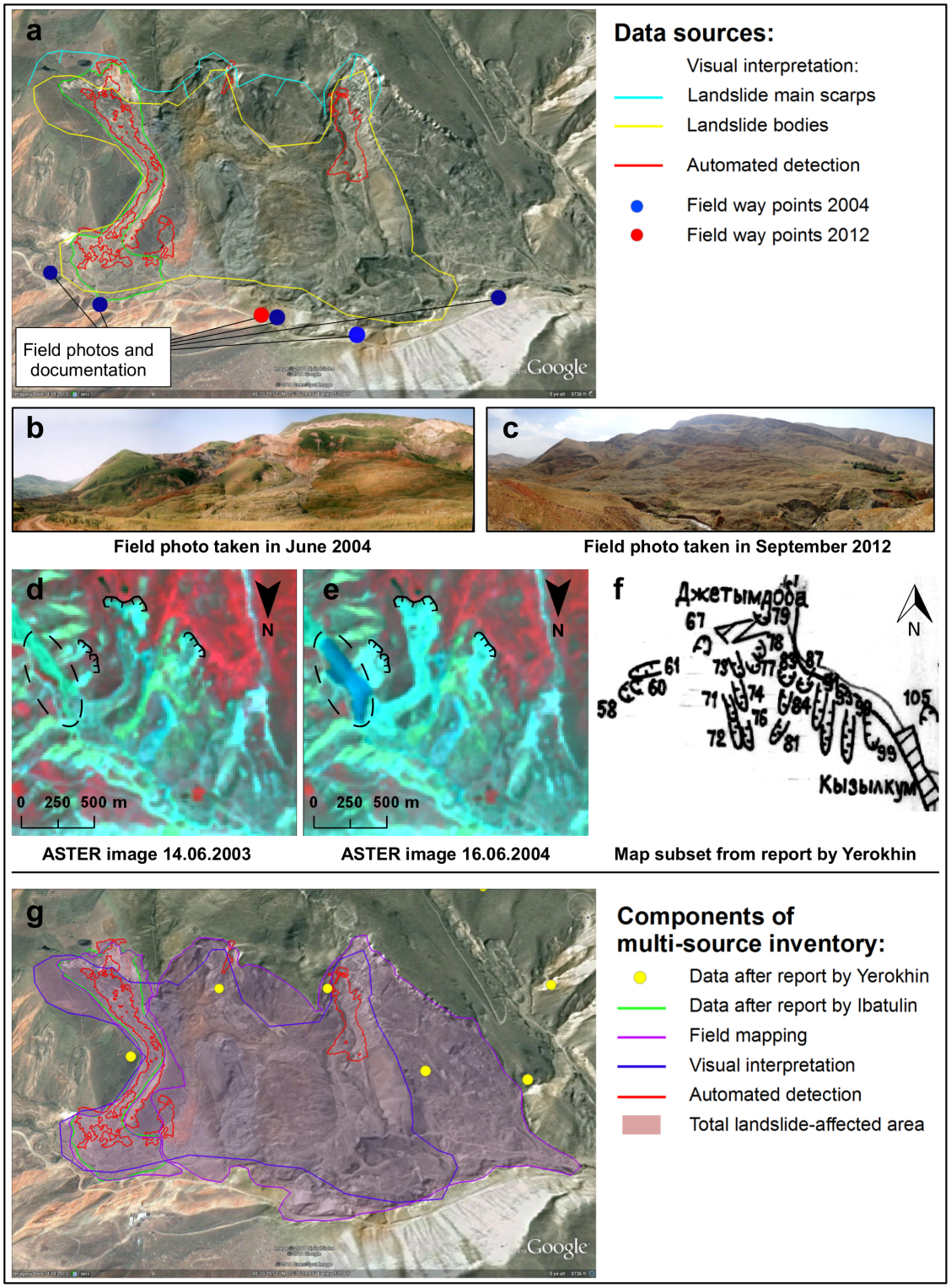

Figure 2.4: (a-f) Input data from various sources of landslide information including field photos, pre-event and post-event ASTER images from the multi-temporal satellite remote sensing database and maps from the report by Yerokhin (1999), (g) results of multi-source landslide mapping for a landslide-prone slope in the Kara-Tuz river valley. Google and the Google logo are registered trademarks of Google Inc., used with permission.

slope and the determination of their spatial extent were carried out using post-event satellite images. Sometimes, verbal information from reports concerning additional features such as landslide-dammed lakes or damage to buildings was helpful to localize the landslide in imagery acquired soon after the landslide failure. The longer the time between the slope failure and the image acquisition the more the landslide features have already been subject to erosion, revegetation and reactivations within the same slope. Often, Google Earth^{TM} was used to supplement the multi-temporal satellite imagery due to the higher spatial resolution, convenient functionality for generating perspective views and easy-to-use digitalization tools offered by this software package.

Slope failures documented in multiple data sources were used to verify the data, correct inconsistencies, improve localization of the landslides and determine the time of their failure with higher accuracy and reliability. Even though the heterogeneous landslide data could be processed to a more consistent and mutually comparable form, differences between the data from the various sources could not be completely eliminated. Therefore, it is important to document the data source for each landslide as part of the metadata, which allows judgments about the properties and precision of the data.

Additional information, such as photos, descriptions and other types of metadata, can be linked to the spatial landslide data via ids or using spatial proximity. We used ids to link attribute tables from the report by Yerokhin (1999) to landslide locations and a spatial link between landslides and GPS waypoints recorded during field surveys, which, in turn, contain references to field photos and landslide descriptions from field journals.

The data contained in the resulting multi-source landslide inventory for the landslide-prone slope in the Kara-Tuz river valley are illustrated in an exemplary way in Fig. 2.4. The report by Ibatulin (2011) documents a failure which occurred in 2004 within this slope. This description contains additional information that the landslide dammed the river and formed a lake. This failure could be localized in the left part of the slope due to the availability of a post-event ASTER image where the lake is clearly visible. The location of the lake is indicated in the pre-event (Fig. 2.4d) and post-event image (Fig. 2.4e) with an ellipse. Landslides recorded in the report by Yerokhin (1999) (Fig. 2.4f) prove that all parts of the slope had already been subject to landsliding prior to the 2004 event. The results of automated landslide detection show that there were further activations within this slope in the period between 26.5.2009 and 14.5.2011 (red outlines in Fig. 2.4). This location was visited in 2004 and 2012 during field work when field photographs were taken and subsequently integrated into the GIS-based photo archive (Figs. 2.4b, 2.4c). This archive allows a better understanding of spatio-temporal dynamics of landslide-prone slopes. During field work, the whole landslide-affected slope was mapped as a single polygon because it was not possible to distinguish between individual failures. Thus, the dated landslide events occupy a relatively small area within the landslide-prone slope. However, this information is valuable for the evaluation of landslide activity in this area, and the undated landslide information allows mapping larger landslide-affected areas. The total extent of the landslide-affected area within the slope was derived as a spatial union of all landslide polygons described above and used for the calculation of landslide density as shown in Fig. 2.6b.

2.3.4 Derivation of Additional Landslide Information

One of the components of the landslide inventory information system is a QGIS plugin written in the Python programming language. The plugin contains a set of customized functions implemented for the needs of working with the multi-temporal landslide inventory. It enables customized queries of the multi-source landslide data with an emphasis on temporal attributes. Furthermore, it provides spatial functionality for the derivation of landslide attributes, e.g. by automated referencing of landslides to spatial mapping units or finding highest points within a landslide body as an approximation of the landslide main scarp location. This type of analysis is based on the combination of vector data on landslides and spatial mapping units with a DEM. An exemplary result is shown in Fig. 2.5.

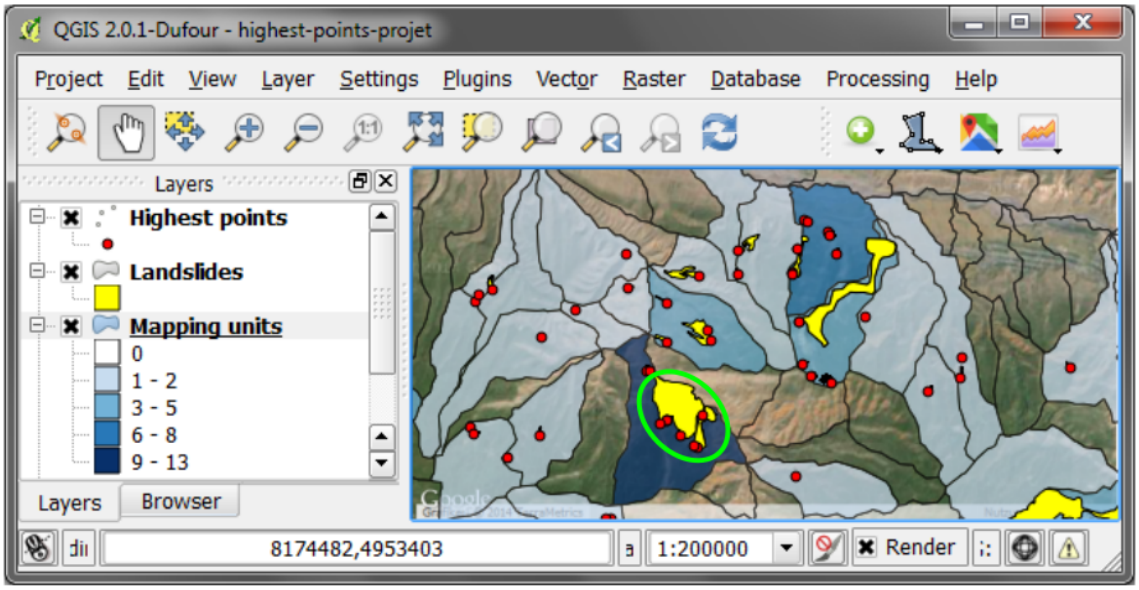

Figure 2.5: QGIS window with landslides south of the Tar river (mapped after report by Ibatulin (2011), results of field surveys, visual and automated analysis of satellite imagery), landslide highest points and spatial mapping units indicating the number of landslides assigned to them. The green circle shows the position of the complex landslide-prone slope in the Kara-Tuz river valley used as example in the methodological description of section 3. Satellite imagery by Google via OpenLayers plugin. Google and the Google logo are registered trademarks of Google, Inc., used with permission.

2.4 Results and Discussion

The resulting multi-temporal landslide inventory contains over 1200 landslides which could be mapped as polygons based on the various sources of information (Tab. 2.2). The summary table also contains the total area covered by complex sequences of failures, where it has not been possible to identify individual landslides due to long-term process activity within these landslide-affected slopes. The table also shows differences in the size of the mapped landslides, e.g. the report by Ibatulin (2011) documents a limited number of large slope failures, whereas automated landslide

Table 2.2: Summary statistics representing the current stage of the landslide inventory according to different data sources.

Source	**Period of assessment**	**Number of landslides**	**Landslide area, km²**	**Landslide type**
Report by Ibatulin (2011)	1970s – 2014	67	22.0	Single failures
Report by Yerokhin (1999)	1956 – 1986	1532	n/a	Single and complex failures
Ministry tables	2002 – 2011	73	n/a	Single failures
Field mapping by GFZ (status 2014)	not dated	555	119.9	Single and complex failures
Visual interpretation	not dated	n/a	172.9	Complex failures
Automated detection	2009 – 2013	625	8.2	Single failures

detection from multi-temporal satellite imagery has made it possible to map systematically landslides of all sizes including the small ones. Visual image interpretation allows mapping complex landslide-affected areas of large spatial extent, although individual failures cannot be distinguished. Automated detection enables reliable identification of the spatial extent of single slope failures. The level of detail for the temporal information depends on the availability of satellite imagery, which determines the length of the time interval between the pre-event and post-event satellite images used for dating automatically detected slope failures. The most detailed temporal information (exact day of the failure) is provided by the report by Ibatulin (2011), although the landslide extents are imprecise. Results of visual interpretation of landslide-prone slopes from satellite images and the information from the report by Yerokhin (1999) contain no temporal information on landslide occurrence but document more landslides and a larger landslide-affected area than other sources. Thus, a trade-off between the inventory completeness, spatial and temporal information content can be observed. The integration of landslide information from multiple sources provides a way of improving the quality of the resulting inventory on these three aspects.

Fig. 2.6a shows the complete content of the multi-source landslide inventory for a 20 by 20 km^2 subset of the study area situated south of the Tar river and characterized by high recent landslide activity. The largest part of the mapped landslide area has been derived by visual interpretation of satellite remote sensing data in combination with field mapping (areas outlined in purple and filled in pink). Using the same combination of data sources, it has been possible to map selected large landslides contained in the report by Ibatulin (2011) in a spatially explicit way (landslides outlined in green). For these cases, the failure dates are known, all of them occurred before 2005. The areas outlined in red depict the landslide objects that have been automatically detected based on the multi-temporal RapidEye data available for the time period between 2009 and 2013. These objects include areas of fresh failures as well as areas of reactivation within previously active landslide-prone slopes.

In a second step, the total area which has been mapped as affected by landslides was derived and related to the spatial mapping units outlined in blue in Fig. 2.6a by calculating the landslide density as the ratio between the landslide-affected area and

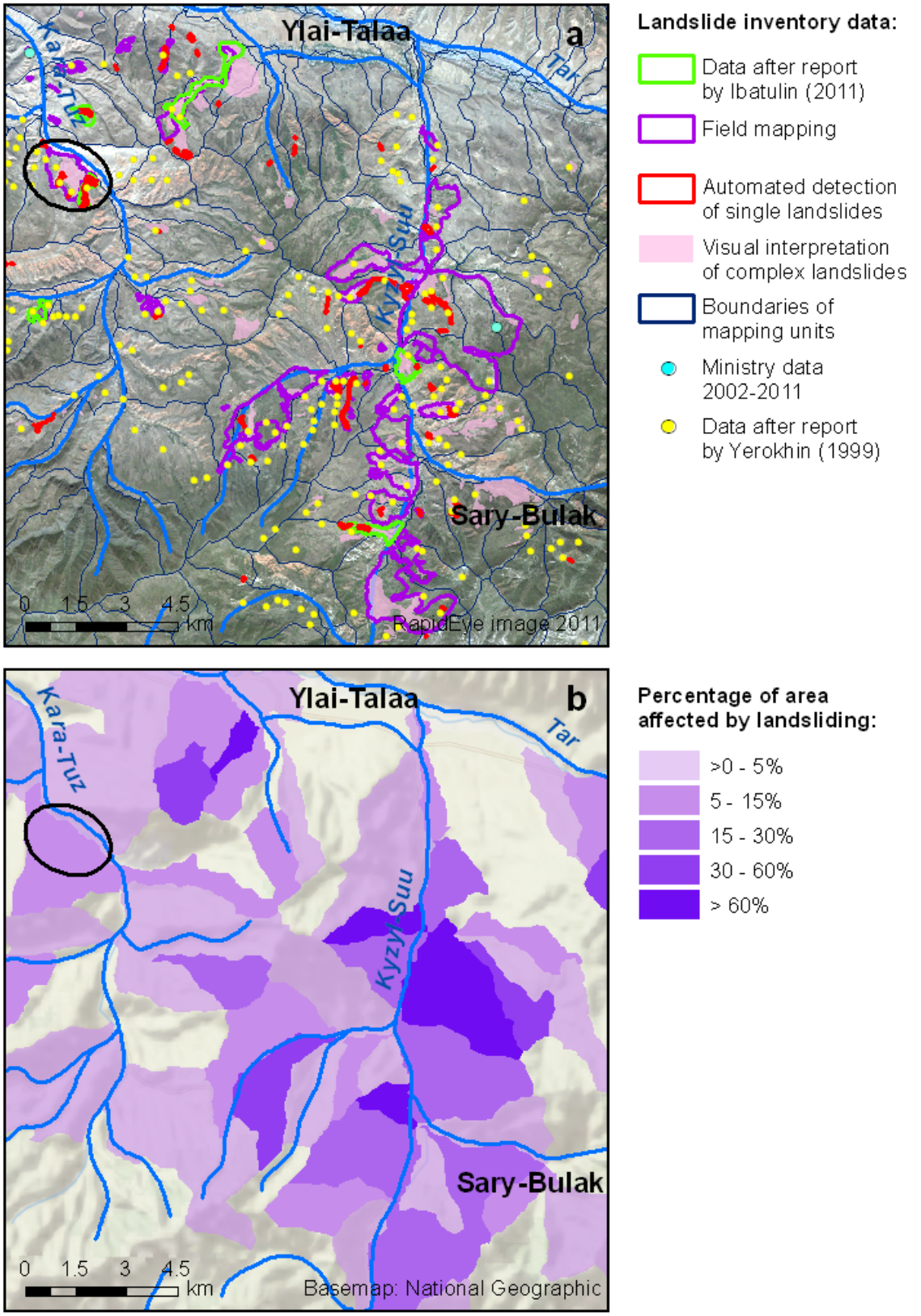

Figure 2.6: Results of multi-source landslide mapping: (a) according to available data sources, (b) percentage of landslide-affected area per spatial mapping unit calculated using data from report by Ibatulin (2011), field mapping, visual interpretation of satellite imagery and automated landslide detection. The black ellipse shows the position of the landslide-prone slope in the Kara-Tuz river valley used as example in the methodological description of section 3.

the total area of the respective mapping unit (Ghosh et al., 2012). The results shown in Fig. 2.6b indicate an especially high concentration of landslide-affected areas on the slopes along the Kara-Darya, Kyzyl-Suu and Kara-Unkyur river valleys. Overall, higher landslide densities can be observed for slopes of northern, northwestern and northeastern expositions. The use of a common spatial reference has enabled the detection of surface cover changes in a more precise way allowing the assessment of reactivations within an already known landslide complex. The precise spatial location of landslide-affected areas within a slope unit indicates the potential for the continuation of landslide activity within that slope unit. In the case of the landslide in the Kara-Tuz river valley, mass wasting has not affected the upper part of the slope unit yet, and that landslide activity may advance towards the watershed.

Although multiple sources of data on landslides have been used, each of them only provides information on a subset of the slope failures that have occurred in the study area. The degree of completeness varies depending on the examined period of time and the available data sources. Visual interpretation and automated landslide analysis based on satellite imagery allows the systematic detection of landslides independently of their proximity to settlements, whereas the completeness depends on their detectability in the image data and the temporal sequence of the imagery. However, due to the limited temporal resolution of the satellite imagery before the availability of multi-temporal RapidEye data, temporal information derived from satellite remote sensing data represents longer periods of occurrence ranging from several months to several years.

In contrast, the report by Ibatulin (2011) contains temporally explicit information on failure dates exceeding the time span which is covered by satellite remote sensing data. In case of failures that occurred before 1990, it represents the only source of temporal information on landslide events unless they have been documented otherwise. However, this information lacks explicit spatial reference and most of it has been acquired in the vicinity of settlements. Such explicit spatial information and extent of slope failures can be derived from remote sensing data, whereas the resulting accuracy is highest if the satellite imagery was acquired shortly after the occurrence of the failure. However, visual interpretation of satellite remote sensing data also allows mapping of older landslides which already have experienced several stages of revegetation and in parts have been affected by subsequent reactivations. In fact, this is the only way of mapping old landslides that had failed even before the start of landslide observations in the study area. Due to the use of the results of visual interpretation of satellite imagery, the resulting multi-source inventory combines features of both multi-temporal and historical landslide inventory mapping. The resulting spatially explicit assessment of landslide-affected areas can be used for subsequent GIS-based landslide susceptibility mapping.

2.5 Conclusions and Outlook

In this paper, we have demonstrated the use of remote sensing and GIS technologies for the development of a landslide inventory information system which is capable of integrating multi-source information on landslide activity for the study area in Southern Kyrgyzstan. Special attention has been paid to spatially explicit landslide mapping and to the temporal dimension of landslide information. In this study

area, satellite remote sensing data represent a valuable source of spatial and temporal information on landslide activity. Visual interpretation is especially suitable for mapping complex slope failures. Automated analysis allows the detection of single landslide events in an object-based form for the most recent period of time. Since none of the used sources is capable of providing a complete inventory, the combination of all of them has been required in order to derive a comprehensive landslide inventory. In this context, GIS-based data integration including homogenization and evaluation played an important role in the derivation of consistent and reliable multi-temporal information, which can be used in subsequent susceptibility and hazard analysis.

Moreover, multi-temporal satellite remote sensing data have been used as spatial reference information for establishing the multi-source GIS database since they are available in high spatial resolution and consistency for the complete study area. GIS technologies have also enabled efficient customized data access and joint processing in order to prepare all available information for subsequent landslide hazard assessment. For this purpose, a QGIS plugin is under development. Future work will focus on the development of GIS-based methods for susceptibility and hazard assessment which are capable of accommodating the spatially and temporally differentiated input information into the analysis including the results of ongoing monitoring of landslide activity in this area. In this context, special attention will be paid to the spatio-temporal assessment of landslide triggering factors, such as precipitation and seismicity in their relation to landslide activity.

Acknowledgements

Research presented in this paper has been funded by the German Ministry of Research and Technology (BMBF) as a part of the Tien Shan âĂŞ Pamir Monitoring Program (TIPTIMON) and PROGRESS projects. We kindly thank our colleagues from the Ministry of Emergency Situations of Kyrgyzstan K.V. Ibatulin and A.K. Sarnogoev for providing information on landslide activity in the region and joint field work. We are grateful to developers of open-source GIS and providers of free-of-cost geodata.

Chapter 3

Automated Derivation and Analysis of Landslide Attributes

Automated derivation and spatio-temporal analysis of landslide properties in southern Kyrgyzstan

Darya Golovko, Sigrid Roessner, Robert Behling, Birgit Kleinschmit

Originally published in Natural Hazards (2017), 85, 1461-1488
https://doi.org/10.1007/s11069-016-2636-y

Abstract

The study area located in southern Kyrgyzstan is affected by high and ongoing landslide activity. To characterize this activity, a multi-temporal landslide inventory containing over 2 800 landslide polygons was generated from multiple data sources. The latter include the results of automated landslide detection from multi-temporal satellite imagery. The polygonal representation of the landslides allows for characterization of the landslide geometry and determination of further landslide attributes in a way that accounts for the diversity of conditions within the landslide, e.g., at the landslide main scarp opposed to its toe. To perform such analyses, a methodology for efficient GIS (geographic information system)-based attribute derivation was developed, which includes both standard and customized GIS tools. We derived a number of landslide attributes, including area, length, compactness, slope, aspect, distance to stream and geology. The distributions of these attributes were analyzed to obtain a better understanding of landslide properties in the study area as a preliminary step for probabilistic landslide hazard assessment. The obtained spatial and temporal attribute variations were linked to differences in the environmental characteristics within the study area, in which the geological setting proved to be the most important differentiating factor. Moreover, a significant influence of the different data sources on the distribution of the landslide attribute values was found, indicating the importance of a critical evaluation of the landslide data to be used in landslide hazard assessments.

3.1 Introduction

Landslide inventories are an essential element of landslide hazard assessments. They are the basis for calculating the spatial, temporal and magnitude probabilities of landsliding (Guzzetti et al., 2005). A landslide inventory is a systematic record of landslide activity in a specific area that details the locations and dates of landslides, as well as other attributes that vary from study to study, e.g., landslide length, width, lithological properties, type, stage of activity, and so forth.

A substantial number of publications use landslide inventories to assess landslide susceptibility (e.g. Legorreta Paulín et al., 2016; Su et al., 2015; Mancini et al., 2010), to calculate the temporal probability of landslide occurrence (e.g., Corominas and Moya, 2008; Guzzetti et al., 2005) or to characterize the influence of triggering events (e.g., large earthquakes and intense rainstorms) on landslide formation (e.g., Malamud et al., 2004; Gorum et al., 2011; Hovius et al., 2011). Such studies generally concentrate on the location and extent of landslides, dates of their (re)activation and their area and/or volume. Geo-environmental attributes, when included, are typically assigned to mapping units that cover the entire study area rather than to individual landslides. However, the attributes of individual landslides are valuable in the analysis of landslide geometry (e.g., for runout modeling), in the determination of landslide types (Van Westen et al., 2008; Costanzo et al., 2012), as a preparatory step for susceptibility modeling, in the model interpretation and in the indirect evaluation of the inventory completeness (Trigila et al., 2010).

Landslide attributes are often determined through field-based investigations or

by visual interpretation of remote sensing data (e.g., Longoni et al., 2014; Ghosh et al., 2011; Tang et al., 2016). In such cases, field observations and expert judgment are used to determine a relatively large number of attributes for a comparatively low number of landslides in an area of limited size. However, these techniques cannot readily be adopted for large regional inventories. Such inventories have become more widespread due to the broader availability of suitable satellite imagery, which allowed for the introduction of (semi-)automated methods for inventory generation (e.g., Martha et al., 2013; Mondini et al., 2013). In this study, we determine the attributes of individual landslides contained in a multi-temporal, multi-source inventory featuring over 2 800 landslide polygons for a study area in southern Kyrgyzstan (Golovko et al., 2015) that covers more than 12 000 km^2. A large portion of the inventory was automatically generated from multi-temporal optical satellite imagery (Behling et al., 2014b, 2016). Automated landslide detection makes it possible to efficiently update the inventory whenever new satellite images become available. Each time that the inventory is updated, it is necessary to determine the attributes of the newly included landslides.

For this purpose, efficient (semi-)automated methods of attribute derivation are needed. However, to our knowledge, a systematic methodology for attribute derivation has not yet been developed. In this study, we use pre-existing and newly implemented GIS tools and remote sensing data to automate the process of attribute derivation and make it more objective than manual determination. Because the inventory was compiled from multiple sources of landslide information, we also compare the quality of the different sources and evaluate the effect of the data collection method on the distribution of landslide attribute values. Finally, we analyze the spatial and temporal differentiation of landslide properties. This is the first multi-temporal landslide inventory for the study area that represents landslides with polygons. In a substantial part of the inventory, the polygons reflect the spatial extent of a single slope failure at a particular point in time. Such representation is rare for inventories with several thousands of landslides, particularly for data-scarce regions such as southern Kyrgyzstan. This detailed multi-temporal landslide inventory enables landslide analyses that were not previously possible, such as a systematic multi-temporal study of the geometric parameters of the landslides. The developed methodology is especially suitable for improving the knowledge of landslides in areas with limited and heterogeneous spatial data availability. In principle, this methodology can be applied in any landslide-prone region of the world.

3.2 Study area

The study area is located in southern Kyrgyzstan at the eastern rim of the Fergana basin at the foothills of the Tian Shan (Fig. 3.1). The region experienced two major folding stages: the Hercynian and Neotectonic orogeny. The oldest and highest structures are composed of igneous and metamorphic rocks of the Proterozoic and Paleozoic. They encircle the intramountain Fergana basin. At elevations below 2200 m a. s. l., these consolidated cores are overlaid by Jurassic–Oligocene formations, which consist of folded layers of clays, argillites, sandstones, limestones, marls, gypsum and conglomerates (Havenith et al., 2009). The folding decreases the stability of these structures, and the alternating permeable and impermeable layers

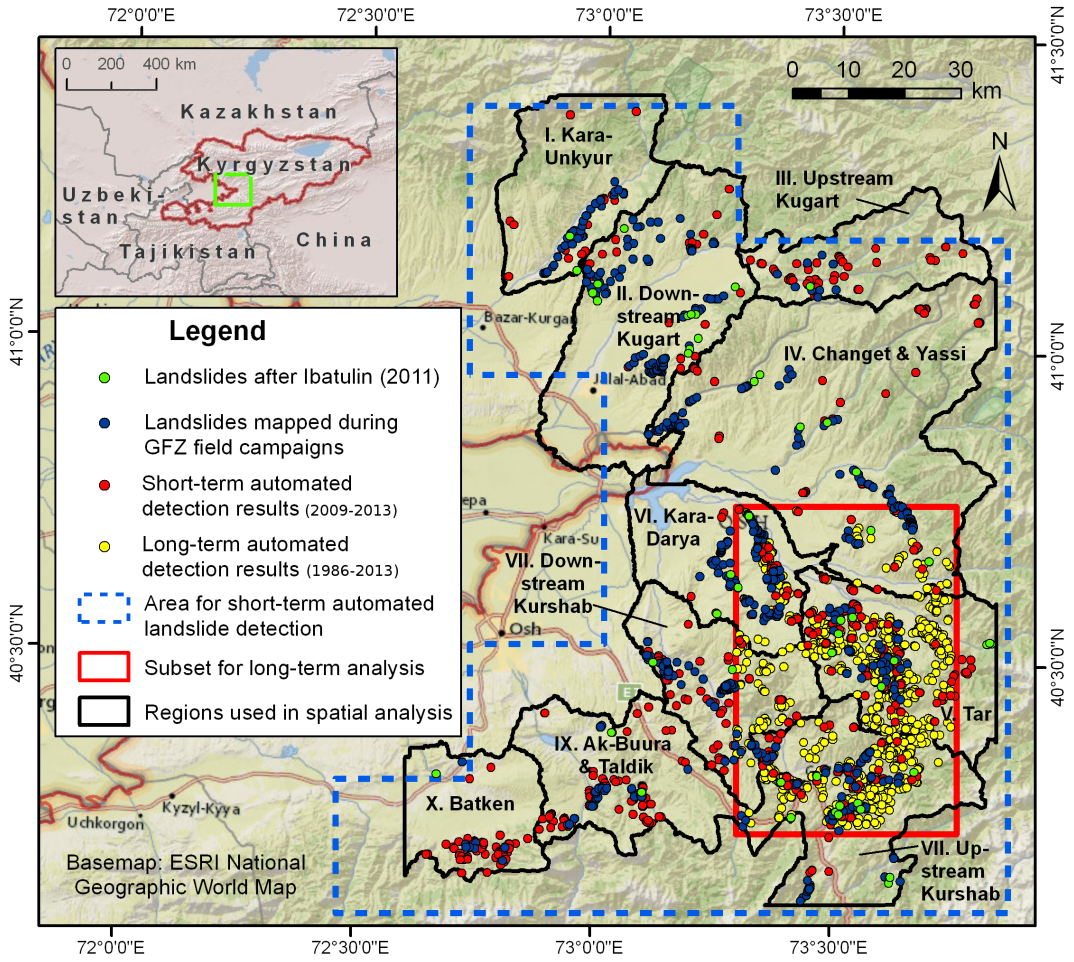

Figure 3.1: Study area in southern Kyrgyzstan and locations of the landslides contained in the multi-source inventory

in the folds create favorable conditions for water accumulation and the formation of sliding surfaces. Quaternary loesses of varying thickness cover these units. The core of the basin is occupied by younger unfolded structures (Wetzel et al., 2000). The lithological composition of the stratigraphic units is shown in Tab. 3.1.

Large rotational and translational slides in the areas of Jurassic–Oligocene folded sedimentary rocks have affected settlements and infrastructure the most. Landslides in massive Quaternary loess units are particularly dangerous due to their rapid avalanche-like movements. They combine rotational and dry flow movement with long runout zones and are most common in the northern part of the study area, where loess deposits reach their maximum thickness (Roessner et al., 2005). Some of these landslides are part of large deep-seated slope deformations (Bedoui et al., 2009; Lebourg et al., 2014; Zerathe and Lebourg, 2012) that experience persistent and very slow movements in their core part, whereas the Quaternary loess cover on top is subjected to faster and discrete slope failures. The less abundant slope failures in basement units occur predominantly in the form of shallow landslides. Large rockfalls are present in the vicinity of faults. The Upper Neogene and Lower Quaternary sediments are rarely affected by landslides. They are composed of conglomerates and weakly consolidated gravels with interbedded loess-like loams. These deposits are more stable due to their high porosity and permeability (Wetzel et al., 2000).

Table 3.1: Lithological units in the study area (following Roessner et al. (2006))

Geological period	**Abbreviation**	**Lithological units**
Upper Quaternary	Q3-Q4	alluvial sediments, glacial moraines, loesses
Middle Quaternary	Q2	glacial moraines, loesses, alluvial sediments
Lower Quaternary	Q1	gray conglomerates, loesses
Tertiary: Neogene (Pliocene)	N2	conglomerates, gravels, loess-type loams
Tertiary: Paleogene (Oligocene) - Neogene (Miocene)	PG3-N1	red sandstone, conglomerates, clays
Tertiary: Paleogene (Lower Eocene - Oligocene)	PG1-PG2	sandstones, gypsolytes, limestones, marls, clays, aleurolites
Upper Cretaceous (Cenomanian) - Paleogene (Lower Eocene)	CR1-CR2	red sandstone, conglomerates, gravels, gypsolytes, limestones, clays, aleurolites
Jurassic	J1-J3	sandstones, aleurolites, slates
Basement units	Basement	metamorphic and igneous rocks

The major faults in the study area are the Madin-Taldi-Suu, Aldiyar, South-Nookat, North- and South-Kuvin fault systems (Feld et al., 2015; Lemzin, 2005). Areas where the major faults converge are particularly landslide prone, e.g., the slope southeast of the town of Uzgen. The study area is subjected to high and ongoing tectonic activity expressed by frequent but relatively low-magnitude earthquakes (Haberland et al., 2011).

The study area is characterized by increased precipitation levels compared to the territories situated further east due to the function of the Tian Shan as an orographic barrier. Snow cover is typically established in the winter months with significant annual variations (Ibatulin, 2011). Monthly precipitation levels reach their maximum in March with a second peak in November (Torgoev et al., 2010). The precipitation maximum in March often coincides with the onset of snowmelt further increasing surface water infiltration into the ground. This leads to an increase in groundwater levels as one of the major factors for the onset of deep-seated slope failures, which represent the main type of landslides in the study area.

The temporal relationships between the occurrence of landslides in the region and variations in the hydrometeorological and seismic conditions are complex. Well-defined single triggering events are not typical for the region. Rather, the onset of slope failures is caused by the cumulative effect of these factors over prolonged periods of time (Danneels et al., 2008) and their interaction with predisposing factors, such as the lithological and tectonic structures. Most landslides occur in the months from March to May as a result of snowmelt and increased precipitation during this period (Torgoev et al., 2010). Significant variations in the process intensity over the years have been observed, which have been linked to differences in the amount of winter precipitation and the specific characteristics of snow accumulation (Ibatulin, 2011; Torgoev et al., 2010).

The interrelations between these factors and the mechanisms of landslide initiation in the region have not yet been sufficiently determined. Therefore, precise spatio-temporal information on landslide occurrence is important for a better understanding of the complex mechanisms for the onset of slope failures in this region.

Table 3.2: Landslide data sources

Source	Number of landslides	Landslide area, km^2
Data after Ibatulin (2011)	63	20.8
Field mapping by GFZ	554	119.7
Automated detection 2009-2013	624	8.2
Automated detection 1986-2013 for a subset of study area	1583	33.2

3.3 Landslide inventory maps

In Kyrgyzstan, slope failures result in numerous casualties and economic losses. From 1973-2010, landslides in southern Kyrgyzstan caused 211 fatalities (Ibatulin, 2011). The local Ministry for Emergency Situations (MES) has been conducting landslide investigations in this region since the 1950s. These investigations include repeated field surveys of known landslide-prone slopes and landslide catalogization efforts, e.g., Yerokhin (1999); Ibatulin (2011), and in recent years, field landslide mapping in selected districts by the Central-Asian Institute for Applied Geosciences (CAIAG). These records provide valuable insights into the properties of landsliding in the region. However, they represent an approach that relies on field investigations and expert knowledge. Moreover, the investigations of the MES have been conducted for the purpose of disaster mitigation and have thus been limited to parts of the study area with a risk to the population and infrastructure. Furthermore, no regular landslide monitoring has been conducted in the region since 1991 due to the lack of funding following the collapse of the former Soviet Union; consequently, the completeness of the landslide record varies considerably for different periods. An objective and comprehensive landslide mapping with a uniform coverage for the entire study area has not yet been performed. To address these issues, we have compiled a more comprehensive inventory that combines archive information, field mapping and the identification of landslides in satellite images. The inventory consists of four components, which are presented in Tab. 3.2.

The first component is based on the report by Ibatulin (2011), which verbally describes a small number of particularly large, destructive or otherwise remarkable landslides in the study area. The report is a result of 40-year-long landslide investigations by the MES. It specifies the dates of most recorded landslide events as precisely as the day of the failure. Additional effort was necessary to transfer these textual descriptions into spatial data in the form of polygons. A set of high-resolution satellite imagery (Behling et al., 2014b), topographic maps and field visits were useful in this process. Often, the spatial extent of the landslides could only be determined approximately, particularly if a long time had passed since their failure. Despite the limited spatial accuracy, this data source provides the most precise information on the landslide failure dates.

The second inventory component, field mapping by GFZ, represents the result of regular visits to the study area by scientists from Section 1.4 of the GFZ German Research Centre for Geosciences since 1998. Most landslide polygons in this data source represent a cumulative effect of multiple slope failures without a differentiation of their failure dates and may include very old slope failures. The field mapping

results are complementary to the previous inventory component, i.e., landslides were not included in the field mapping dataset if they were already mapped after Ibatulin (2011). These two sources of landslide data together will henceforth be referred to as 'field-based sources' in this paper.

To obtain the third and fourth inventory components, an automated approach for the detection of landslides from time series of satellite images was developed by Behling et al. (2014a,b). A co-registered database of optical satellite imagery was created with a total of 729 images acquired in 1986-2013 by various satellites (Landsat, SPOT, ASTER, and RapidEye) with a spatial resolution ranging from 30 m for Landsat to 5 m for RapidEye (Behling et al., 2014b). The temporal resolution varies between six years at the beginning and several weeks at the end of the covered period, whereas at least yearly coverage is available since 1996 with a gap in 2006. A multi-temporal automated approach was applied to these images, which compares pixel NDVI values over time and detects typical landslide NDVI trajectories with an abrupt vegetation decrease at the time of the failure and slow revegetation afterward (Behling et al., 2014a, 2016). Whereas bi-temporal change detection enables the creation of event-based or seasonal inventories, the multi-temporal automated detection approach enables the creation of a multi-temporal inventory, which is more suitable for our study area. If multiple landslide events occur within the same slope and their bodies overlap, their extent can still be correctly determined if an image is available after each of these events.

This approach allows a high degree of spatial and temporal precision and completeness to be achieved and ensures an objective mapping method with equal consideration of the complete study area. The automated landslide detection has been performed (i) for the entire study area with high-resolution RapidEye images for the period of 2009-2013, resulting in 624 landslide polygons ('short-term automated landslide detection'), and (ii) for a subset of the study area using imagery from all sensors for the period of 1986-2013 with 1 583 detected slope failures ('long-term automated landslide detection'). The RapidEye images used for short-term detection that covered this subset were also included in the long-term detection (see Fig. 3.1).

The first (based on Ibatulin (2011)) and second (field mapping) inventory components reflect the conventional approach to landslide mapping based on expert knowledge. Because expert investigations are hardly possible after every single landslide event, at least some of the resulting landslide polygons may not coincide with the spatial extent of single events (Marc and Hovius, 2015). This problem is aggravated if the study area is large and/or difficult to access or if few resources are available for landslide mapping, as is the case in southern Kyrgyzstan. New automated approaches that use multi-temporal satellite imagery can delineate individual failures more accurately. The correspondence between the representation in the inventory and the actual spatial extent of landslide events is not always considered when landslide attributes are determined. The availability of data from different sources in this study makes it possible to compare the influence of the data acquisition method on the attribute values.

Fig. 3.2 shows a subset of the multi-source inventory for an area southwest of the village of Gulcha around the Budalyk river valley. Of all inventory components, the results of field mapping are characterized by particularly large areas affected by landsliding, but the dates of the failures are not specified. Conversely, the results

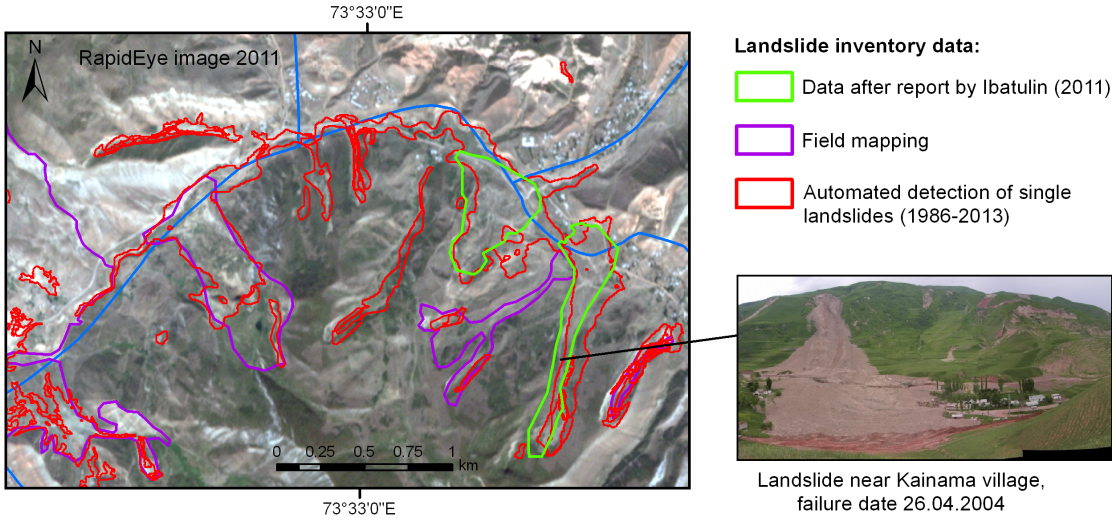

Figure 3.2: Landslides from various data sources for a subset of the study area in the Budalyk river valley and an example of a slope failure

of automated detection contain polygons of smaller sizes because they are able to delineate the spatial extent of a single slope failure and the period of its occurrence. Landslides digitized after Ibatulin (2011) are the least numerous, but their failure dates are documented with the highest temporal precision. These data sources supplement each other due to their different levels of spatial and temporal detail. The resulting multi-source inventory is the most extensive landslide record available for the study area in southern Kyrgyzstan. The representation of landslides in the form of polygons is important both for the more precise spatial localization of landslide objects and for conducting types of analysis that are not possible using point-based data.

3.4 Methods

Depending on the properties of the study area and research objectives, the list of attributes in a landslide inventory can vary (Wieczorek, 1984; Cruden and Varnes, 1996; Van Den Eeckhaut and Hervás, 2012; Xu, 2014; Schlögel et al., 2015; Pellicani and Spilotro, 2015). Attribute determination often relies on field visits and expert knowledge, which cannot be provided for the inventory with over 2 000 landslides. Rather, we use an automated GIS-based approach to derive selected attributes that characterize landslide geometry and geo-environmental properties.

Our approach combines standard and customized (newly implemented) GIS functionality described in the following subsections. Standard GIS procedures were performed using the tools of the proprietary ArcGIS 10.0 and open-source QGIS 2.8 software packages. The customized functionality required for some of the attributes was implemented in the Python programming language as a QGIS plugin (QGIS Development Team, 2015).

For relief-related analyses, we use the freely available digital elevation data in the form of ASTER GDEM Version 2 (2011) with 30-meter resolution. Due to the predominantly treeless character of the vegetation in the study area, this digital

surface model can be used to represent the Earth's topography. A more detailed DEM would be desirable. However, because we aim at an automated approach that can efficiently calculate attributes for a large number of landslides in an inventory, we condone the imprecisions for smaller landslides. Furthermore, the proposed analysis can be conducted again with little additional effort as soon as more detailed digital elevation data become available for the study area, or it can be applied to a less data-scarce region where such a DEM is already available.

Because a lithological map in a sufficient spatial scale (1 : 250 000) is not available, we use the geological map because the geological formations contained in this map are characterized by specific lithological composition and behavior (see Tab. 3.1 for more details). The geological map is a result of a combination and expert reinterpretation of several scanned and georeferenced 1 : 200 000 paper maps, which were published in the Soviet Union prior to 1991. The representation of Quaternary units in this map is incomplete, which does not allow loesses (which are very important for landsliding) to be distinguished from other Quaternary deposits.

3.4.1 Geometrical landslide properties

Area and perimeter are common landslide attributes. They can easily be determined using the standard functionality of any GIS software. By contrast, the calculation of the length and width of a landslide polygon is more complex, despite the apparently simple concept of length and width. In the following subsections, we present our customized method for automated landslide length and width calculations and demonstrate how the length and width information can be further used to calculate the landslide compactness as an indirect indicator of the landslide movement type.

Landslide length and width

One of the methods for calculating the length and width of a complex polygon is to derive an enclosing ellipse and use the two axes of the ellipse as the polygon length and width (Burger and Burge, 2009). For landslide-related applications, this method may result in errors, particularly for rotational slides and small failures, when the width of a landslide is greater than or comparable to its length. Our approach is based on the fundamental property of gravitational mass movements to move down the slope. We combine landslide polygons with raster digital elevation data to derive the landslide length. This calculation method can be executed automatically for a large number of landslides.

In the first stage, the highest and lowest points are calculated for each landslide polygon (Fig. 3.3a). This is achieved using a combination of vector landslide data with raster digital elevation data. The DEM raster is clipped to the landslide polygon in question, and the center of the pixel with the highest or lowest elevation value is calculated.

In the second stage, a line ('length line') is drawn between these two points. If this line is completely inside the landslide polygon, then the algorithm stops, and the length of the line is considered to be the landslide length. Otherwise, new points need to be added recursively to the length line. In each recursive step, a

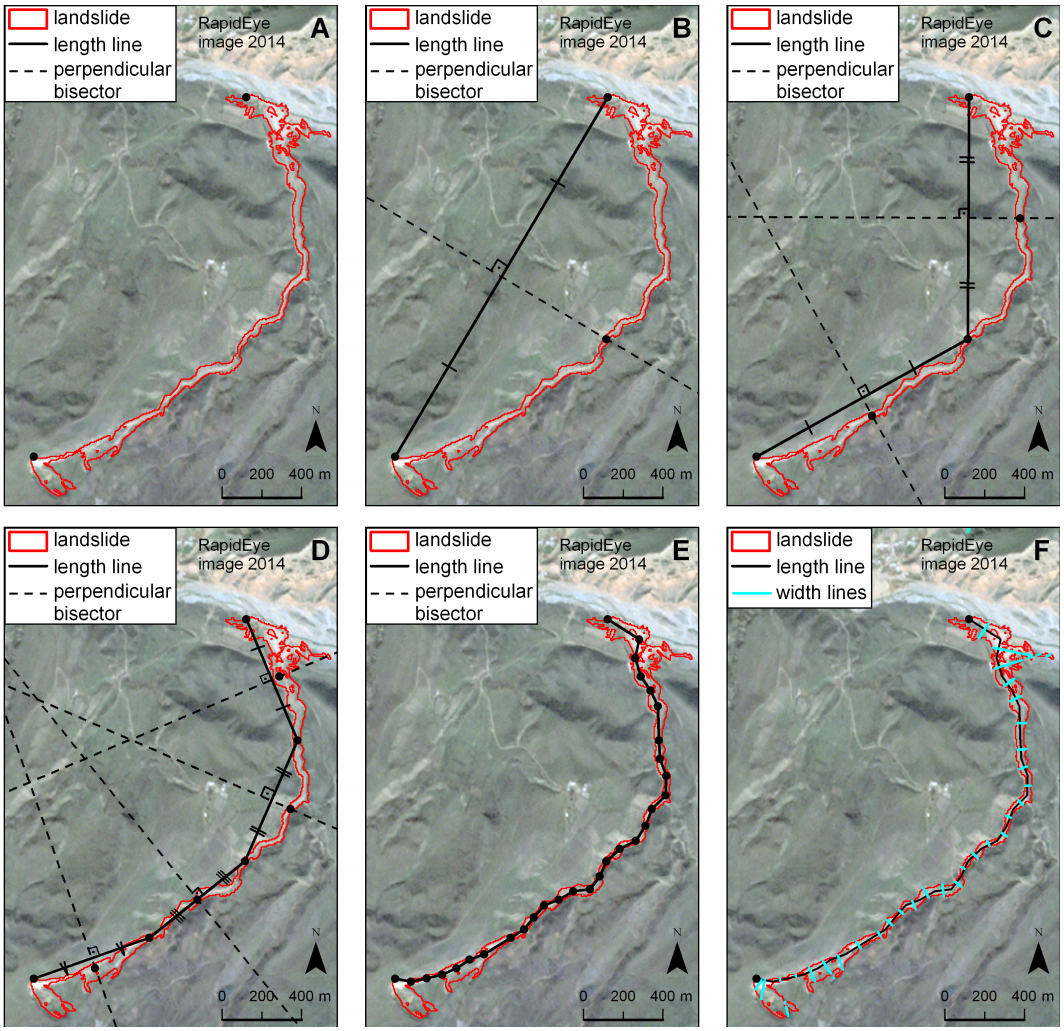

Figure 3.3: Approach for landslide length and width calculation: A - landslide polygon with its highest and lowest points; B - length line connecting the highest and lowest points, its perpendicular bisector and the new point in the middle of the intersection of the perpendicular bisector with the landslide polygon; C, D - the same procedure is performed with each new segment of the length line that is not completely inside the landslide polygon; E - final length line; and F - width lines calculated using perpendicular bisectors of the length line segments.

perpendicular bisector of the length line is constructed (Fig. 3.3b). A new point is added to the length line at the middle of the intersection of the perpendicular bisector with the landslide polygon. Each of the two new segments of the length line is then subjected to the same procedure, and new points are added until the complete length line is inside the landslide polygon (Fig. 3.3c-e).

The segments that result from the intersections of the perpendicular bisectors with the landslide polygon are used to determine the width of the landslide polygon at multiple positions (Fig. 3.3f). The mean, median, maximum, minimum and standard deviation values of all width segments associated with the same landslide are then recorded in the attribute table of the landslide shapefile to characterize the width of each landslide polygon as a whole.

Compactness

Compactness is a measure of how wide or narrow a landslide polygon is relative to its length. It also offers a way to indirectly describe the type of landslide movement. The movement type is often included as an attribute in landslide inventories. The most reliable approaches for determining compactness are field studies and expert judgment. However, the direct determination of the movement type for landslides detected using remote sensing is difficult. Furthermore, the large size of the inventory and its updatable character make expert evaluation a labor-intensive task, which is why an indirect inference on the landslide movement type from the landslide shape using the measure of compactness can be useful. In addition, the compactness value can point to the relationship between the landslide area, which is easy to derive in a GIS, and the landslide volume because more compact landslides tend to have larger volumes for the same area (Havenith et al., 2015).

A common approach for calculating the compactness of a polygon is the isoperimetric quotient Q (Osserman, 1978), also referred to as elongation factor (Havenith et al., 2015):

$$Q = \frac{4\pi A}{P^2}, \tag{3.1}$$

where A is the polygon area and P is the polygon perimeter. The quotient can have values in the range $(0, 1]$, with a value of 1 corresponding to the most compact shape, a circle, and lower values indicating less compact polygons.

However, using the isoperimetric quotient is problematic in the case of the multi-source inventory for southern Kyrgyzstan. This is because the landslides that were automatically detected from remote sensing imagery preserve their pixel-based zigzag boundaries, leading to substantially higher perimeter values that are incomparable to other sources of landslide data. Therefore, we have used the landslide length rather than the perimeter to calculate compactness:

$$C = \frac{A}{L^2}, \tag{3.2}$$

where A is the polygon area and L is the polygon length. In the general case, when the length is the most extended dimension of a polygon, the range of this function is $(0, 0.25\pi]$. In the present application, however, the landslide length is not necessarily the largest dimension of the landslide polygon; thus, the range of the compactness function is a right-open interval. Similar to the isoperimetric quotient, greater values indicate more compact landslides.

3.4.2 Geo-environmental landslide properties

Information on geo-environmental landslide properties is typically available in the form of vector or raster maps that cover territory beyond the extent of a single landslide. Therefore, the challenge in the process of determining geo-environmental landslide attributes for a polygon-based inventory is the transition from the terrain properties to the properties of a single landslide. A landslide inventory can encompass a variety of geo-environmental attributes. In this study, we derive four attributes of this group: slope, aspect, geology and distance to stream.

Landslide slope values are calculated as the mean of the slope values of all pixels that are within a landslide polygon. However, this approach is inapplicable for aspect. Aspect is an example of data on a circular scale. Thus, the addition and division of multiple aspect values ranging from 0° to 360° to find their mean is unreasonable. Rather, we classify the aspect raster into eight classes for each cardinal and intercardinal direction. Then, we use the 'majority' option of the zonal statistics function in ArcGIS, which adopts the value of the most frequent class as the aspect attribute of the landslide.

In this study, geology is available in the form of a vector map. A landslide polygon can intersect several geology classes; in fact, the succession of stratigraphic units along the slope is common for many slopes. Therefore, one is confronted with several potential geological classes for each landslide. A straightforward solution is to select the class that occupies the largest area within the landslide polygon. However, this approach can result in errors when the largest class is not representative of the conditions that led to the slope failure. Instead, we suggest using the landslide highest point (see Section 3.4.1) because the geological conditions at the landslide main scarp are crucial for the initiation of most landslides in the study area. This approach leads to a better representation of more rare classes, which might be absorbed into larger units when the maximum-area method is used.

To calculate the distance to stream for each landslide, we derived the stream network from the DEM using the standard GIS routine that involves the derivation of flow direction and flow accumulation. A 1 : 100 000 topographic map was used to correctly set the threshold on the flow accumulation raster and to differentiate stream pixels from non-stream pixels. Subsequently, the Euclidean distance between the landslide polygon and the stream was calculated using the ArcGIS tool 'Near'. For each landslide, this tool identifies two closest segments, one from the landslide polygon and one from the stream dataset, and calculates the shortest distance between them (ArcGIS Help, 2016).

3.5 Results

The attributes area, length, compactness, mean slope, dominant aspect, geology and distance to streams were successfully derived for the multi-source inventory. The length lines and values were manually corrected for some landslides. Most of them were very small or had complex geometries.

The attribute distributions were analyzed separately for each landslide data source to investigate the effect of the mapping method on the properties of the landslide inventory (Section 3.5.1). Furthermore, the degree of completeness was compared between the inventory components. In the second step, the spatial and temporal differentiation of the attributes was examined (Sections 3.5.2 and 3.5.3).

3.5.1 Variations of landslide properties by data source

The landslide properties differ depending on the source of the landslide data. Fig. 3.4 illustrates the differences in landslide sizes (areas). In our study, the automated

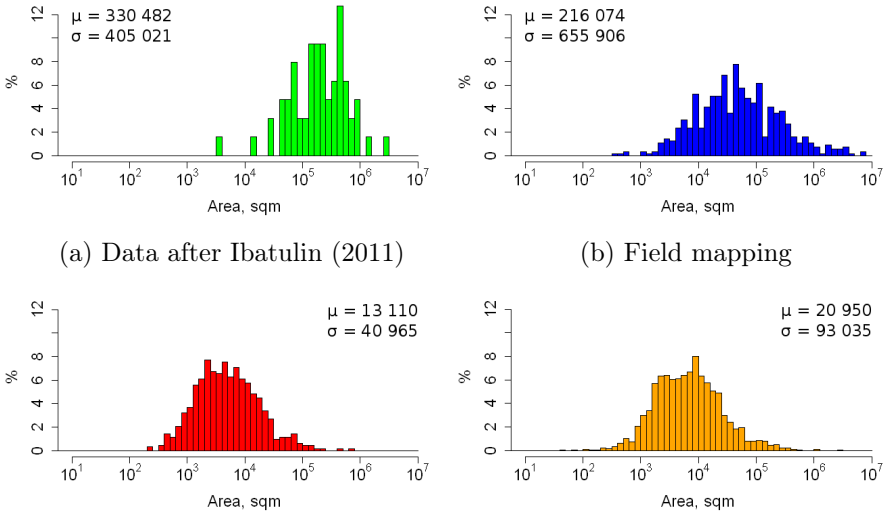

(a) Data after Ibatulin (2011)

(b) Field mapping

(c) Automated detection 2009-2013

(d) Automated detection 1986-2013

Figure 3.4: Distribution of landslide area values (decimal logarithm of landslide area) by landslide data source

detection results have the highest frequency on the logarithmic scale in the range of 10^3–10^4 m^2, whereas the two field-based data sources already exhibit a decrease at this size range. Thus, smaller landslides are underrepresented in the field-based sources. The histograms for both automatically derived datasets are similar, but smaller landslides are better represented by the automated detection results for 2009-2013. This is because the years 2009-2013 are characterized by relatively low landslide activity compared to the entire time period of the long-term analysis (1986-2013). The specific shape of the histogram for the long-term results with a peak around 10^4 m^2 is due to the lower resolution of satellite images in earlier years, which did not permit such an extensive mapping of small landslides as was possible in the more recent periods. Landslides after Ibatulin (2011) have a narrow distribution around larger sizes. Landslides mapped during the field campaigns include a wider range of sizes.

With this in mind, the distribution of further landslide attributes (Fig. 3.5) can be analyzed. The larger landslide complexes documented in the field-based data sources are characterized by greater lengths, gentler slopes, and their toes are located closer to streams. These tendencies are even stronger for the landslides mapped after Ibatulin (2011) than for the field mapping results. The distribution of compactness values does not exhibit significant differences between the data sources, which indicates the independence of the compactness calculation from the landslide mapping approach.

The distribution of landslides by geology class is similar for all landslide data sources. It is characterized by the prevalence of landslides within Cretaceous and Paleogene units (Fig. 3.6). Basement units and the unfolded Neogene platform sediments are less favorable for the development of landslides in the study area. A relative increase of landslides in the basement units is observed for the results of automated landslide detection in 2009-2013, which is due to the lower landslide activity in this period. This decrease in landslide activity was more significant for areas composed of weakly consolidated sediments than for the metamorphic

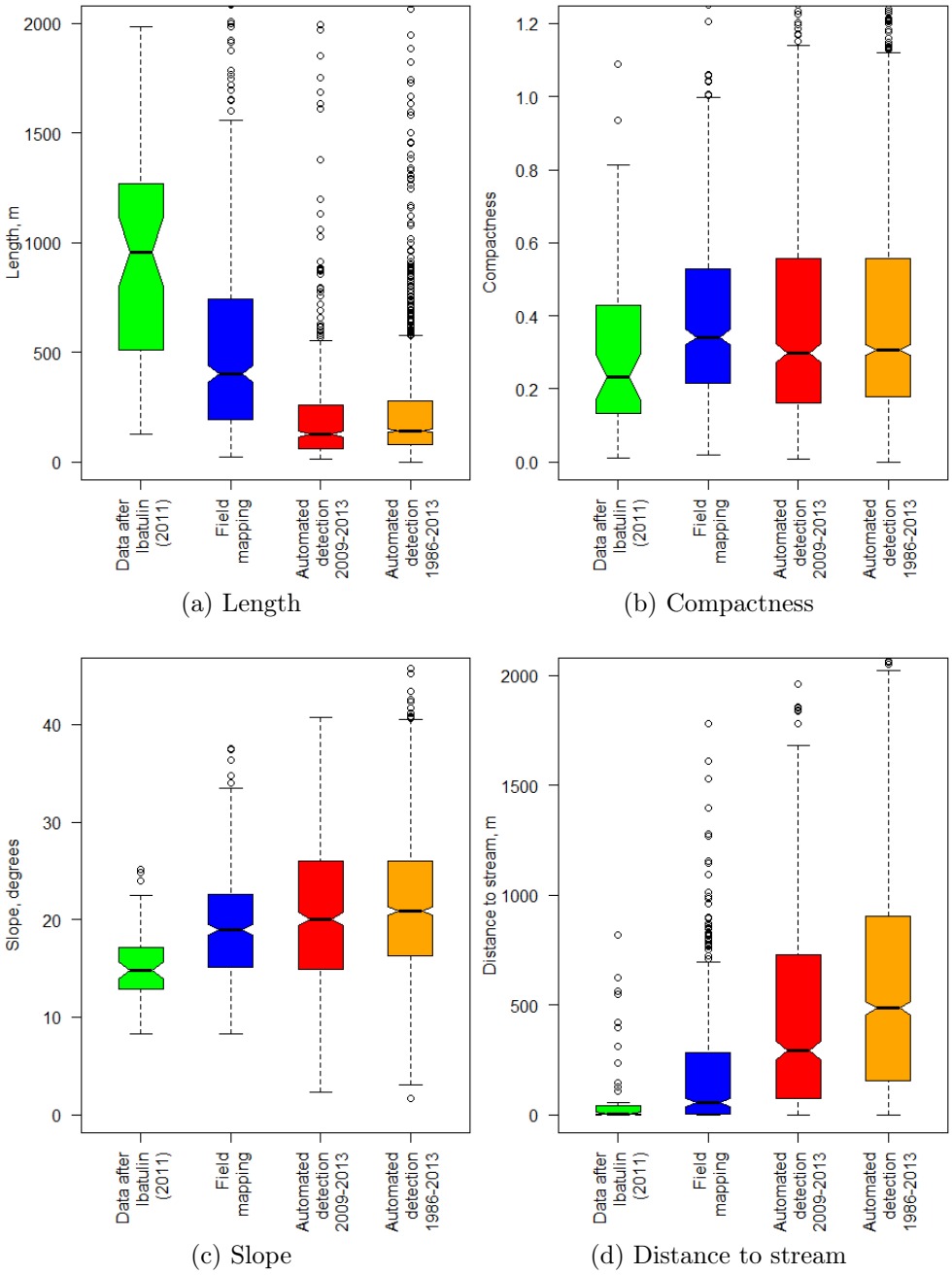

(a) Length (b) Compactness

(c) Slope (d) Distance to stream

Figure 3.5: Distribution of landslide attribute values by landslide data source

basement rocks. Furthermore, many landslide locations had not been mapped prior to the availability of the automated detection method, and this especially applies to landslides outside of the major landslide hotspots.

Fig. 3.7 shows the distribution of the landslides by aspect for each data source. For all the data sources, the landslide activity is higher on the northern, northwestern and northeastern slopes than on the southern, southwestern and southeastern slopes. The automated landslide detection results show the dominance of the northeastern aspect in the distribution of landslide areas. That is, large landslides particularly occur on northeastern slopes. This tendency is milder for landslides described in Ibatulin (2011), and the northwestern direction prevails for the field mapping results in terms of both number and area. An explanation for this phe-

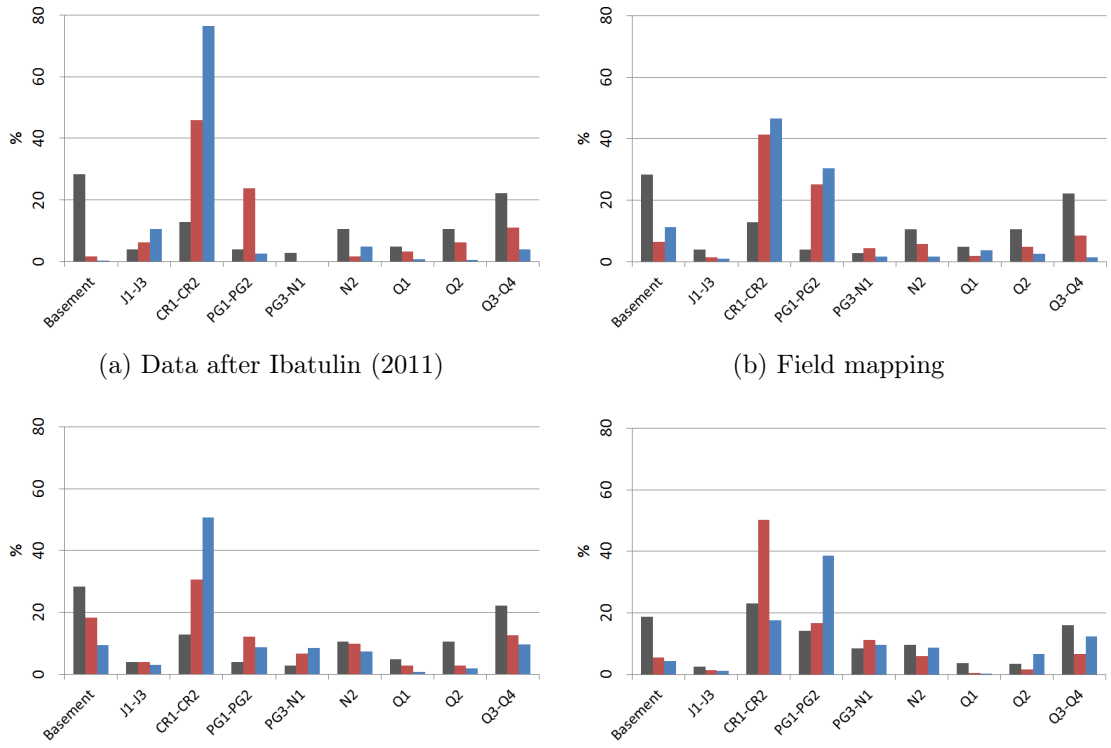

(a) Data after Ibatulin (2011)

(b) Field mapping

(c) Automated detection 2009-2013

(d) Automated detection 1986-2013

Figure 3.6: Landslide occurrence related to geology class by landslide data source (for lithological characterization of the geology classes, see Tab. 3.1). Red columns (in the middle) show landslide number, blue columns (on the right) show landslide area, and black columns (on the left) show the distribution of geology classes in the study area or in the study area subset.

nomenon is that the northern parts of the study area, particularly the regions of Kara-Unkyur and Downstream Kurshab with thick loess deposits, have experienced strong landslide activity since the start of landslide observations by the local authorities and especially during the very active year 1994. Due to the orientation of the river valleys and the patterns of loess accumulation in these regions, northwestern slopes have experienced the most landslides. In 2009-2013, however, no substantial landslide activity occurred in the northern part of the study area. Instead, the most important landslide hotspot in the period of regular satellite observations after 1998 was the slope southeast of the town of Uzgen. Because no settlements are located in the runout zone of this very active landslide complex, it received little attention from the local authorities compared to the magnitude of the landslide activity it experienced.

3.5.2 Spatial variations of landslide properties

Thus far, the landslide data have been examined by information source with no further differentiation. However, the study area in southern Kyrgyzstan is not homogeneous. For the spatially differentiated analysis, the study area was subdivided into ten regions based on natural watershed boundaries (Tab. 3.3). The spatial differentiation of landslide properties in the study area was analyzed using the au-

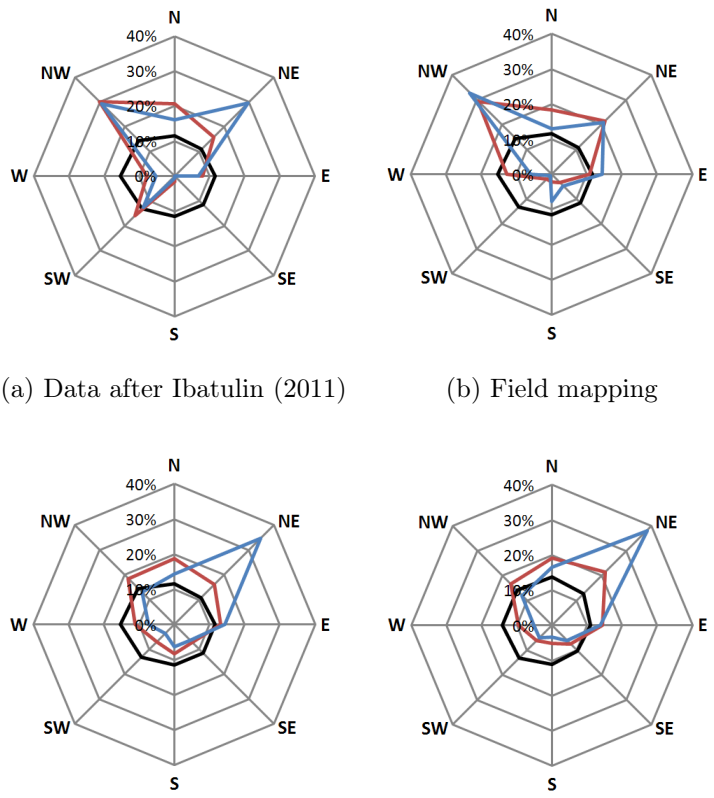

(a) Data after Ibatulin (2011)

(b) Field mapping

(c) Automated detection 2009-2013

(d) Automated detection 1986-2013

Figure 3.7: Distribution of aspect values for different landslide data sources. Red lines show landslide number, blue lines show landslide area, and black lines show the distribution of aspect classes in the study area or in the study area subset.

tomated detection results for the period 2009-2013 (624 landslides) because this dataset covers the study area in the most systematic way, regardless of how remote individual parts of it may be.

Table 3.3: Distribution of landslides by region and data source

№	Region	Number of landslides after Ibatulin (2011)	Number of landslides mapped in field	Number of landslides detected automatically (2009-2013)
I	Kara-Unkyur	2	40	22
II	Downstream Kugart	15	106	27
III	Upstream Kugart	1	9	49
IV	Changet and Yassi	8	92	55
V	Tar	12	39	101
VI	Kara-Darya	5	96	55
VII	Upstream Kurshab	12	76	81
VIII	Downstream Kurshab	2	56	63
IX	Ak-Buura and Taldik	5	33	99
X	Batken	1	8	72

An association between the dominant geology and aspect classes can be traced

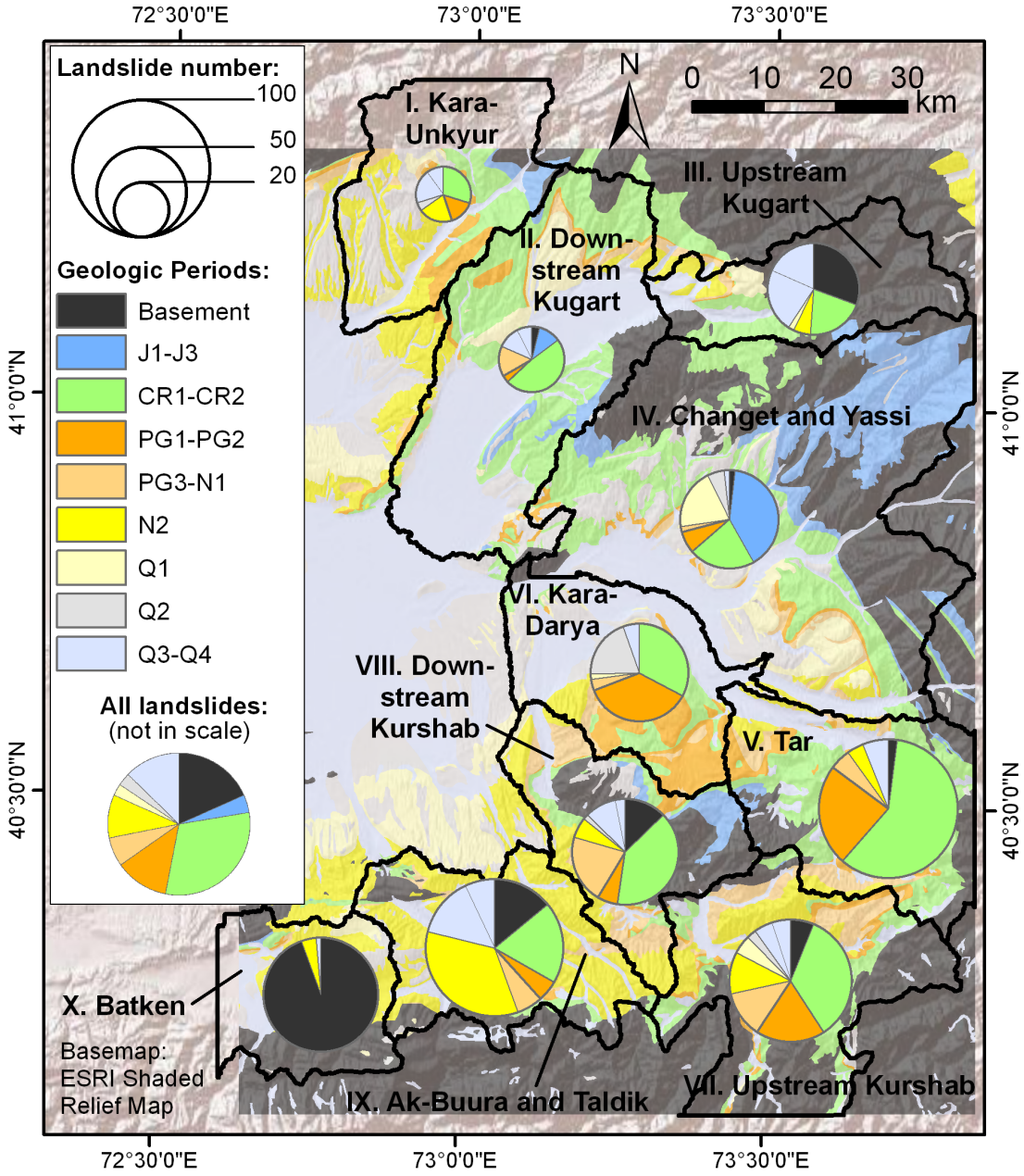

Figure 3.8: Landslide occurrence related to geology class by region (for lithological characterization of the geology classes, see Tab. 3.1)

over all the regions (Figs. 3.8 and 3.9). The prevalence of landslide-prone geological structures on particular sides of the river valleys often explains the dominating aspect values. For example, in the Kara-Unkyur valley, most landslides are located on the left river bank in folded Cretaceous and Paleogene deposits (in contrast to the right river bank composed of more stable unfolded sediments), and therefore, the northwestern landslide aspect is prevalent. The same is true for Downstream Kugart with its northwestern, western and eastern orientations of river valley sides with Cretaceous and Paleogene sediments. In Upstream Kugart, the northern and southern aspects are the most prominent, which reflects the course of the river from east to west at lower elevations, whereas the westward slopes in the higher upper part are composed of less landslide-prone basement rocks. In Downstream Kugart, the northwestern, northern and northeastern aspects are dominant due to the southern

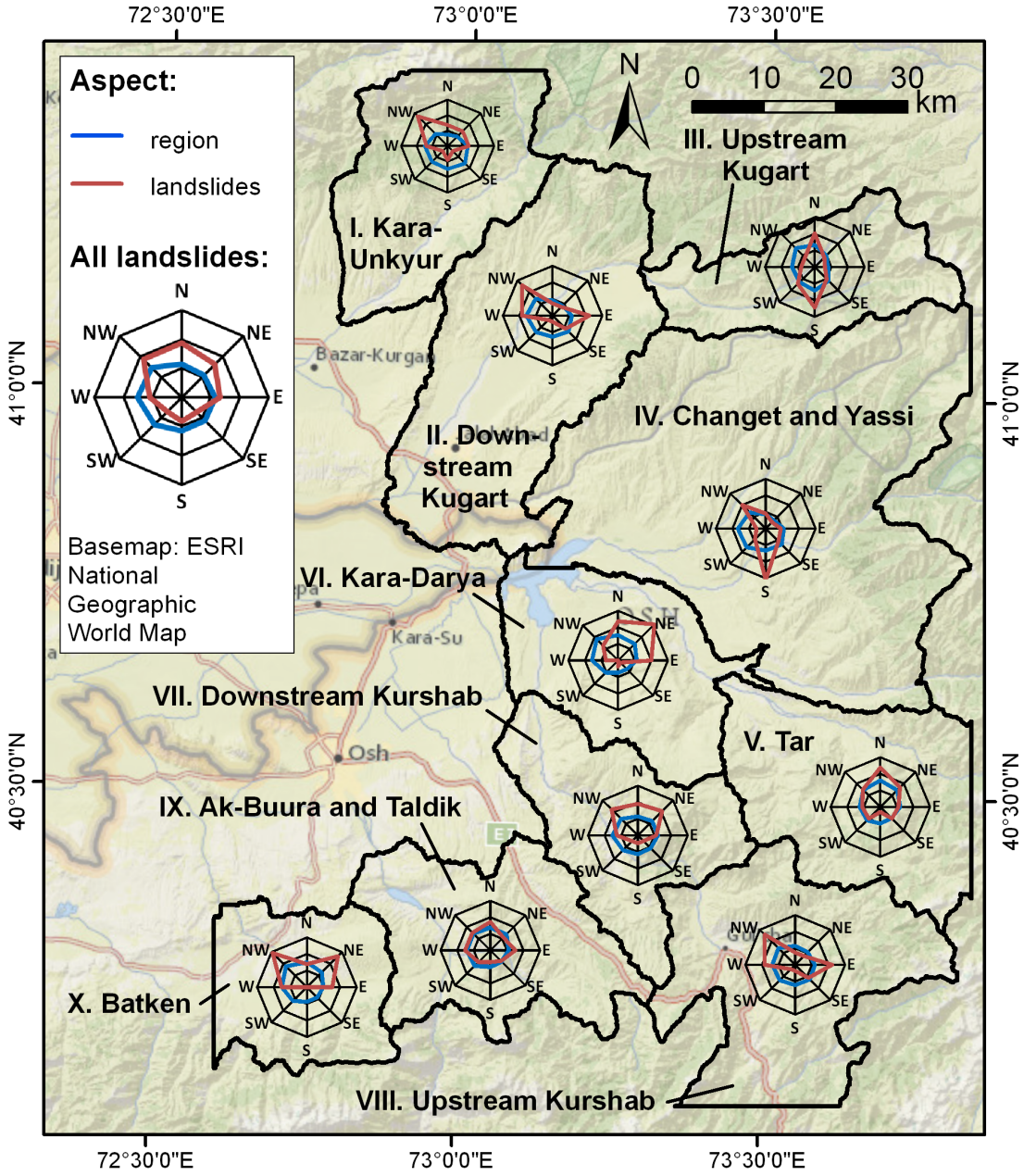

Figure 3.9: Distribution of landslide aspect values by region

orientation of the slopes with basement rocks. In Changet and Yassi, Kara-Darya, Upstream Kurshab, and Batken geology classes are distributed more or less evenly among the aspect classes; thus, the dominant aspect classes in the landslide data reflect the dominant orientations of the river valley sides. For the Tar and Ak-Buura and Taldik regions, landslides exhibit a similar distribution of aspect classes as the region as a whole with a slight tendency toward the north, which could be linked to more favorable conditions such as higher moisture and longer snow cover duration on north-facing slopes. The close association between aspect and geology values in these areas reveals that the structural setting is the dominant factor determining the spatial differences in landslide occurrence.

Some regions within the study area exhibit landslide characteristics that are comparable to those derived for the study area as a whole (Figs. 3.8, 3.9 and 3.10). Such regions are located at lower elevations and include downstream parts of the

basins of the principal rivers in the study area: Kara-Unkyur, Downstream Kugart and Downstream Kurshab. Landslides in the Kara-Darya and Tar regions differ from the study-area-wide averages only in their greater distance to streams due to the presence of landslide-prone slopes with high relative heights and reactivations in the upper slope parts.

Regions located in the upstream parts of the river basins differ more due to their geological composition. The Batken area in the southwest is particularly different: almost all landslides here develop in basement rocks and on steeper slopes than in other regions. The landslide processes here are dominated by shallow landsliding and debris flows. The large share of shallow landslides is reflected in their short length and compact shape. In fact, it is the inclusion of this region in the automated analysis that increases the share of landslides in basement units in the automated detection results for 2009-2013 (Fig. 3.6).

A feature of the Ak-Buura and Taldik regions is the abundance of landslides in Neogene rocks, which are not prone to landsliding in other parts of the study area. A possible explanation is the incomplete inclusion of Quaternary sediments in the geological map and the high tectonic activity, which leads to instabilities of slopes that are otherwise stable in other parts of the study area.

Upstream Kugart is well characterized by a higher share (approximately one third) of landslides in basement units. This region also exhibits particularly low distances to streams (Fig. 3.10e), which is because approximately 40% of the automatically detected landslides here are actually a result of the Kugart river and its tributaries undercutting the river banks. Furthermore, many landslides (at least a quarter) are reactivations within large old landslide complexes at a distance from the main scarp, which explains the tendency toward low slope values for landslides here.

The geological composition of the Upper Kurshab region is similar to the study area as a whole. However, the region exhibits the highest median value of the landslide length and the lowest median value of compactness, which points to the prevalence of flows in this region. This may be a result of steeper slopes, which are a manifestation of high tectonic activity.

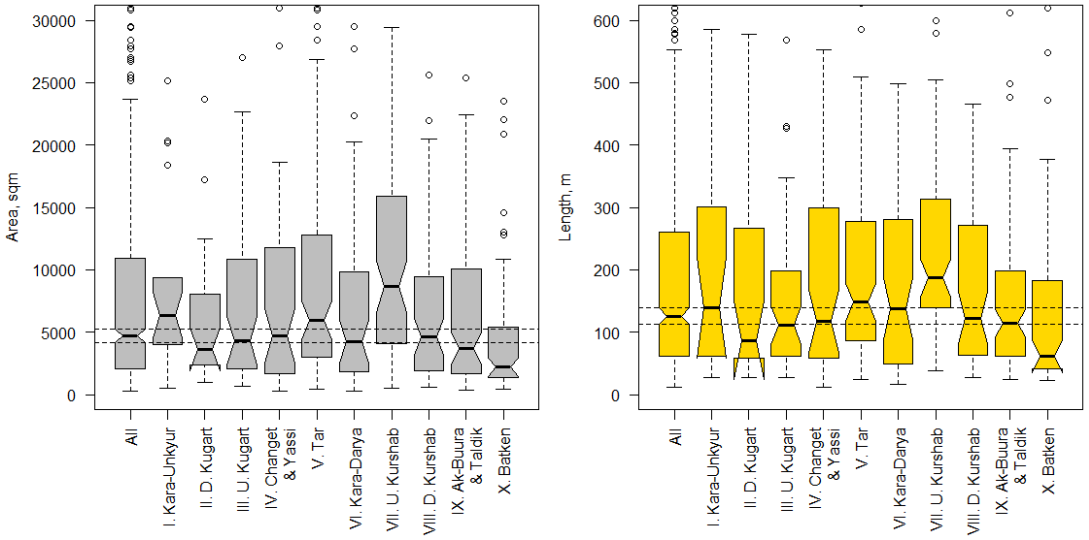

(a) Area

(b) Length

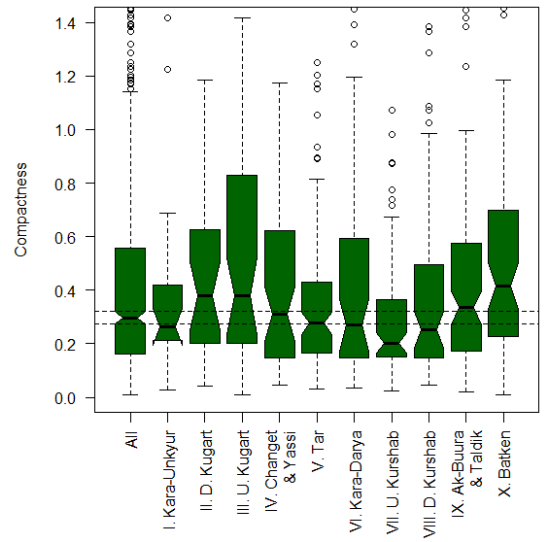

(c) Compactness

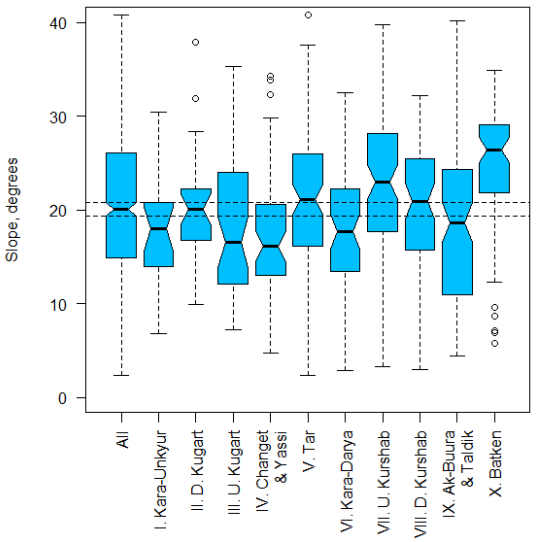

(d) Slope

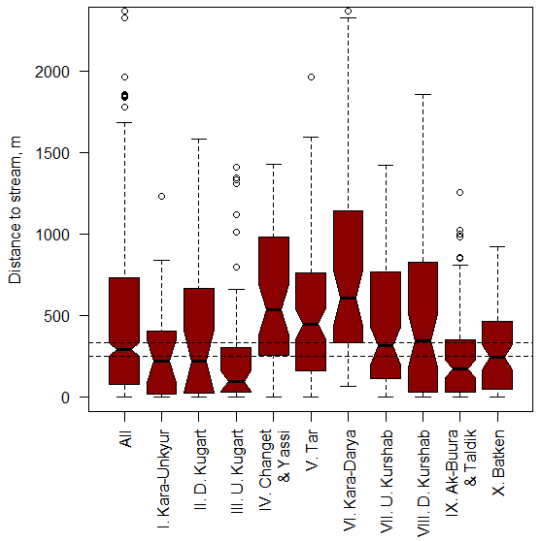

(e) Distance to stream

Figure 3.10: Distribution of landslide attribute values by region

Thus, the substantial differences in the attribute value distributions observed in some regions are mostly a result of the presence of different types of gravitational mass movement processes in these parts of the study area. Regions where the distributions of the attribute values are similar to those for the complete study area are characterized by larger landslides and higher landslide density. Differences in the geological composition of the territory play the dominant role in the variability of landslide properties between the regions. The systematic consideration of all parts of the study area in the process of automated landslide detection reveals the large variety of gravitational mass movement processes in the study area, which had not been fully considered before in the frame of the field-based landslide data sources. This once again highlights the subjectivity of these data sources and their focus on the identification of landslides in already known landslide hotspots of certain prevailing landslide types.

3.5.3 Temporal variations of landslide properties

To analyze the change of landslide properties over time, the automated detection results for the period 1986-2013 (1 583 landslides) were used. This analysis covers a 75x50 km large subset of the study area south of the Tar river (see Fig. 3.1). The landslides were divided into 11 periods based on the acquisition dates of the imagery used for the automated detection. This division (Tab. 3.4) was chosen because it can be applied to the complete subset of the study area while preserving most of the temporal detail for the landslide data. The boundaries of the 11 periods were chosen in summer or late spring such that the time of intensive landsliding during and after snowmelt fits completely within a single period.

Table 3.4: Landslide number and frequency by period

A	B	C	D	E	F
Period	**Length in years**	**Number of land-slides**	**Number of land-slides per year**	**Number of landslides with area A≥10 000 m²**	**Number of landslides per year with area A≥10 000 m²**
12.07.1986 – 02.06.1990	4	51	13	39	10
02.06.1990 – 11.08.1998	8	113	14	69	9
11.08.1998 – 08.06.2001	3	62	21	39	13
08.06.2001 – 14.06.2003	2	477	239	161	81
14.06.2003 – 16.06.2004	1	311	311	125	125
16.06.2004 – 05.07.2005	1	86	86	22	22
05.07.2005 – 25.06.2007	2	27	14	5	3
25.06.2007 – 17.05.2009	2	69	35	6	3
17.05.2009 – 14.05.2011	2	266	133	83	42
14.05.2011 – 24.05.2012	1	48	48	15	15
24.05.2012 – 08.06.2013	1	65	65	11	11

The breakdown of these 1 583 landslides by time periods is shown in Tab. 3.4. Due to the varying length of the time periods, the landslide numbers and frequencies were divided by the length of each period for better comparability in columns D and F. Eight landslides were assigned to no period because the time of their occurrence could only be determined with lower temporal resolution and thus corresponds to

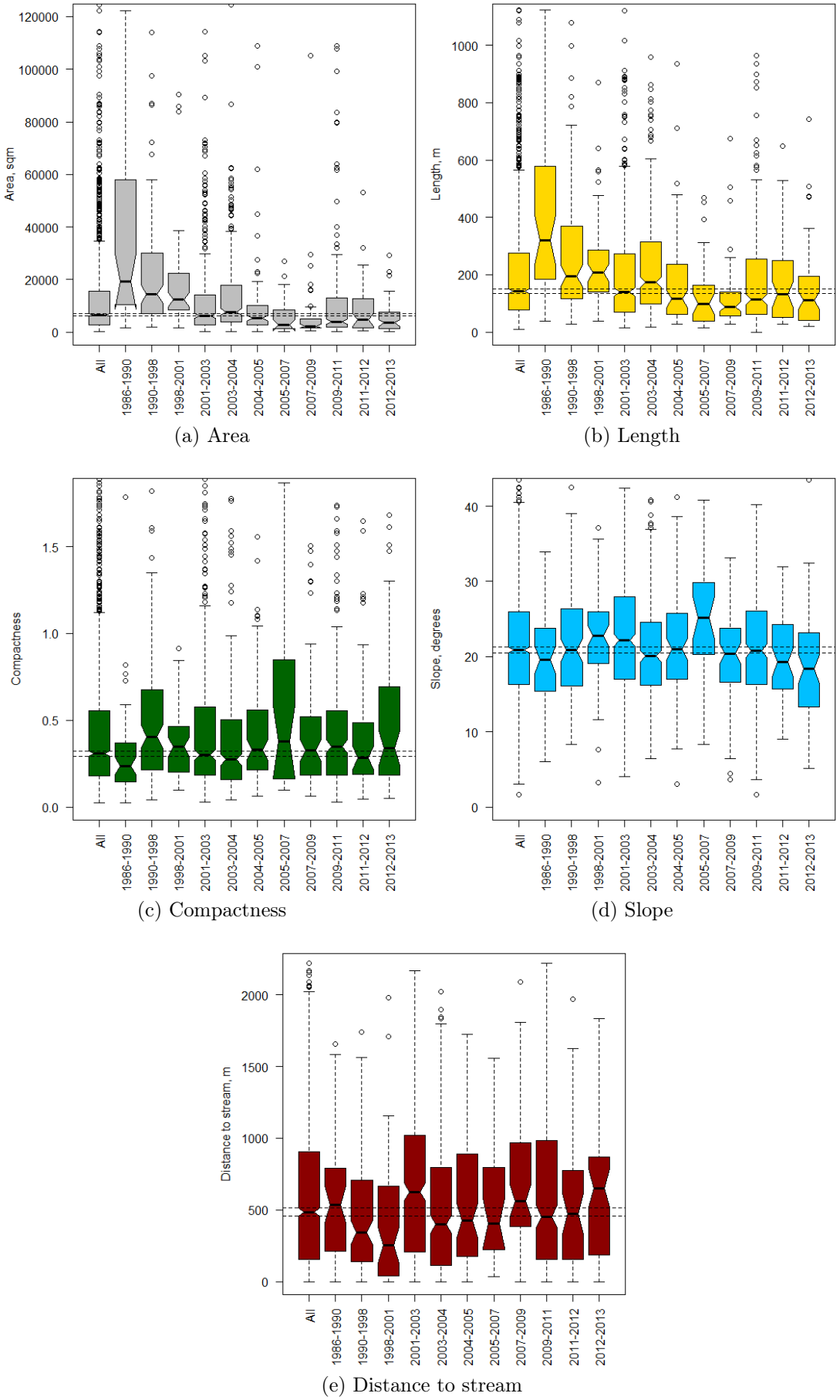

(a) Area

(b) Length

(c) Compactness

(d) Slope

(e) Distance to stream

Figure 3.11: Distribution of landslide attribute values by period

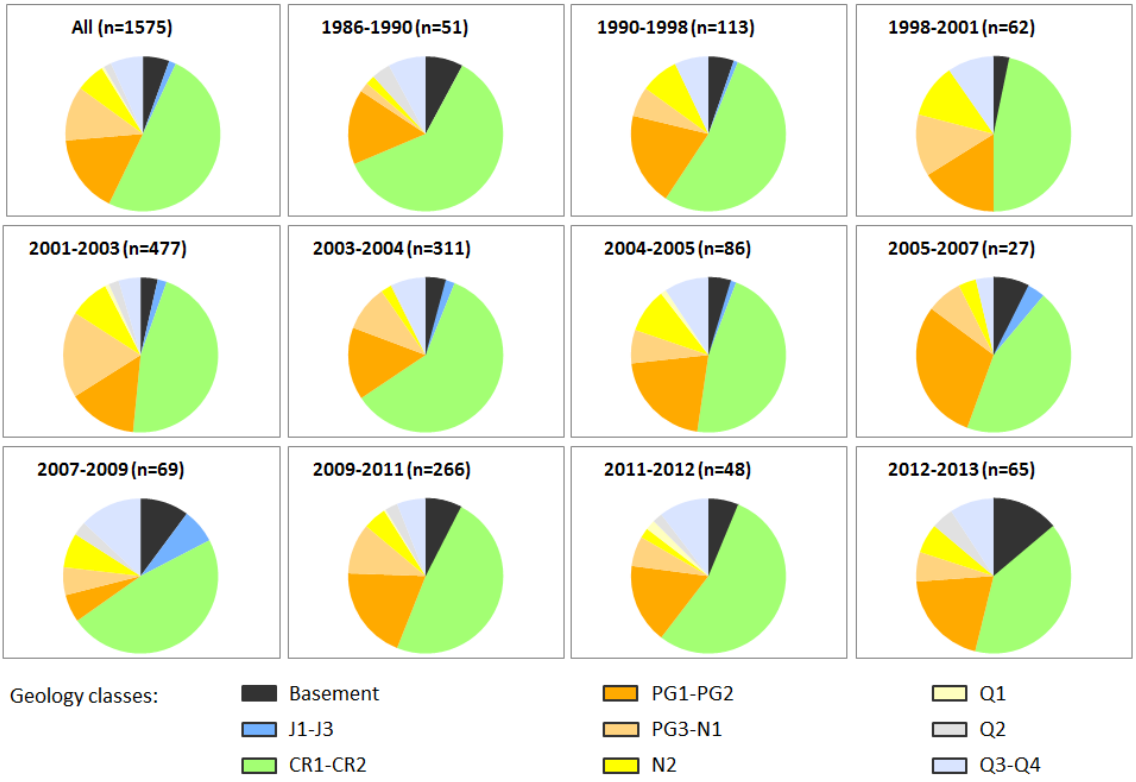

Figure 3.12: Landslide occurrence related to geology class by period (for lithological characterization of the geology classes, see Tab. 3.1)

multiple time periods. The peaks of landslide activity were in the periods 2001-2003 and 2003-2004, when the yearly landslides numbers were 4-5 times higher than the long-term average. These observations are consistent with the information of local experts (Torgoev et al., 2010; Ibatulin, 2011) that the winters of 2002-2003 and 2003-2004 were especially rich in snow. Furthermore, there was a less significant increase in landslide activity in 2009-2011. The periods prior to 1998 have few landslides, which contradicts the fact that the year 1994 witnessed an exceptional number of landslides in the study area (Ibatulin, 2011). This inconsistency is due to the lower spatial and temporal resolutions of the satellite imagery available for the earlier years of the analysis, thus leading to incomplete landslide detection.

Despite the significant differences in the intensity of landslide activity between the periods, the landslide attributes vary less in time than they do spatially between different parts of the study area. The landslide geometry attributes (Fig. 3.11a-c) reflect the lower resolution of satellite imagery used in the automated landslide detection for the periods prior to 2001. These periods are characterized by a higher median area and length of the landslides than the periods after 2005. Large landslides follow the same pattern of temporal distribution as the entire dataset, with peaks in the periods of maximum landslide activity and a decrease in periods with less landsliding. However, landslides on average become larger in the most active periods, independently of the image resolution (Fig. 3.11a, b, Tab. 3.4).

The geology values do not exhibit significant differences between the periods (Fig. 3.12). During the peak periods of landsliding, the number of landslides increases for each stratigraphic unit, but the increase for the Jurassic-Oligocene folded sediments is even stronger. Altogether, 50% of the landslides recorded in 1986-2013

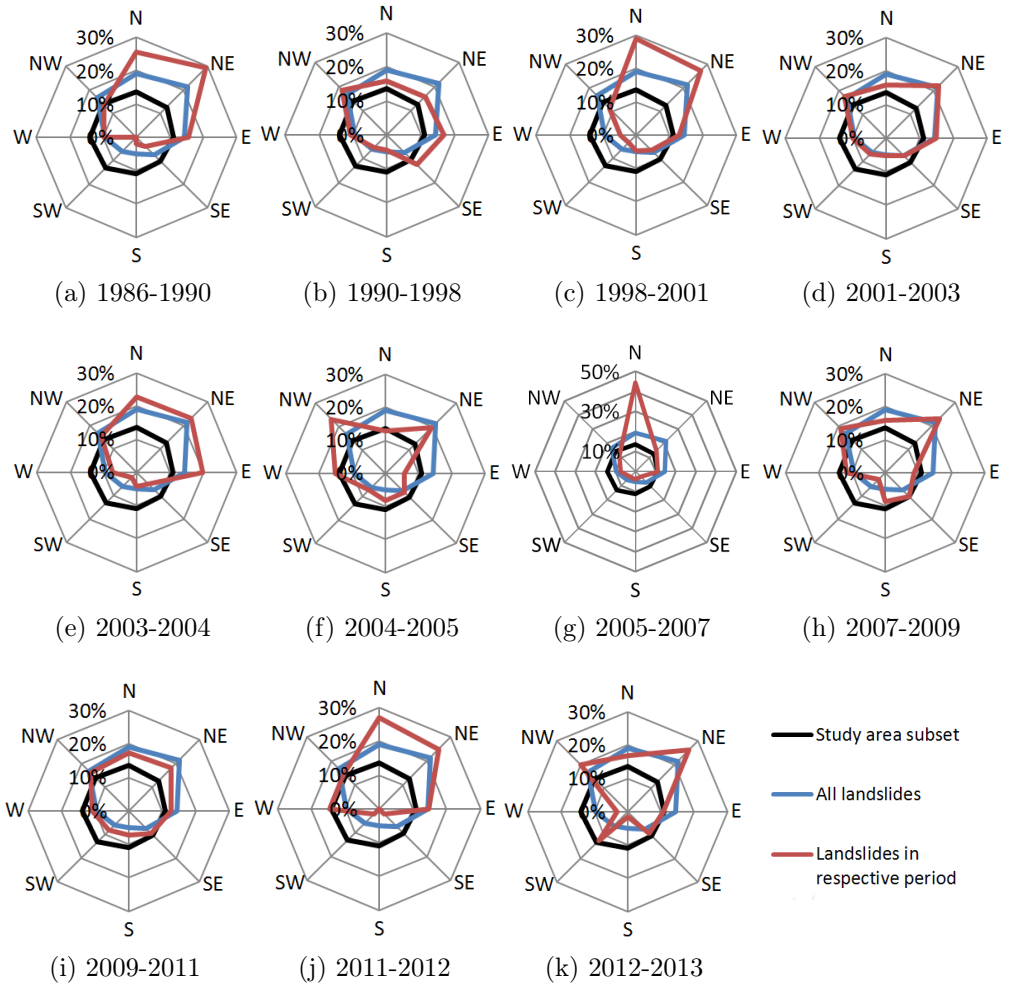

(a) 1986-1990 (b) 1990-1998 (c) 1998-2001 (d) 2001-2003

(e) 2003-2004 (f) 2004-2005 (g) 2005-2007 (h) 2007-2009

(i) 2009-2011 (j) 2011-2012 (k) 2012-2013

Figure 3.13: Distribution of landslide aspect values by period

occurred in the two periods 2001-2003 and 2003-2004, which correspond to the abundant winter precipitation in 2002-2004 (Ibatulin, 2011). However, a 51%-65% increase was observed for the Jurassic-Oligocene rocks, and only a 13%-42% increase was observed for basement units. That is, the folded Jurassic-Oligocene units are more responsive to changes in the hydrometeorological factor. The saturation of permeable rocks with water in wet years activates the sliding surface in folds where permeable deposits are located above impermeable sediments and makes those areas particularly susceptible to landsliding.

The temporal changes in the distribution of aspect values do not exhibit a particular trend, except that their distribution in periods with more active landsliding is closer to the long-term average (Fig. 3.13). The slope values tend to be higher in periods with lower landslide activity, especially in 2005-2007 (Fig. 3.11d), when a particularly large share of the landslides occurred in basement rocks that correspond to a steeper terrain. The distance to stream attribute exhibits low values for the periods 1990-1998 and 1998-2001 (Fig. 3.11e) due to the larger size of landslides in these periods. Higher values are found in 2001-2003 because of many smaller landslides in Upper Oligocene–Neogene platform deposits away from streams and in 2012-2013 due to the prevalence of small landslides in this period.

3.6 Discussion and conclusions

We derived a set of landslide attributes for a multi-source multi-temporal inventory with over 2 800 landslide polygons for the study area in southern Kyrgyzstan using a GIS-based approach. Standard GIS tools were combined with newly implemented functionality. The latter was used to calculate the landslide length, width, compactness and geological properties based on the highest and/or lowest points of the landslide polygon. These tools have been successfully applied to the landslide inventory in southern Kyrgyzstan. However, they can be applied to any landslide database that contains landslides in the form of polygons. For the derivation of topographic attributes, the 30 m cell size of the ASTER GDEM was sufficient for most landslide polygons, but problems arose with some of the smallest landslides. The applicability of the developed approach in other regions depends on how the landslide size in the region compares to the resolution of the available spatial data. A lower resolution of the available thematic maps and of the DEM is more tolerable for regions dominated by very large landslides, but it is more critical for study areas with smaller landslides.

The proposed algorithm for the automated calculation of landslide length and width consists of fitting a polyline inside the landslide polygon to represent its length. The algorithm performed adequately for the majority of the landslides. Unsatisfactory results were produced for the smallest landslides and those with irregular shapes, which required manual correction. Another problem occurred for automatically detected landslides with very long runout zones located on flat terrain or along the river bed. The proposed length calculation method may result in an overestimation of the length of such landslides. Such cases can be detected if an alternative length calculation is performed based on the elevation drop and the mean slope of the landslide polygon. In a recent publication, Nikulita (2016) proposed a method for the automated calculation of landslide length and width using minimum oriented bounding boxes of the landslide polygons and a DEM. His approach is also based on the combination of elevation and vector data, and it differentiates between long versus wide landslides to handle them differently.

The integration of multiple sources of landslide data in the inventory revealed that landslide polygons that were automatically detected from satellite images have more irregular zigzag boundaries than polygons digitized by hand. This difference led to the selection of the formula for compactness calculations in this study. It may also be important for the derivation of further geometric attributes in other cases.

Collaboration with local specialists is necessary to adjust the selection of the attributes to their needs. Furthermore, steps toward the development of a unified methodology for the determination of selected attributes may be beneficial. Guzzetti et al. (2012) addressed the need for standards and the definition of best practices for the preparation of landslide inventories. This should involve not only the documentation of landslide locations and extents but also the methodology for attribute determination. This process could include the implementation of standardized procedures in the form of open-source code that can be shared among interested users and run as extensions for popular GIS software.

The multi-source character of the inventory used in this study enabled investigating the influence of landslide data sources on the distributions of the derived

attributes. In the case of the two field-based sources, the inability to differentiate between single slope failures and the omission of smaller landslides led to a bias toward features typical for very large landslides, e.g., greater length, more gentle slope values, and shorter distance to streams. Due to the concentration of field campaigns on areas that had been previously known to experts as being landslide prone, the documentation of some landslide types was more complete than that of other types. In turn, the short-term results of the automated detection suffer from the short time period covered since the period 2009–2013 was characterized by low landslide activity. Because many studies use a single inventory data source, it is important to understand possible distortions of the landslide data. The more complete the landslide inventory, the more reliable the results of the consecutive hazard assessment. The availability of methods that can automatically detect landslides from satellite imagery is crucial for systematic analyses of landslide occurrence. This will be even more possible in the future because the availability of suitable optical remote sensing data will continue to increase. The recent launch of the Sentinel-2 system will provide new opportunities for acquiring imagery with sufficient spatial and temporal resolutions.

The present study enabled a quantification of the temporal variations of landslide occurrence. It was revealed that the spatial variations of landslide properties within the study area have been more significant than their differentiation in time. In the spatial aspect, the geological setting is the major factor that influences the distribution of landslide activity in the study area. In the temporal aspect, periods with the highest number of landslides also tend to have larger landslide sizes. For the assessment of the landslide hazard, this implies that similar factors influence the temporal and magnitude probability of landsliding. The lower spatial resolution of the satellite imagery available prior to 1998 has an effect on the distribution of attribute values over time, which reduces their comparability between the earlier and later time periods.

Because the results of long-term automated landslide detection from satellite imagery are only available for a 58 x 29 km large subset of the study area, the comparison of landslide attributes in time reflects the properties of this subset only. It would be desirable to extend the investigation of the long-term variation of landslide properties to the entire study area. However, the data availability is not sufficient for all parts of the study area. A better characterization of the geo-environmental properties of the study area, such as a geological map and a DEM of higher resolution, would also improve the derivation of landslide attributes. The geological map used in this study does not provide a systematic record of the superficial Quaternary deposits. A map of Quaternary deposits with an adequate representation of loess in the study area would be advantageous.

Due to the possibility of updating the inventory, it would be interesting to investigate the distribution of the landslide attributes based on a longer landslide record. The existing inventory reflects the period of high landslide intensity between the years 2002 and 2004. However, another strong peak of landslide activity in 1994 is not fully represented in the inventory. This is because the multi-temporal remote sensing data coverage in the most severely affected northern part of the study area was not sufficient to perform long-term automated detection of landslide occurrence. Furthermore, the rather low spatial and temporal resolutions of satellite images available for this period might have prevented the detection of some slope

failures within the subset. If such peaks of landslide activity occur in the future, the availability of remote sensing data would allow a more complete documentation. In that case, the understanding of the temporal variability of landslide properties can be improved and compared to the changes in the hydrometeorological and seismic parameters over time. The availability of methods for efficient attribute derivation, which this paper addresses, is the basis for updating the landslide attribute values and performing these comparisons.

The knowledge on landslide properties acquired by analyzing landslide attributes provides the basis for defining and interpreting multivariate statistical models used in the calculations of landslide susceptibility and temporal probability of landsliding. In southern Kyrgyzstan, the attribute analysis has shown that some regions within the study area differ significantly from the rest. If an analysis of landslide susceptibility is to be conducted, our findings indicate that it may be necessary to subdivide the study area into several parts and set up the models separately for each of those parts to accommodate the existing regional variability within the study area.

Acknowledgements

The research presented in this paper has been funded by the German Ministry of Research and Technology (BMBF) as part of the Tian Shan - Pamir Monitoring Program (TIPTIMON) and PROGRESS projects. We kindly thank our colleagues from the Ministry of Emergency Situations of Kyrgyzstan and the Central Asian Institute for Applied Geosciences (CAIAG) in Bishkek and Hans-Ulrich Wetzel for providing the geological map. We thank the anonymous reviewers for their valuable comments.

Chapter 4

Susceptibility Assessment

Evaluation of of Remote-Sensing-Based Landslide Inventories for Hazard Assessment in Southern Kyrgyzstan

Darya Golovko, Sigrid Roessner, Robert Behling, Hans-Ulricht Wetzel, Birgit Kleinschmit

Originally published in Remote Sensing (2017), 9(9):943
https://doi.org/10.3390/rs9090943

Abstract

Large areas in southern Kyrgyzstan are subjected to high and ongoing landslide activity; however, an objective and systematic assessment of landslide susceptibility at a regional level has not yet been conducted. In this paper, we investigate the contribution that remote sensing can provide to facilitate a quantitative landslide hazard assessment at a regional scale under the condition of data scarcity. We performed a landslide susceptibility and hazard assessment based on a multi-temporal landslide inventory that was derived from a 30-year time series of satellite remote sensing data using an automated identification approach. To evaluate the effect of the resulting inventory on the landslide susceptibility assessment, we calculated an alternative susceptibility model using a historical inventory that was derived by an expert through combining visual interpretation of remote sensing data with already existing knowledge on landslide activity in this region. For both susceptibility models, the same predisposing factors were used: geology, stream power index, absolute height, aspect and slope. A comparison of the two models revealed that using the multi-temporal landslide inventory covering the 30-year period results in model coefficients and susceptibility values that more strongly reflect the properties of the most recent landslide activity. Overall, both susceptibility maps present the highest susceptibility values for similar regions and are characterized by acceptable to high predictive performances. We conclude that the results of the automated landslide detection provide a suitable landslide inventory for a reliable large-area landslide susceptibility assessment. We also used the temporal information of the automatically detected multi-temporal landslide inventory to assess the temporal component of landslide hazard in the form of exceedance probability. The results show the great potential of satellite remote sensing for deriving detailed and systematic spatio-temporal information on landslide occurrences, which can significantly improve landslide susceptibility and hazard assessment at a regional scale, particularly in data-scarce regions such as Kyrgyzstan.

4.1 Introduction

The eastern rim of the Fergana Basin in southern Kyrgyzstan is a tectonically active region that experiences regular landslide occurrences. The threat to people and infrastructure posed by this high landslide activity requires a systematic and objective assessment of the landslide hazard, which has not yet been performed for this region. Although analyses of landslide susceptibility have been conducted by local experts, these analyses have been of a qualitative nature and concentrated on areas in the vicinity of settlements and roads. Factors that complicate this task are the large size of the study area (approximately 2300 km^2) and the limited availability of spatially detailed and up-to-date information on landslide occurrences and predisposing factors.

In such a setting, the use of satellite remote sensing has high potential for large-area detailed characterization of predisposing factors and for the generation of improved landslide inventories. Using time series of archived remote sensing data enables multi-temporal reconstruction of backdated landslide occurrences for large areas covering a time period of several decades. However, such a task requires ana-

lyzing large amounts of remote sensing data, which can only be accomplished using automated methods. We have developed such a method for the automated object-based detection of landslide occurrences using multi-sensor time series of optical satellite images (Behling et al., 2014b, 2016). This method is based on the analysis of normalized difference vegetation index (NDVI) trajectories (Behling et al., 2014a) and has been successfully applied in this study area (Behling et al., 2016). In this paper, we investigate the suitability of the resulting systematic multi-temporal landslide inventory covering a 30-year time period for conducting subsequent analyses of landslide susceptibility and hazard.

Landslide susceptibility analysis is the first step in the overall framework of landslide hazard and risk assessment (Guzzetti et al., 2005, 2012; Van Westen et al., 2008; Corominas et al., 2014). This analysis requires spatial information on past landslide occurrences (landslide inventory) and spatial characterization of landslide predisposing factors to evaluate the spatial probability of where landslides may occur in the future. The reliability of susceptibility mapping is significantly influenced by the quality and completeness of the landslide inventory. To achieve a high degree of completeness, different information sources have to be analyzed, thus resulting in different types of landslide inventories.

Guzzetti et al. (Guzzetti et al., 2012) distinguish between the following inventory types: archive inventory (based on records in archives, newspapers, and so on), historical inventory (showing the cumulative effect of landsliding over a long period of time without further temporal differentiation), event-based inventory (landslides caused by a single triggering event, such as a strong earthquake), seasonal inventory (landslides triggered within one active season) and multi-temporal inventory (continuous monitoring of landslide activity over longer periods of time independent of particular triggering events). The multi-temporal inventory is the most labor-intensive inventory type and the only one with the potential for spatio-temporal completeness, and it generally requires the use of remote sensing (Behling et al., 2016).

The majority of the research on landslide hazard focuses on assessing landslide susceptibility, often because of difficulties in obtaining the multi-temporal information on landslide occurrences required for landslide hazard analysis (Fressard et al., 2014). At the methodological level, many papers compare results obtained using different susceptibility calculation approaches, such as logistic regression, frequency ratio, and neural networks, among others Brenning (2007); Pourghasemi et al. (2013); Pradhan (2013); Yilmaz (2009). Since all of these methods are data-driven methods, the resulting models also largely depend on the type and quality of the input data, although this aspect generally receives less attention. However, several publications also discuss the influence of the type and quality of the used landslide inventory information on the results of susceptibility mapping (Steger et al., 2016; Pellicani and Spilotro, 2015; Galli et al., 2008; Fressard et al., 2014).

In our investigation, we focus on the influence of the inventory properties on landslide susceptibility and hazard analysis with special consideration of the contribution of satellite remote sensing. For this purpose, we derived two landslide inventories: (i) a systematic multi-temporal inventory generated by automated landslide detection from time series of satellite remote sensing data and (ii) a historical inventory prepared by an expert based on the visual interpretation of high-resolution satellite

remote sensing data as well as incorporating already existing knowledge on landslide occurrences. Detailed descriptions of the methodologies used for the derivation of these two inventories can be found in Behling et al. (2016, 2014b); Golovko et al. (2015, 2017a).

The historical inventory represents the more conventional approach to landslide mapping, and it requires the time-consuming involvement of an expert. This inventory allows the cumulative assessment of landslide activity that has occurred in an area up to the time when the inventory is prepared. Since the historical inventory incorporates all available records, the quality of the inventory also depends on the overall availability of historical information for a specific region. Using high-resolution satellite remote sensing can partially compensate for missing historical documentation as long as the morphological indicators for past landslide activity are still present in todayâĂŹs relief. Historical inventories are generally limited in terms of temporal information on landslide occurrences. However, such information is needed to provide the temporal component required for landslide hazard analysis (Guzzetti et al., 2012).

Preparing the necessary multi-temporal inventories including multiple time steps—ideally after each triggering event and/or period of landslide activation—imposes limits on manual approaches of landslide mapping, particularly if large areas need to be analyzed. Therefore, remote-sensing-based automated approaches become increasingly more important. In this study, we pose the question of to what extent the use of an automatically derived multi-temporal remote-sensing-based landslide inventory leads to different results in the susceptibility analysis compared to the historical inventory prepared by an expert. Furthermore, we aim to investigate the potential of the multi-temporal nature of the automatically derived inventory for assessing the temporal component of landslide hazard, which to date has received less attention among the scientific contributions toward improved hazard assessment because of the widespread lack of suitable multi-temporal data on landslide occurrences.

4.2 Study Area and Database

4.2.1 Study Area

The approximately 60-by-40-km-large study area is located in Osh Province (oblast) of Kyrgyzstan (Figure 4.1) at the foothills of the Tian Shan. This territory is primarily composed of weakly consolidated Mesozoic and Cenozoic rocks, which have been folded by subsequent tectonic deformations, thus contributing to their instability. Loess cover of varying thickness is deposited in the folds, which leads to particularly fast and dangerous slope failures. Rather than being associated with individual triggering events, most landsliding in the study area occurs in the spring months with significant variations in landslide intensity among the years. These variations have been linked to snow accumulation in the winter months, intensity of snow melting and additional precipitation during the snow melt Ibatulin (2011); Torgoev et al. (2010).

Earthquakes contribute to the destabilization and can act together with the

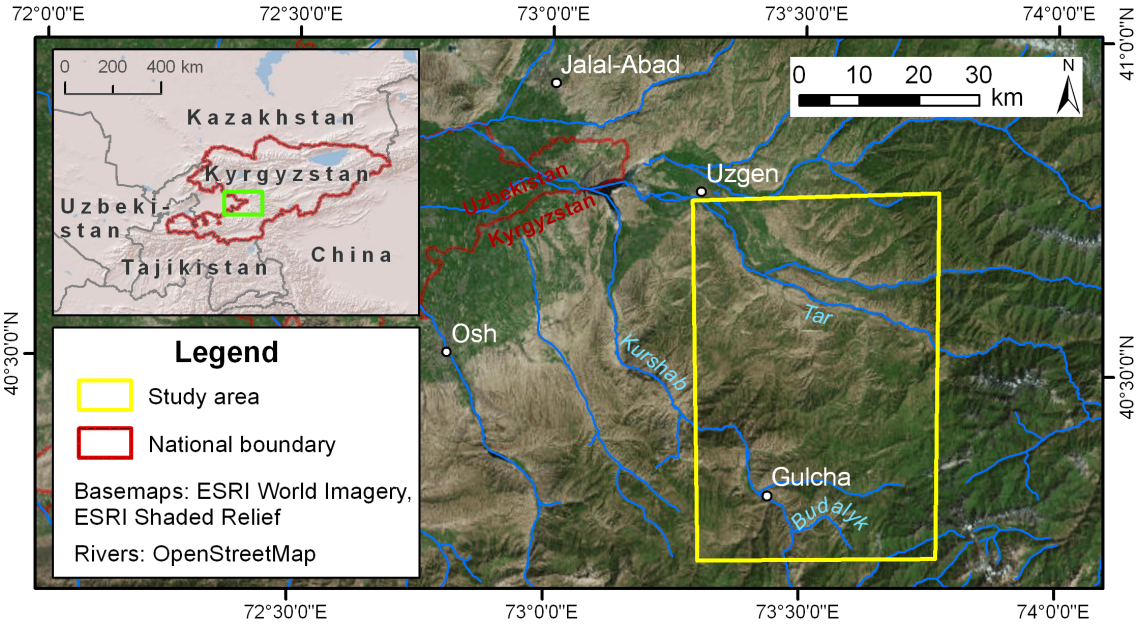

Figure 4.1: Location of the study area.

hydrometeorological factor (Danneels et al., 2008).

The study area is a part of a larger region (approximately 12,000 km^2 in size) that is affected by intensive landsliding. If the hazard analysis is to be extended to the larger area, then the automated detection allows the analysis to be extended with less effort compared to the expert identification, which would be practically as labor intensive as it was in the smaller study area. In this case, it is important to know whether the quality of the analysis based on the automated detection results is different from that of the analysis based on the expert interpretation results.

4.2.2 Landslide Inventory

Regular landslide monitoring in southern Kyrgyzstan was conducted by the local authorities until 1991, with a substantial decrease in the 1990s followed by a gradual resumption. To characterize the landslide activity in the region as fully as possible, multiple information sources need to be combined, each with its strengths and limitations (Golovko et al., 2017a, 2015). The landslide datasets used in this study were prepared using two different methods:

- Automated detection. This dataset was obtained using an automated object-oriented landslide mapping approach that utilizes multi-temporal satellite-based imagery acquired by different optical sensors (Landsat E(TM), SPOT 1-5, ASTER, IRS-1C LISS III, and RapidEye) between 1986 and 2016 (Behling et al., 2014a, 2016, 2014b; Behling and Roessner, 2017). The resulting landslide dataset is composed of 1846 polygons. Each polygon represents the spatial extent of an individual landslide failure. For each landslide polygon, the date of occurrence was determined as the period between two consecutive image acquisitions (before and after the slope failure). The temporal resolution depends on the length of the period between the before and after images. The resolution varies between several years at the beginning and a few weeks at the

end of the time span covered by the multi-temporal remote sensing database. The polygons overlap if multiple failures occurred within the same slope over time, which makes it possible to reconstruct the history of landslide reactivations. The resulting dataset is a systematic record of the landslides in the study area that occurred during the past 30 years. This may appear to be a short landslide record, particularly compared to some European countries with very extensive spatial data on landsliding. However, for southern Kyrgyzstan, this dataset is of unprecedented quality and completeness. The length of the period covered by this dataset will increase as new high-resolution satellite images are acquired, but an evaluation of the properties of the dataset and its influence on the susceptibility results can already be performed with the 30-year coverage.

- Expert interpretation. Areas that experienced landsliding in the past and that still exhibit morphological evidence of these past slope failures were mapped visually by an expert. The mapping was based on RapidEye images acquired between 2012 and 2015, a digital elevation model (DEM) and geological information. The resulting dataset represents the cumulative result of landsliding with no information on the failure dates and without the differentiation of the spatial extents of individual activations. Thus, in contrast to the automatically detected dataset, the results of expert interpretation do not contain individual landslide objects but rather a mask that shows whether the given location was affected by landsliding in the past.

The area covered by the expert interpretation dataset is seven times the size of the area covered by the automatically detected dataset (Table 4.1). Approximately two thirds of the landslide-affected area of the automatically detected dataset falls into the results of the expert interpretation. Figure 4.2 shows the spatial distribution of the landslides in the study area and its two subsets. Subset S1 experienced little landsliding over the past 30 years, whereas subset S2 was affected by high landslide activity. Overall, large parts of the study area are subjected to ongoing landslide activity, which is particularly high in several landslide hotspots.

Table 4.1: Landslide area documented in the two landslide datasets.

Dataset	**Area, km^2**	**Portion of Study Area, %**
Landslide area according to the results of automated detection	28.5	1.23
Landslide area as interpreted by the expert	197.8	8.52
Overlapping landslide area of both datasets	19.8	0.86
Area not affected by landsliding in either dataset	2115.0	91.10

4.2.3 Predisposing Factors

The data on the landslide predisposing factors are available in the form of a geological map and the Advanced Land Observation Satellite (ALOS) DEM World with a 30 m resolution (ALOS DEM World - 30m, 2017). The geological map was created through expert reinterpretation of multiple digitized 1:200,000 geological paper maps published prior to 1991. Because a lithological map of the study area is unavailable,

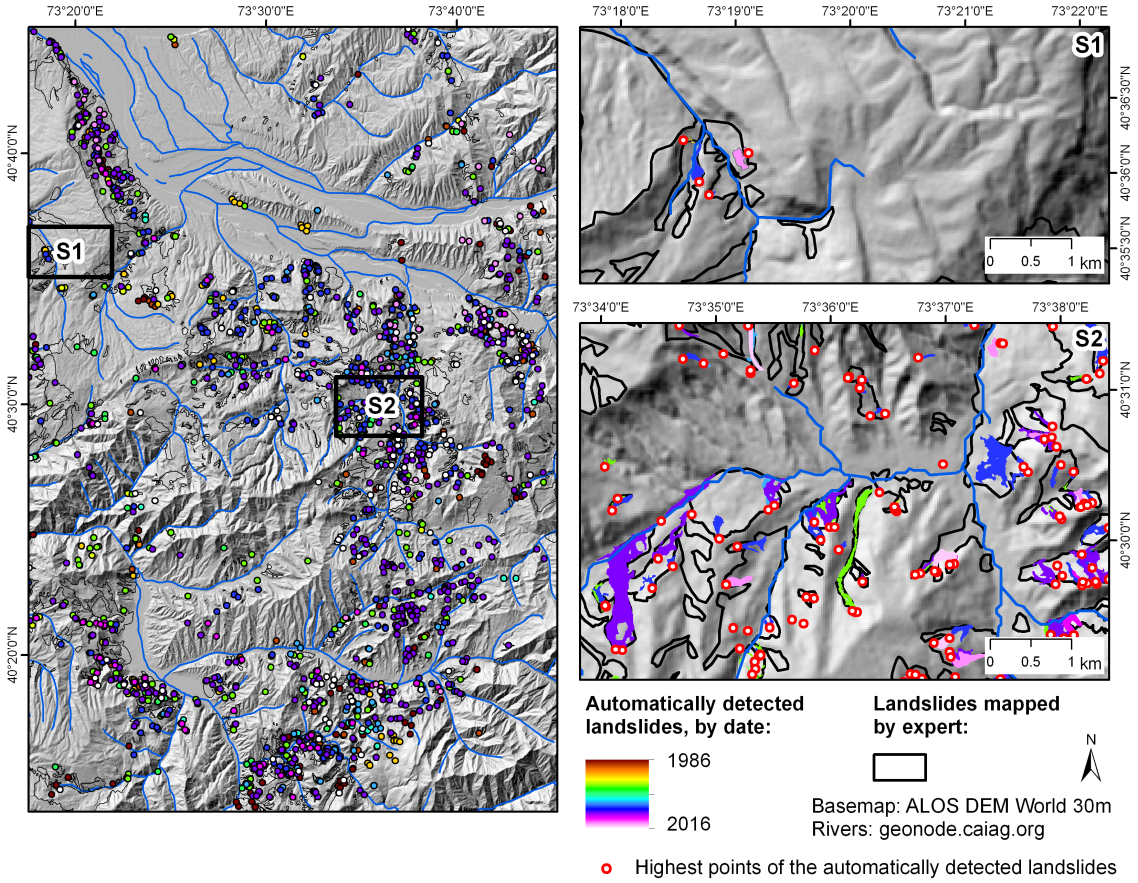

Figure 4.2: Landslides in the study area mapped by expert interpretation (black contours) and automated detection (colored polygons and points). The points in the overview map are the centroids of the automatically detected landslide polygons. The representation with points is for visualization purposes only; the actual dataset contains polygons.

we use the structural geological units to characterize the lithology. The following structural units are distinguished (following (Roessner et al., 2005)):

- Basement: Metamorphic and igneous rocks;
- Jurassic (J1–J3): Sandstones, siltstones, and slates;
- Upper Cretaceous—Paleogene (Cr1–Cr2): red sandstones, conglomerates, gravels, gypsolytes, limestones, clays, and siltstones;
- Lower Eocene—Oligocene (Pg1–Pg2): sandstones, gypsolytes, limestones, marls, clays, and siltstones;
- Oligocene—Miocene (Pg3–N1): red sandstones, conglomerates, and clays;
- Pliocene (N2): conglomerates, gravels, and loess-type loams;
- Lower Quaternary (Q1): gray conglomerates and loesses;
- Middle Quaternary (Q2): glacial moraines, loesses, and alluvial sediments;
- Upper Quaternary (Q3–Q4): alluvial sediments, glacial moraines, and loesses.

The open source software packages SAGA GIS (version 2.2.7) and QGIS (version 2.14.3) were used to derive the following factors from the ALOS DEM for each raster cell using its 8-cell neighborhood:

- Aspect shows the exposition of the slope, classified into eight cardinal and intercardinal directions.
- Slope characterizes the steepness of the slope.
- Stream power index (SPI) is a function of the product of flow accumulation and the local slope that describes the potential erosion power at a specific point of the surface (Jebur et al., 2014; Moore et al., 1991).

4.3 Methods

Landslide susceptibility indicates how likely a landslide is to occur at a location with a certain combination of predisposing factor values (Guzzetti et al., 2005; Corominas et al., 2014). We calculate the landslide susceptibility for both landslide datasets: the results of automated detection and expert interpretation. For the former dataset, we perform the susceptibility analysis (i) using all of the landslide extents and (ii) using a single point at the landslide initiation zone (cf. Section 4.3.4). We compare and validate the results. Finally, we calculate the exceedance probability of landsliding using the multi-temporal inventory.

4.3.1 Frequency Ratio Method

n our study, we use the frequency ratio method (Lee and Talib, 2005; Intarawichian and Dasananda, 2011). This method calculates the frequency ratio value for each factor class by comparing the landslide density within that class to the average landslide density in the study area:

$$FR_{\mathrm{i}} = \frac{N_{\mathrm{pix(S_i)}}/N_{\mathrm{pix(N_i)}}}{\sum N_{\mathrm{pix(S_i)}}/\sum N_{\mathrm{pix(N_i)}}}, \tag{4.1}$$

where
$N_{\mathrm{pix(S_i)}}$ is the number of landslide pixels in each class i;
$N_{\mathrm{pix(N_i)}}$ is the total number of pixels that have class i in the study area;
$\sum N_{\mathrm{pix(S_i)}}$ is the total number of landslide pixels in the study area;
and $\sum N_{\mathrm{pix(N_i)}}$ is the total number of pixels in the study area.

The class boundaries for each factor are determined by the researcher prior to the calculation based on expert knowledge and the data distribution. The landslide susceptibility index (LSI) is then calculated by adding the frequency ratio of each factor for the given pixel. To ensure comparability between susceptibility models

with different numbers of factors, the sum is divided by the number of factors:

$$LSI = \frac{1}{n}\sum_{i=1}^{n} FR_i \implies$$

$$LSI = \frac{FR(geology) + FR(aspect) + FR(slope) + FR(abs.\ height) + FR(SPI)}{5}. \tag{4.2}$$

4.3.2 Validation of Susceptibility Assessment

To evaluate the susceptibility models, we use receiver operating characteristic (ROC) curves, which plot the model sensitivity (i.e., the portion of known landslide pixels correctly classified as susceptible) against its specificity (i.e., the portion of landslide-free pixels correctly classified as not susceptible) (Begueria, 2006; Van Den Eeckhaut et al., 2009). The area under the curve (AUROC) varies between 0.5 and 1.0, with higher values indicating a better fit of the model. The model is validated by comparing it to a landslide dataset that is not used for calibrating the model (Chung and Fabbri, 2008; Remondo et al., 2003). The subdivision of the landslide data into the training and validation parts is generally performed randomly or using non-overlapping temporal or spatial subsets of the landslide inventory (Chung and Fabbri, 2008).

We use the following pairs of training and validation datasets:

- The datasets obtained by automated detection (both the landslide highest points and the landslide masses) are divided into training and validation parts. This is a standard approach for validating the susceptibility results when a single landslide dataset is available (Chung and Fabbri, 2008; Van Den Eeckhaut et al., 2009). We divide the datasets into 50%/50% parts.

- The expert interpretation dataset is used for training the model, and the automated detection dataset (landslide masses) is used for validating the model. The goal is to understand whether the automatically detected dataset, which is based on a relatively short 30-year observation period, is capable of producing results that are comparable to the labor-intensive geomorphological mapping.

- The automated results of 2009–2016 (landslide masses) are used to train the model, and the automatic detection dataset of 1986–2009 is utilized to validate the model. This is an attempt to evaluate the reliability of the susceptibility mapping in a scenario where only RapidEye satellite images are available.

4.3.3 Temporal Probability of Landsliding

To explore the spatial variations in the landslide activity in time, we calculate the exceedance probability of landslide occurrence using a binomial distribution, as follows:

$$P = 1 - e^{-\lambda t}, \tag{4.3}$$

where λ is the annual landslide frequency (per mapping unit) and t is the length of the period (in years) for which the exceedance probability is calculated (Corominas and Moya, 2008; Guzzetti et al., 2005).

The completeness of a landslide inventory is crucial for the correctness of the exceedance probability calculations because the omission of landslides from the underlying inventory leads to an underestimation of the hazard. However, the completeness of landslide inventories is limited, particularly in data-scarce regions. Landslide size-frequency behavior follows a power law distribution with a roll-over for smaller events (Havenith et al., 2015; Malamud et al., 2004), which is a result of the incomplete mapping of landslides below a certain size. Prior to calculating the exceedance probability of landsliding, we assess the completeness of the automated landslide detection results based on their size-frequency distribution.

4.3.4 Mapping Units

Mapping units are a result of partitioning the space into non-overlapping parts that together cover the territory of the study area in question. These units are used to transition from discrete and possibly overlapping landslide objects to analyses at the scale of the study area, e.g., in the course of the landslide hazard assessment (cf. Guzzetti et al. (1999); Van Den Eeckhaut et al. (2009); Erener and Düzgün (2012)).

In this study, the susceptibility calculation is performed on the basis of 30-m pixels for both landslide datasets. The complete extent of the landslide mass is rasterized and used as the input data for the susceptibility analysis. Additionally, we calculate the susceptibility using a single point for each landslide of the automatically detected dataset. The point representative of the landslide polygon should be located in the landslide initiation zone. To automate the process, we use the highest point within the landslide as an approximation of the landslide main scarp. The highest point is calculated by clipping the DEM raster to the landslide polygon in question and using the center of the pixel that has the highest elevation value. The procedure is automatically performed as a part of the QGIS plugin Landslide Tools (QGIS Plugin Landslide Tools, 2017) implemented by one of the authors. The susceptibility calculation using the highest points cannot be performed with the results of expert interpretation because this dataset does not distinguish between individual landslide objects. The choice of the landslide representation determines the interpretation of the resulting susceptibility model: the model based on the landslide highest points indicates the likelihood of a pixel to initiate a landslide, whereas the model based on complete landslide extents represents the likelihood of the given location to be affected by a landslide.

It is possible to calculate the exceedance probability in a similar pixel-based manner. However, a typical landslide-prone slope in the study area is characterized by recurring landslide failures. Each slope failure may only occupy a part of the slope, whereby the multitude of such events over the years eventually affects the entire slope. The differentiation in the landslide frequency on such slopes is often a result of the short observation period. The absence of landslides in the inventory in the presumably unaffected parts of such slopes does not imply that these areas are safe. In fact, the opposite may be true in the short term. We solve this contradiction by introducing larger mapping units. In this study, slope units have been used as

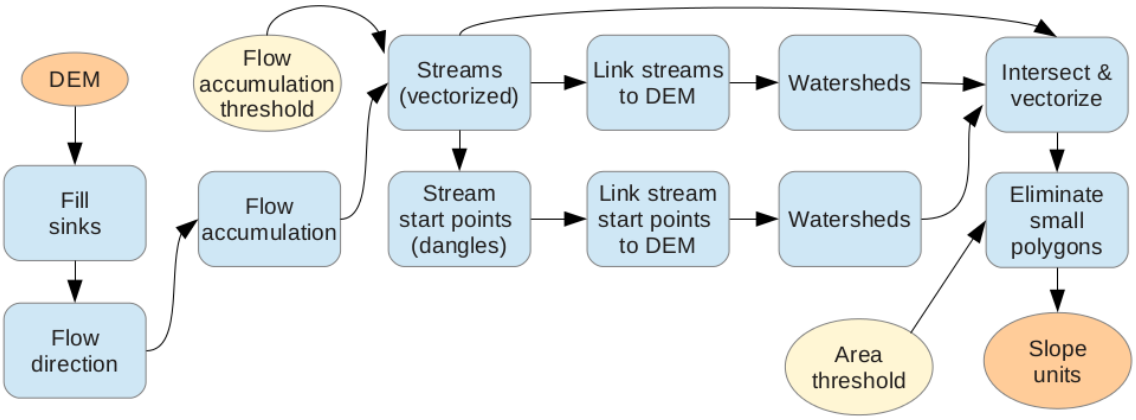

Figure 4.3: Workflow for the derivation of slope units.

mapping units because they reflect the physical properties of the relief as a major landslide predisposing factor.

We derived the slope units from digital elevation data using an approach based on watershed delineation in ArcGIS. A simplified overview of the approach is presented in Figure 4.3. We followed the standard ArcGIS procedure, which consists of deriving the stream network by setting a threshold on the flow accumulation raster and then using the branch-off points of the resulting streams to delineate individual watersheds. However, the result of this procedure does not allow distinguishing between opposite slopes of a river valley that touch the same stream segment. Therefore, an additional step was introduced. This step subdivides the watersheds obtained in the previous step into two polygons by intersecting them with the stream lines. For upstream watersheds, an additional third sub-watershed is delineated that drains to the highest point of the stream and represents the uppermost part of the river valley. This approach allows for a more consistent aspect within the resulting slope units. This modified procedure includes two user-defined parameters: the flow accumulation threshold and the area threshold. The flow accumulation threshold is used to vary the size of the resulting slope units to account for the properties of the study area and the scale of the analysis. The area threshold serves to remove resulting polygons that are too small to represent a slope by merging them with their larger neighbors. We assign each landslide to a slope unit based on the location of the landslide highest point.

In the final step, we combine the spatial and temporal aspects into a landslide hazard index, which is done at the level of the slope units using the susceptibility map based on the automatically detected landslide masses. We reclassify the susceptibility map into three classes of equal size (tertiles). The "Majority" function of the QGIS Zonal Statistics tool is used to determine the prevalent susceptibility tertile for each slope unit. From the slope units with the highest susceptibility tertiles, we select the units that have experienced multiple (at least two) landslide failures since 1998. We consider these slope units to have the highest landslide hazard index.

4.4 Results

4.4.1 Landslide Susceptibility

Model Results

The frequency ratio values were calculated for all three of the landslide datasets (Table 4.2). The predisposing factor datasets were reclassified according to these frequency ratio values. To evaluate the ability of individual factors to differentiate between pixels with high and low susceptibilities, the AUROC values of susceptibility models based on a single factor were calculated (Table 4.3). Geology is the main factor determining the differentiation of landslide susceptibility in the study area in each of the three models. This factor is responsible for the most global level of the study area zonation because it is indicative of the different structural settings of its parts. In the northern part of the study area in particular, the main differences between susceptibility values can be linked to the boundaries of lithological units. Cretaceous deposits (Cr1–Cr2) are consistently the most affected geology class across all three models. The model based on the results of expert interpretation assigns higher susceptibility to Jurassic rocks (J1–J3). The model that uses the automatically detected landslide masses results in high frequency ratio values for Middle Quaternary deposits (Q2). This result is due to the extensive landsliding on the Uzgen slope, where the areas severely affected by landsliding were classified as Q2 in the geological map. The aspect factor behaves similarly among all three of the models. The model based on the landslide highest points assigns higher frequency ratio values for steeper slopes and higher terrain than the other models.

Comparison of Susceptibility Maps: Automated Detection vs. Expert Interpretation

Figure 4.4 shows the susceptibility maps produced for both landslide datasets. Both susceptibility maps are similar in subset S2. In subset S1, the model based on the automatically detected landslides shows lower susceptibility levels than the model based on the results of expert interpretation.

To compare the susceptibility values of both maps, their difference was calculated (Figure 4.5). The differences between the two maps can be linked to the frequency ratio values of the predisposing factor classes in both susceptibility models (see Table 4.2). For example, the automatically detected landslides are more rare in Jurassic and Paleogene deposits than landslides mapped by the expert. Consequently, these areas received lower susceptibility in the model based on the automated detection results (see highlighted areas A and B in Figure 4.5). The very active slope near the town of Uzgen in the very northwest of the study area (highlighted area C in Figure 4.5) has a substantial influence on the susceptibility model based on the automatically detected landslides. The consequence is a large frequency ratio value for northeastern slopes in the susceptibility model based on automatically detected landslides. This reflects not only on the Uzgen slope itself but also in other parts of the study area, e.g., highlighted area D in Figure 4.5. No landslides have been recorded in highlighted area D, but a visual assessment of the satellite imagery from

Table 4.2: Frequency ratio values of the predisposing factors by landslide data source. Classes with FR > 1 are more favorable for the development of landslides than the study area on average

Factor	Class	Automated Detection 1986-2016, Highest Points	Automated Detection 1986-2016, Landslide Masses	Expert Interpretation
Geology	Basement	0.281	0.131	0.228
	J1-J3	0.588	0.289	1.345
	Cr1-Cr2	2.134	2.309	2.070
	Pg1-Pg2	1.214	0.956	1.370
	Pg3-N1	1.325	0.646	0.507
	N2	0.622	0.443	0.129
	Q1	0.176	0.030	0.053
	Q2	0.478	1.923	0.954
	Q3-Q4	0.426	0.806	0.973
Aspect	North	1.415	1.382	1.479
	Northeast	1.742	2.108	1.668
	East	1.242	1.423	1.343
	Southeast	0.750	0.705	0.847
	South	0.431	0.423	0.659
	Southwest	0.463	0.435	0.483
	West	0.616	0.542	0.558
	Northwest	1.250	0.964	0.991
Slope, degrees	<5	0.079	0.395	0.518
	5 - <10	0.259	1.035	1.395
	10 - <15	0.490	1.283	1.640
	15 - <20	0.938	1.347	1.376
	20 - <25	1.474	1.137	0.998
	25 - <30	1.832	0.968	0.704
	30 - <35	1.872	0.760	0.424
	35 - <40	1.456	0.610	0.244
	40 - <45	1.689	0.796	0.198
	≥45	1.601	0.998	0.152
Absolute height, m	<1200	0.243	0.767	0.694
	1200 - <1400	0.305	1.277	0.860
	1400 - <1600	0.760	1.658	1.040
	1600 - <1800	1.500	1.929	1.492
	1800 - <2000	1.706	1.686	1.393
	2000 - <2200	1.400	0.749	1.228
	2200 - <2400	0.935	0.316	0.962
	2400 - <2600	0.433	0.161	0.366
	≥ 2600	0.104	0.027	0.042
SPI	<4	0.044	0.183	0.297
	4 - <6	0.456	0.579	0.901
	6 - <7	0.889	0.812	0.989
	7 - <8	1.412	1.129	1.015
	≥8	1.609	1.887	1.349

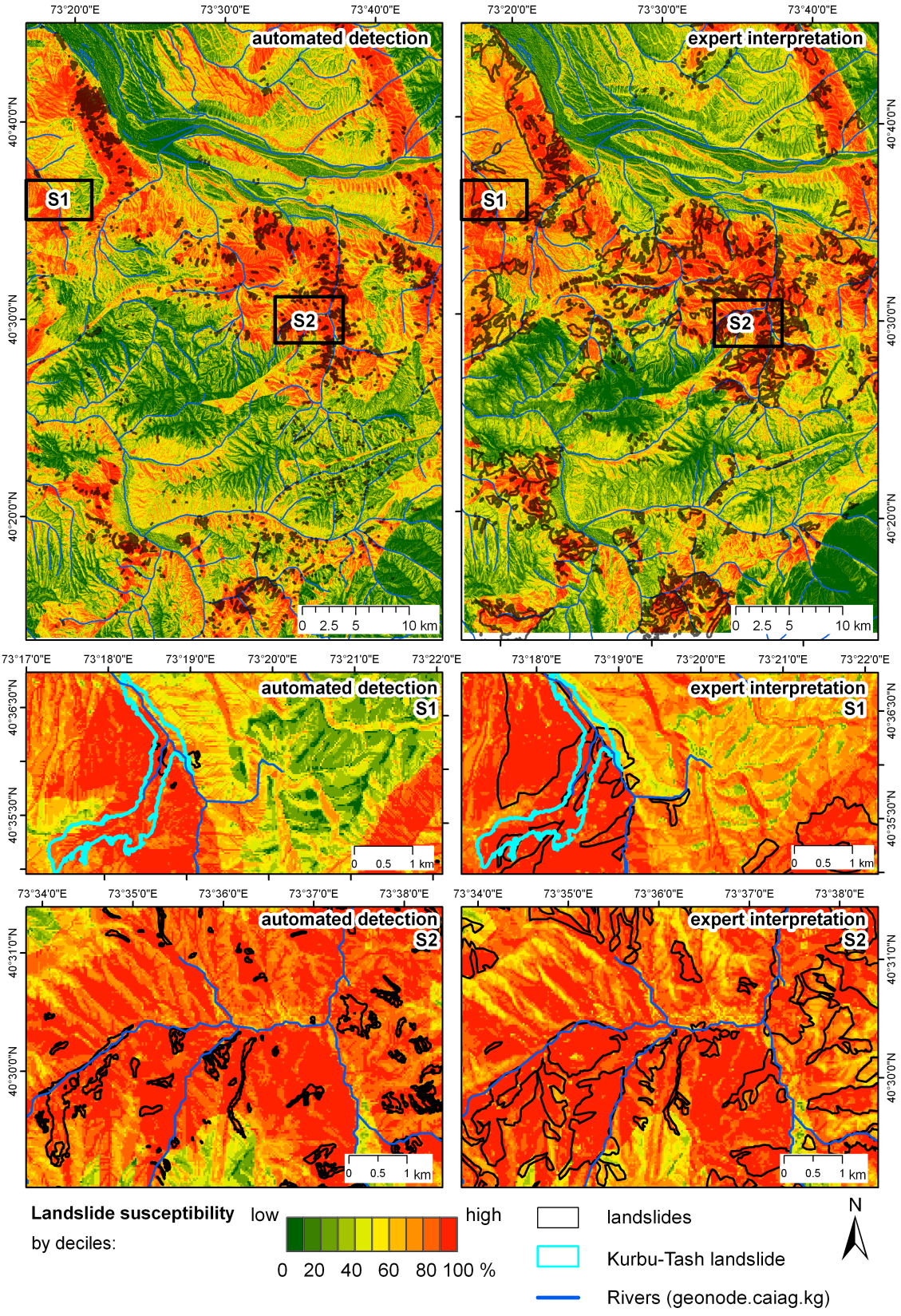

Figure 4.4: Results of susceptibility assessment produced using automatically detected landslide masses (1986–2016) and landslides obtained by expert interpretation: study area and two subsets.

Table 4.3: Discrimination ability of predisposing factors: area under the receiver operating characteristic (AUROC) curve values of susceptibility models based on a single factor.

Factor	Automated Detection 1986-2016, Highest Points	Automated Detection 1986-2016, Landslide Masses	Expert Interpretation
Geology	0.6960	0.7232	0.7221
Aspect	0.6265	0.6615	0.6303
Slope	0.6820	0.5876	0.6486
Absolute height	0.6560	0.6912	0.6270
SPI	0.6354	0.6318	0.5605

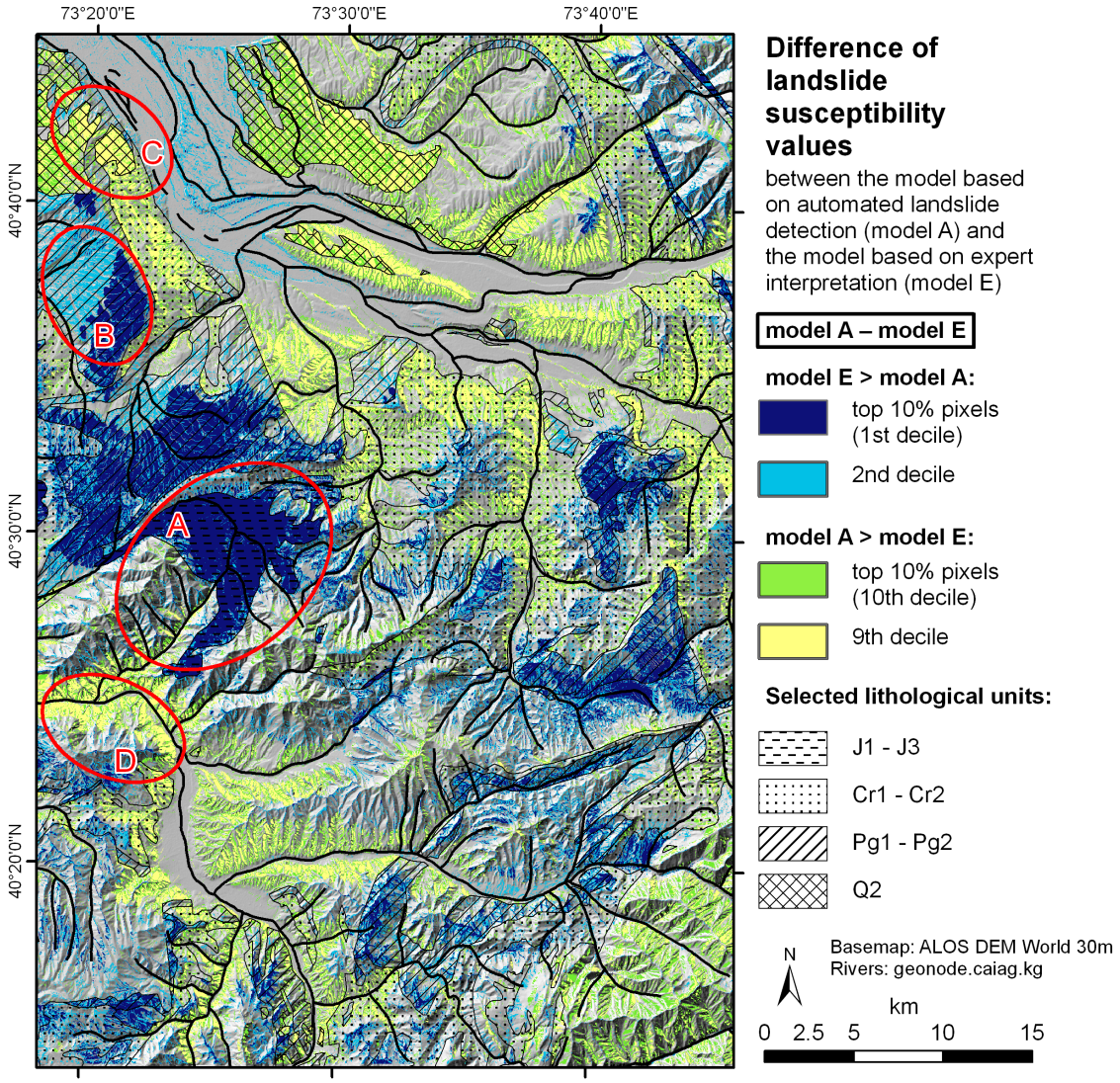

Figure 4.5: Difference between susceptibility maps produced using the results of automated detection (landslide masses, "model A") and expert interpretation ("model E").

Google Earth (by Google Inc., Mountain View, California) indicates that landsliding is plausible here.

Comparison of Susceptibility Maps: Landslide Masses vs. Highest Points

The differences between the susceptibility models based on the landslide highest points and the landslide masses reflect the nature of the input data. The model calculated using the highest points assigns higher susceptibility values to upper parts of the slope (e.g., subset S4 in Figure 4.6). Furthermore, it results in lower susceptibility for Middle Quaternary (Q2) deposits (e.g., the Uzgen slope in subset S3 in Figure 4.6) and higher susceptibility for areas with more consolidated rocks due to the higher elevation and slope values there. Landslides in the areas with more consolidated rocks are small, but because the landslide size has no influence on the susceptibility model based on landslide highest points, small landslides receive more weight in this model.

Validation

After selecting the best susceptibility models, we assess their predictive power in a validation procedure. We also use this opportunity to analyze how the input landslide data quality affects the susceptibility assessment results.

Table 4.4: Validation results.

Row	Training Dataset	Validation Dataset	AUROC*
1	Automated detection 1986-2016, highest points (50%)	Automated detection 1986-2016, highest points (50%)	0.7998
2	Automated detection 1986-2016, landslide masses (50%)	Automated detection 1986-2016, landslide masses (50%)	0.8142
3	Expert interpretation	Automated detection 1986-2016	0.7730
4	Automated detection 2009-2016, landslide masses	Automated detection 2009-2016, landslide masses	0.8053

*area under the receiver operating characteristic curve

The AUROC values presented in Tab. 4.4 suggest that the susceptibility mapping results are acceptable for all the landslide datasets. The highest values were achieved using the landslide masses detected automatically in 1986-2016. Even the shorter dataset covering the period between 2009 and 2016 with high-resolution RapidEye images results in an AUROC value of 0.8. This result implies that the susceptibility assessment can be extended to the territory adjacent to our study area, provided that RapidEye images are available.

4.4.2 Temporal Probability of Landsliding

We calculated the exceedance probability of landsliding using the results of automated landslide detection. This dataset covers the 30-year period between 1986 and 2016. According to data from the local authorities, the year 1994 experienced an exceptional number of landslides in southern Kyrgyzstan: a third of all slope failures

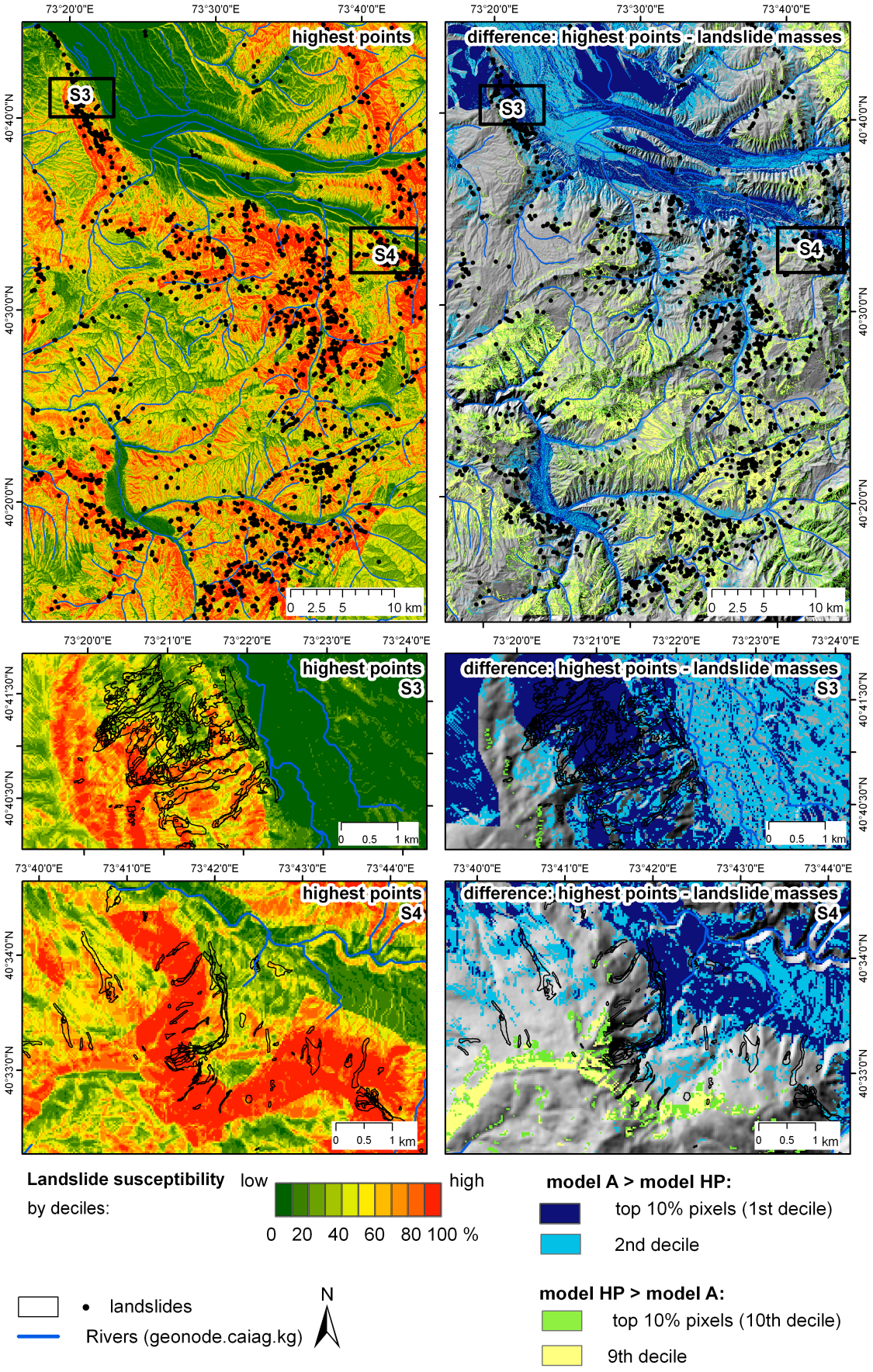

Figure 4.6: Results of susceptibility assessment produced using landslide masses (model A) and landslide highest points (model HP) of automatically detected landslides (1986–2016): study area and two subsets.

registered from 1986–2010 occurred in 1994 (Ibatulin, 2011). However, this exceptional landslide activity is not reflected in the automated detection results. The automatically detected landslide dataset contains 1846 landslides, but only 164 of them failed in 1986–1998. One reason for this result is that the statistics from the local authorities refer to a territory that is larger than our study area, and the hotspot of landslide activity in 1994 was north of the study area. However, a more important reason is the low temporal resolution of the imagery used for the automated detection. The earliest image acquisition dates were in 1986, 1990 and 1998. The interval between 1990 and 1998 is so long that some of the slope failures could not be detected using remote sensing due to revegetation and/or subsequent failures on the same slope during the same time period. This is, e.g., the case for the landslide in the Kandava river valley next to the village of Komsomol that failed on 26 March 1994 and caused 28 fatalities (Ibatulin, 2011). Furthermore, the spatial resolution of the images available for the early periods is lower and thus simply does not enable smaller landslides to be detected. To avoid an underestimation of landslide hazard, we only use landslide data of 1998–2016 in the following analysis of the temporal component.

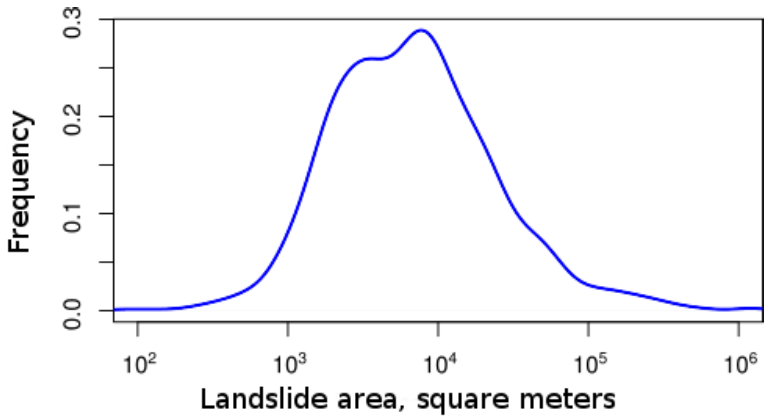

Figure 4.7: Size-frequency distribution of automatically detected landslides in 1998–2016.

The assessment of the size-frequency distribution for these landslides (Figure 4.7) shows a roll-over effect in the probability density curve for landslide areas under 10,000 m^2. Therefore, the available data permit the calculation of the exceedance probability only for landslides of this size or larger.

The exceedance probabilities of the occurrence of landslides larger than 10,000 m^2 for periods of 5 and 10 years are presented in Figure 4.8a,b. The exceedance probability of landslide occurrence for the period of 5 years is over 80% on the Uzgen slope, in parts of the basins of left tributaries of the Tar river, around the village of Gulcha and in the Budalyk river valley. Large landslides over 100,000 m^2 are particularly likely on the Uzgen slope (Figure 4.8c,d).

After combining the exceedance probability map with the susceptibility map based on the automated landslide detection results (landslide masses), we select the slope units with the highest landslide index (Figure 4.9). They largely coincide with the distribution of the main landslide hotspots in the study area.

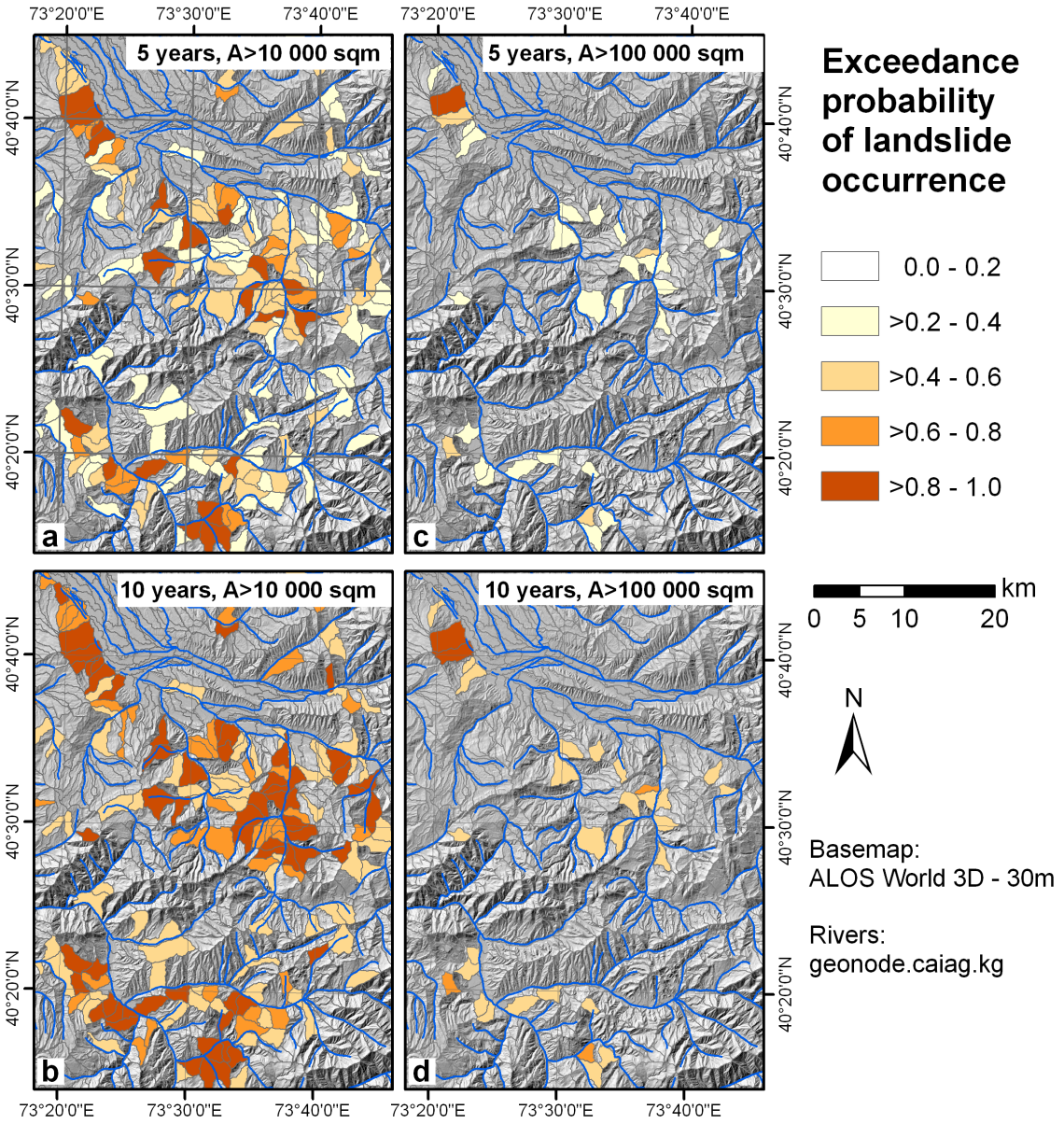

Figure 4.8: Exceedance probability of the occurrence of a landslide with an area over 10,000 m^2 (**a,b**) and over 100,000 m^2 (**c,d**) by slope unit.

4.5 Discussion

We have calculated landslide susceptibility for the study area in southern Kyrgyzstan using two versions (highest points of landslide initiation and complete landslide masses) of a multi-temporal landslide inventory and a historical landslide inventory and five predisposing factors (geology, aspect, slope, absolute height and stream power index). The multi-temporal inventory was generated by automated landslide detection from time series of optical satellite images covering the period between 1986 and 2016. The historical inventory was derived by expert mapping using a combination of satellite remote sensing interpretation and already existing knowledge on landslide occurrence.

The good performance (AUROC values between 0.77 and 0.81) of the models for all three types of landslide input data and a visual assessment of the resulting

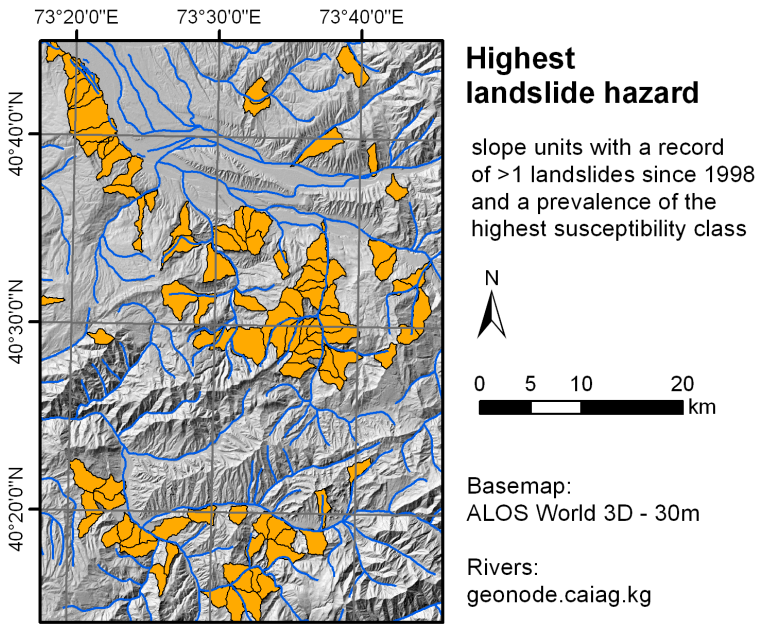

Figure 4.9: Slope units with the highest landslide hazard index, i.e., slope units where (i) more than one landslide failure occurred since 1998 and (ii) the highest susceptibility tertile occupies a larger area than any other tertile.

maps indicate that the automated landslide detection method is a valid and more precise alternative to the labor-intensive manual mapping. Although the quantitative AUROC metrics are commonly accepted for quality assessment within landslide susceptibility studies, they need to be complemented with an assessment of the potential biases contained in the input landslide and factor data and of geomorphic plausibility checks (Steger et al., 2017). Moreover, the results of susceptibility analysis should be compared to independent landslide occurrences, e.g., slope failures of 2017.

The differences in the susceptibility values of individual factor classes between the historical and multi-temporal inventories can be traced back to the fact that the landslides mapped by the expert occupy a larger area and span over a wider range of natural conditions and a longer time period of occurrence. This explains why some factor classes (e.g., Jurassic and Paleogene rocks) are represented with a higher significance in the model based on the landslide inventory derived by the expert compared to the inventory derived by automated remote sensing analysis. We conclude that the recurrence intervals of landslides in such areas exceed the 30-year-long time period for which satellite remote sensing time series data of sufficient spatial resolution are available for the study area.

The spring of 2017, which is not yet covered by the inventory used in this study, represents an extraordinary period of landslide activity caused by a threefold increase in winter precipitation between October and March compared to the long-term average (Ministry of Emergency Situations of the Kyrgyz Republic, 2017). These extraordinary meteorological conditions led to the activation of a high number of landslides of partially very large extent. Within our study area, a 4.3-km-long landslide occurred at the end of April 2017 near the village of Kurbu-Tash, destroying approximately 60 houses whose residents had been evacuated prior to the main failure (Figure 4.10) (Petley, 2017a; AKIpress, 2017). The landslide occurred on a

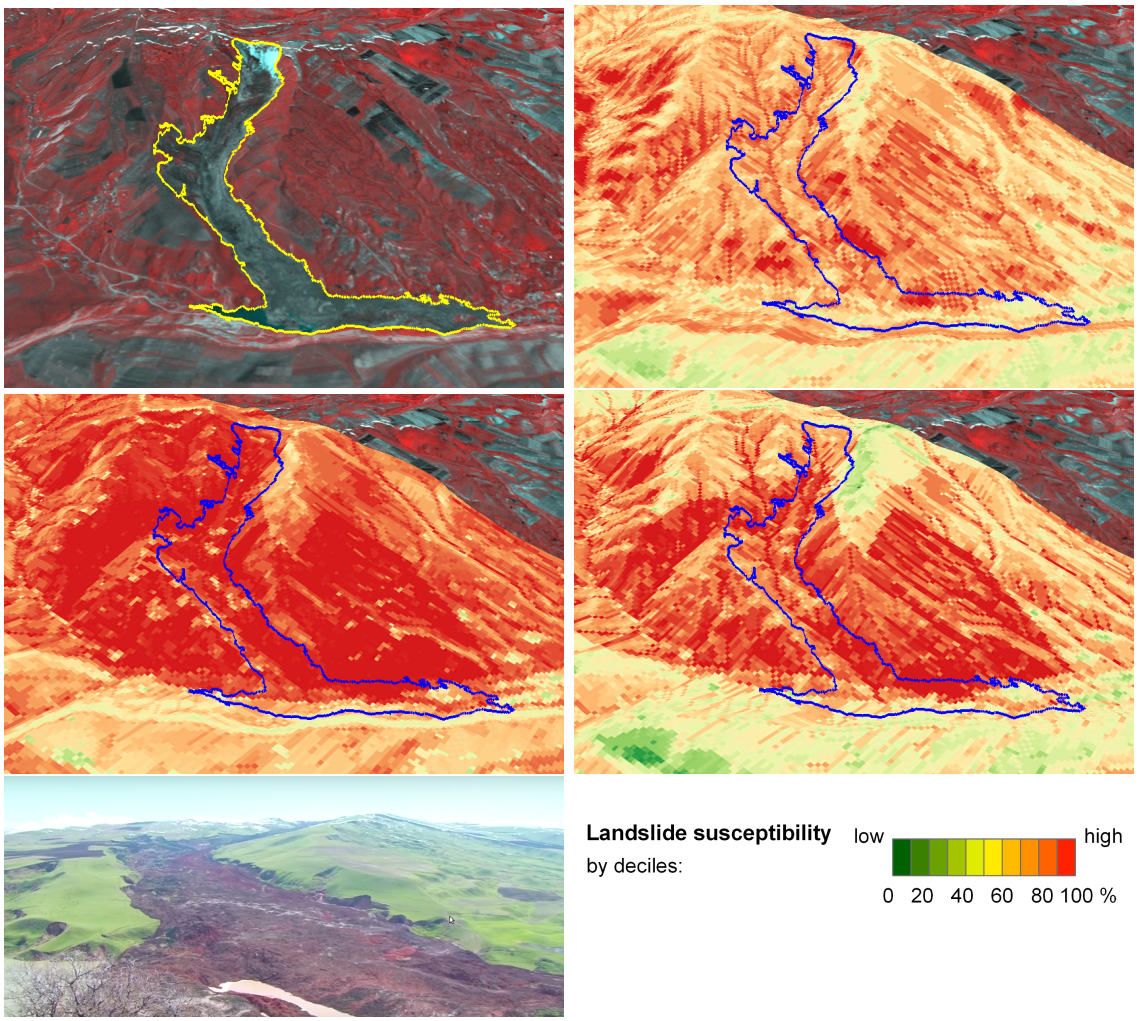

Figure 4.10: The 4.3-km-long Kurbu-Tash landslide that occurred in April 2017 (extent determined by automated detection) overlaid over a false-color near-infrared RapidEye image acquired on 2 May 2017 (**top left**). Overlay with the susceptibility map based on the highest points of automatically detected landslides (**top right**), masses of automatically detected landslides (**middle right**) and expert interpretation (**middle left**). (**Bottom left**): a video frame by AKIpress (AKIpress, 2017) acquired in the first half of May 2017 showing the landslide mass. Elevation data: Google Earth.

slope within subset S1 of the study area (Figure 4.4), which had not been affected by landsliding over the past 30 years. However, the expert-based landslide mapping had revealed morphological indicators of ancient landsliding, which were included in this inventory. Nevertheless, both susceptibility maps depict the highest susceptibility values for similar regions and are characterized by acceptable to high predictive performances.

Overall, the multi-temporal landslide inventory results in a susceptibility assessment that better reflects the landslide properties observed in recent decades. Whether this is an advantage or a disadvantage also depends on the ratio between the length of the observation period and the landslide recurrence intervals in the study area. The model based on the inventory derived by automated detection underestimates the susceptibility of predisposing factor combinations that are only

activated under conditions not observed over the past 30 years. However, the automated approach does not require the involvement of a landslide expert who is capable of performing the manual landslide mapping. Therefore, it can be used to generate an inventory that is suitable for an initial susceptibility assessment, which can then be further evaluated.

Moreover, in the case of a large area of interest, the derivation of a historical inventory may be too labor intensive to perform. In contrast, the detailed analysis of a smaller area may require a spatially more focused inventory incorporating all available information sources, whereas the automated inventory allows outlining those parts of the study area that are characterized by the highest recent landslide activity. Therefore, we consider both types of inventories as valuable information sources on landslide occurrence that complement each other, and both need to be considered in a comprehensive susceptibility analysis.

When comparing the susceptibility models resulting from incorporating different landslide properties—polygon-based whole landslide masses versus the point-based approximation of landslide initiation zones—a spatial shift of higher susceptibility values toward the more elevated parts of the slope is observed. Moreover, the susceptibility model based on highest points is biased toward small landslides because they receive the same weight in the model as very large slope failures. In the study area, small landslides are mostly found in more consolidated rocks (which are less likely to experience highly hazardous slope failures), whereas the weakly consolidated sediments produce the largest and most dangerous landslides. Thus, the approach based on highest points effectively underestimates the hazard in the most affected areas. Therefore, the susceptibility model based on whole landslide masses also needs to be considered. The two susceptibility models can complement each other and should both be taken into account for comprehensively characterizing the different aspects of landslide susceptibility. This also points to the advantage of GIS-based landslide susceptibility and hazard assessment over conventional expert-based mapping approaches consisting of the flexible consideration of different input information for deriving a variety of complementary models that can be further evaluated by landslide experts.

This situation is also illustrated by the example of the Kurbu-Tash landslide. For both susceptibility models (expert and automated) that are based on the use of landslide masses, the susceptibility values within the area of the Kurbu-Tash landslide are rather high: a large part of the area covered by the landslide belongs to the 20% of the study area that is characterized by the highest susceptibility. In contrast, the model that uses the highest point of landslide initiation results in lower susceptibility values for the area of the Kurbu-Tash landslide. This example shows the effect of using different landslide properties on the model results, leading to an underestimation of the susceptibility originating from large landslides. Moreover, the high landslide activity in 2017 indicates that there is a considerable need for future continuation of systematic large-area landslide monitoring in southern Kyrgyzstan to further improve the susceptibility and hazard assessment.

Due to the availability of the remote-sensing-based multi-temporal inventory, we were able to assess not only the landslide susceptibility but also the exceedance probability of landsliding. This is the first step in analyzing the temporal aspect of the landslide hazard in this region. Further research is needed to link the differences in

landslide frequency between the years to changes in the potential triggering factors, such as the hydrometeorological conditions. Once high-resolution multi-temporal imagery are available for a period of several decades for southern Kyrgyzstan, landslide hazard assessments can focus more on the temporal analyses derived from the landslide frequencies. In this case, the analyses will no longer be affected by the scarcity of data on predisposing factors.

For this purpose, future continuation of systematic landslide monitoring in the study area is crucial. It will extend the observation period and possibly include landslide locations with a combination of predisposing factors that have not yet been represented in our susceptibility model (Wang et al., 2015). More importantly, the landslide activity in the study area is characterized by occasional very intensive years with a dramatic increase in landslide activity. In such intensive years, landslides may become activated on slopes that have been stable for the past decades and possibly have not been accounted for by the susceptibility model based on the automatically detected data. The results of automated landslide detection have captured the peak in landslide occurrence in 2003–2004 (Behling et al., 2016), but the landslide activity of the even larger peak of 1994 could not be adequately reconstructed because of the lack of suitable satellite remote sensing data. The continuation of monitoring including the most recent peak year of 2017 and beyond provides an opportunity to improve our understanding of the landslide processes in the study area and is thus the basis for subsequent susceptibility and hazard assessments.

The results of this study show that landslide susceptibility and hazard assessments based on satellite remote sensing are particularly suitable for regions with high process activity and, at the same time, for limited information on landslide occurrence and predisposing factors due to insufficient means for landslide mapping and subsequent hazard analysis. Remote-sensing-based hazard assessment allows the efficient identification of the particularly hazardous areas, which can then be subject to more concentrated monitoring and mitigation efforts. In this context, the recent launches of the Sentinel-2A and 2B satellite remote sensing missions are of crucial importance since they provide satellite imagery of suitable spatial and temporal resolutions at the global scale free of charge, enabling multi-temporal landslide monitoring worldwide. We have already performed the first preliminary investigations on the potential of Sentinel 2A/B to automatically derive landslide failures that occurred during the most recent period of high landslide activity of spring 2017 in southern Kyrgyzstan. The first results indicated landslide detection with high spatial detail and completeness over large areas, which will even further increase when the full temporal resolution of the 2A/B Sentinel constellation is enabled worldwide. However, even under the condition of thus far limited revisit time of data acquisition, the principal suitability of these data as a basis for automated derivation of multi-temporal landslide inventories has already been proven.

4.6 Conclusions

Our investigations have shown that satellite remote sensing can support landslide susceptibility and hazard analysis in multiple ways, particularly for large data-scarce regions such as southern Kyrgyzstan. We have utilized remote sensing at every stage of the investigation, whereas the main emphasis has been placed on the influence of

landslide inventory properties on the results of susceptibility and hazard assessments. In our work, we have shown that satellite remote sensing methods can greatly support the expert-based derivation of historical landslide inventories and the derivation of multi-temporal inventories for the entire time period of suitable satellite remote sensing data availability. However, the latter requires the use of automated methods to analyze multi-temporal time series data covering several decades. The resulting systematic spatio-temporal inventories are the main prerequisite for analyzing the temporal component of landslide hazard.

Since both of the derived landslide inventories contain object-based information on past landslide occurrences, we were able to calculate different susceptibility models that emphasize different aspects of landslide activity in the study area. However, for all of these models, AUROC values of approximately 0.8 were achieved. Hence, we conclude that, in our study area, the different models can be used in a complementary way to perform a comprehensive characterization of landslide susceptibility.

The shorter 30-year observation period of the automatically derived multi-temporal inventory results in a susceptibility map with a stronger representation of the properties of the recent landsliding. In contrast, the inventory derived by expert mapping contains a longer time span of landslide occurrence. However, in both susceptibility maps, the highest susceptibility values are observed for similar areas. We conclude that the results of the automated landslide detection provide a suitable landslide inventory for a reliable large-area landslide susceptibility assessment.

We also used the temporal information of the automatically derived multi-temporal landslide inventory to assess the temporal component of landslide hazard in the form of the exceedance probability. Both versions of the susceptibility assessment are useful for showing that the slopes that are more likely to produce a landslide under today's conditions, as well as areas that may have a high hazardous potential in the future when natural conditions might arise again that have already caused intense landsliding in the past.

Moreover, our investigations have shown that the specific landslide properties used in the susceptibility analysis have a significant influence on the results. If the model is based on the highest point covered by the mapped landslide representing an approximation of the main scarp, then the resulting susceptibility model indicates where landslide initiation is most likely to occur. In contrast, using the complete landslide polygons results in a map that emphasizes the areas that are most likely to be covered by landslide masses. Ideally, both maps should be available to provide a better understanding of both aspects of landslide susceptibility analysis.

The presented approach is based on the extensive use of remote sensing and GIS methods, enabling an objective, quantitative and comprehensive characterization of the different aspects of landslide susceptibility and hazard. The temporal component of landslide hazard can only be assessed if a multi-temporal inventory is available. Our investigations have shown that multi-temporal satellite remote sensing has great potential for deriving such inventories, which will further increase upon the global availability of Sentinel-2A/B data.

4.7 Acknowledgments

We thank the three anonymous reviewers and the Editor for their constructive comments, which were very helpful for improving the paper. Research presented in this paper has been funded by the German Ministry of Research and Technology (BMBF) as part of the Tien Shan—Pamir Monitoring Program (TIPTIMON) and PROGRESS projects. We kindly thank our colleagues from the Ministry of Emergency Situations of Kyrgyzstan and Central Asian Institute for Applied Geosciences (CAIAG) in Bishkek for their expert advice, valuable discussions and assistance during field campaigns.

4.8 Author Contributions

Darya Golovko and Sigrid Roessner designed the research and prepared the manuscript. Darya Golovko performed the hazard analysis. Robert Behling developed the method for automated landslide detection and applied it to derive the multi-temporal landslide inventory dataset. Hans-Ulrich Wetzel performed the expert landslide mapping. Sigrid Roessner, Birgit Kleinschmit and Robert Behling contributed to the discussion and general paper review.

4.9 Conflict of Interests

The authors declare no conflict of interest. The founding sponsors had no role in the design of the study; in the collection, analyses, or interpretation of data; in the writing of the manuscript, and in the decision to publish the results.

Chapter 5

Synthesis

5.1 Conclusions

In this section, the research questions posed in the Introduction of this thesis will be answered based on the findings published in the three publications that were presented in the chapters 2-4.

5.1.1 Chapter 2: Multi-Source Landslide Inventory

What data sources on landslide activity can be used and what are their characteristics?

The large size of the study area and the relative data scarcity make it necessary to combine any available information on landslides. For a long time, landslide investigations of the local authorities and field visits were the principal sources of landslide data for the study area. Much of these data were available in the form of text and tables rather than spatial data formats that could directly be used in a GIS. Naturally, the precision of these data was limited. Since 2010, research has been conducted at the German Research Centre for Geosciences (Behling et al., 2014b,a, 2016) to develop an automated approach for a comprehensive, systematic and more accurate detection of landslide objects from multi-temporal optical satellite images. However, the results of the automated detection only covered the time period of 2009-2013 at the time of publication of the first paper (chapter 2 of this thesis). A workflow was developed as part of chapter 2 to prepare the available heterogeneous landslide data for further use for spatial analyses and evaluate the properties of the different data sources.

What types of landslide inventories are suitable in the context of the present research and which of them can be produced for the study area?

The pattern of landsliding in southern Kyrgyzstan is characterized by strong variations in the intensity of landslide activity between the years and frequent reactivations within the same slopes. To document the landslide activity as fully as possible, a multi-temporal landslide inventory is the most suitable inventory type. A multi-temporal inventory makes it possible to carry out analyses related to the landslide frequency and thus to the temporal aspect of the landslide hazard. Fur-

thermore, the delineation of individual landslide polygons with high spatial accuracy enables analyses related to the landslide geometry. However, such an inventory is the most difficult one to obtain.

Out of the landslide information sources available for the study area, only the results of automated landslide detection provide data that can be used as a multi-temporal object-based landslide inventory, albeit the short time period covered by these data. The temporal coverage was significantly extended in later studies by Behling et al. (2016). Other inventory components can be useful depending on the application. E.g. for the susceptibility mapping, the visual landslide interpretation by an expert can be very useful because it covers the largest area, whereas the individual landslide objects and landslide failure dates are irrelevant to this type of analysis. In this case, we can speak of a geomorphological historical inventory (Guzzetti et al., 2012). By contrast, when the temporal information on landslide occurrence over a long time period is needed, the data of the local authorities can be used. These are an example of an archive landslide inventory or a combination of several seasonal inventories (Guzzetti et al., 2012).

What is the role of remote sensing and GIS in the compilation of a landslide inventory for southern Kyrgyzstan?

The role of remote sensing and GIS is a crucial one due to the lack of detailed spatial data from other sources and the large size of the study area.

Optical satellite images are the basis for both automated and manual landslide mapping. The spatial and temporal precision of the resulting inventories is determined by the spatial and temporal resolution of the available imagery. For the manual mapping, the general overview of the region provided by optical images (combined with a geological map) is the basis for the expert evaluation of the geomorphological setting of the surrounding area. Optical satellite images, combined with a topographic map, were used to verify and specify the landslide locations and extents as well as resolve any discrepancies when transferring the landslide information from verbal descriptions into a spatial form.

The digital elevation models were used in this study to clarify the position of landslides in ambiguous cases and to provide an overview of the area and individual slopes affected by landslides. In the other two papers, the DEM is important to calculate geometrical landslide attribues and to derive landslide predisposing factors.

The use of a GIS was important at every stage of the work: to establish the common spatial reference for all the landslide and other data, to enable efficient and precise data queries and analyses. This includes scenarios in which similar types of analyses have to be performed repeatedly, e.g. upon the availability of new satellite imagery or new landslides that were identified with the automated approach. In such cases, the use of customized GIS methods can save a lot of time and effort.

What is the spatial and temporal precision of the available landslide data and how can they be accommodated in a single inventory?

The inventory components are characterized by varying spatial and temporal precision, which is shown in Fig. 5.1. The data collected by the local authorities (report by Ibatulin and the ministry tables) have high temporal precision and cover a long time period but lack spatial accuracy and completeness, especially for smaller

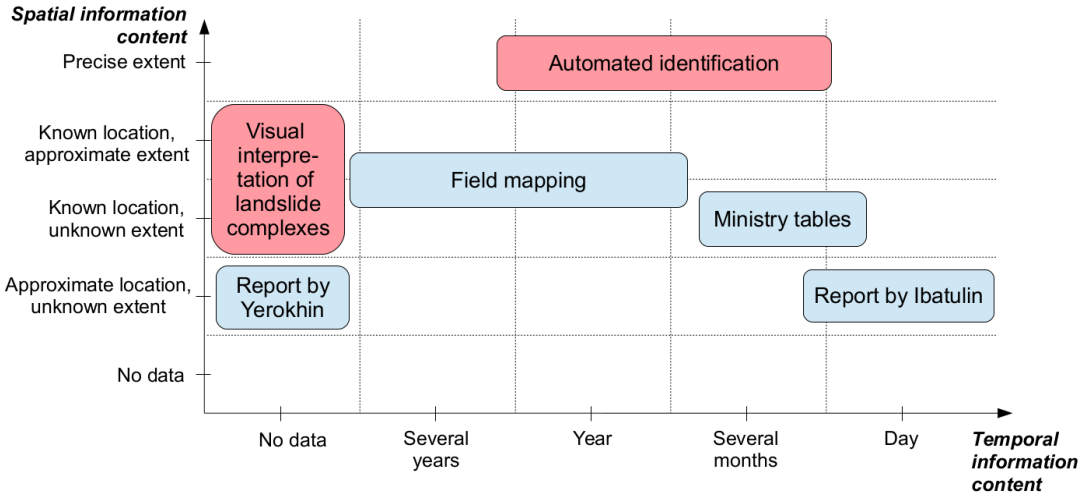

Figure 5.1: Spatial and temporal information content of principle data sources for the landslide inventory.

landslides. The results of visual expert landslide mapping offer the most complete interpretation of the areas that have been affected by landsliding in the past, but without any temporal reference. Results of automated landslide detection are optimal when both the spatial and the temporal precision content are important.

Merging all the inventory components in a single inventory is not possible or desirable. Rather, one or the other component(s) should be chosen depending on the application. For example, if we need the most complete estimate of the areas affected by landsliding in the past (e.g. for susceptibility mapping), then the results of visual image interpretation by an expert are the most suitable dataset. On the other hand, if the dates of landslide occurrence are of interest, then preference is to be given to the results of automated landslide detection (if the inventory completeness is crucial and the breivity time period covered is not a problem) or to the data collected by the local authorities (if we are interested in large landslides over a longer time period).

5.1.2 Chapter 3: Automated Derivation and Analysis of Landslide Attributes

To derive landslide attributes in a GIS, the most suitable landslide data sources are those where the outlines of the landslides are represented by polygons and individual failures are differentiated. Therefore, three of the inventory components from the previous chapter were used: landslides recorded after the report by Ibatulin (2011), landslides mapped in the field and landslides derived with the automated approach from multi-temporal satellite images. Additionally, the results of automated landslide detection covering a longer time period (1986-2013) and a subset of the study area were used as the fourth dataset. This long-term dataset was not merged with the results of automated detection for 2009-2013 for two reasons. Firstly, the longer time period included periods of peak landslide activity, when landslides may have had different characteristics that in the periods of low landslide activity. Secondly, the short-term dataset covers the complete study area, whereas the long-term dataset only covers a subset of it.

Which landslides attributes are often included into landslide inventories and which ones of them can be derived automatically for large inventories?

The attributes that are often included into landslide inventories have been summarized in Tab. 2.1. The exact composition of the attribute list depends on the objective of the inventory, type of landslide processes, the resources available for data collection, etc. Automated derivation using GIS and remote sensing is possible for attributes related to the landslide position, dimensions and geo-environmental characteristics. Provided that data and specific knowledge of the study area in question are available, the automated derivation of other attributes may be possible, e.g. estimates can be made on the landslide types, failure dates, triggers, consequences and elements at risk.

If a landslide inventory is a result of field investigations, landslide attributes can be determined directly during the field mapping. In the case of southern Kyrgyzstan, the most detailed object-based landslide inventory was produced by automated landslide detection from remote sensing data. Thus there is a large number of landslide polygons with known landslide locations and failure dates (periods). For the derivation of the other attributes, efficient GIS-based approaches are an important tool. In this study, landslide length, compactness, slope, distance from landslide toe to stream and geology were derived.

Which values of landslide attributes are particularly frequent in the study area?

In the study area, a significant share of landslides occur in Cretaceous and Paleogene units, especially if the landslide size is taken into consideration. Furthermore, Q2 (Middle Quaternary) is closely linked to landslide occurrence. Other favourable conditions for landsliding are locations of northwestern, northern and northeastern exposition and slopes of 15-25 degrees (for very large landslides, even gentler slopes of ≈15 degrees). Periods of very active landsliding in southern Kyrgyzstan been have found to produce larger landslides.

How do the values of landslide attributes differ for landslides documented from different sources?

The landslides mapped after the report by Ibatulin (2011) concentrate on the largest slope failures. The results of automated landslide detection include smaller landslides, which were mostly omitted by the other data sources. This affects the distributions of the attribute values for each data source.The omission of smaller landslides from the report by Ibatulin (2011) and the field mapping results leads to the underrepresentation of landslides with small length and on steep slopes. The compactness values and the distribution of landslides by the geology class were very similar for all the data sources.

Are there differences in landslide properties between different parts of the study area?

The differences in the landslide properties between the different parts of the study area are very pronounced. They are closely related to the geological formations present in each part. These differences reflect on other attributes as well because the geology formation determines the size of a typical landslide it can produce.

What is the size (maximal and minimal area) of landslides that are sufficiently represented in the database (e.g. in order to estimate their frequency / return period)?

The results of automated landslide detection are the most systematic inventory component. A comparison of the distribution of landslide sizes presented in Fig. 3.4 to the power-law behavior described by Malamud et al. (2004) shows that the results of long-term landslide detection systematically map landslides starting from the size of 10,000 m^2. This limit is somewhat lower for the results of short-term automated landslide detection because they are based exclusively on high-resolution RapidEye images. For the landslides mapped in the field, the limit is at approximately 50,000 m^2. The dataset based on the report by Ibatulin (2011) has fewer than 100 landslides and significant data gaps, so that a comparison with the power-law distribution is not possible.

5.1.3 Chapter 4: Susceptibility Assessment

How do the properties of the underlying landslide inventory influence the results of landslide susceptibility mapping?

By the example of a multi-temporal inventory covering the last 30 years, and a historical inventory recording all visible traces of landsliding over a long period of time with unknown failure dates, a significant influence of the inventory data properties on the resulting susceptibility maps was found. The shorter time period covered by the multi-temporal inventory resulted in a susceptibility assessment more focused on the characteristics of the recent landslide activity. Furthermore, the inclusion of smaller landslides into the multi-temporal inventory in locations outside of the major landslide hotspots led to higher susceptibility values in such locations as compared to when the historical inventory was used. This is important considering that many landslide studies focus on calculating landslide susceptibility with the inventory that is available and do not evaluate the impact of how the inventory choice affected the result. The effect of the inventory can be augmented if the observation period is particularly short or if conditions in the study area have changed (e.g. due to climate change or an outstanding event such as a large earthquake)

What are the most important landslide predisposing factors in the study area?

Five factors were included into the susceptibility model in this study: geology, aspect, slope, elevation and stream power index. Their importance was evaluated using the AUROC value of a single-factor susceptibility model for each of them. Geology was the most important factor in all susceptibility models, whereas all other factors also contributed to improving the model. This choice of factors was largely determined by the ability to derive the factor data from the available DEM. If data had been available on other geo-environmental characteristics (e.g. faults, lithological composition, ground water, etc.), they may have also been important as landslide predisposing factors.

How can remote sensing and GIS contribute to the acquisition and clarification of information on landslide predisposing factors in the study area?

Remote sensing plays a very important role not just for the acquisition of landslide data, but also of the information on landslide predisposing factors in the study

area. The availability of detailed spatial data with sufficient spatial resolution and a coverage of the complete study area is limited. Out of the five factors used in the susceptibility models in chapter 3, four were derived from a DEM (ALOS DEM World - 30m, 2017) using GIS tools availale e.g. in the package SAGA GIS. Remote sensing was essential to obtain data on the fifth factor, geology, as well. The geological map had been created in the process of expert reinterpretation and clarification of several paper maps, which was widely supported by optical satellite imagery.

How can the susceptibility assessment be supplemented to include the temporary aspect of landslide hazard?

The central part of the research presented in chapter 4 focuses on landslide susceptibility. Yet the availability of a multi-temporal inventory allows to involve the temporal aspect of landslide hazard into the analysis as well. In southern Kyrgyzstan, there is no direct temporal link between the occurrence of triggers (hydrometeorological conditions and seismicity) and landslide activations, so that it is difficult to establish a causal relationship between them.

Therefore, an approach was selected based on the landslide frequency as recorded in the multi-temporal landslide inventory. Because of the varying availability of the satellite data used for the derivation of the inventory, the time period with sufficient representation of the landslides had to be determined first.

These results are not exhaustive but rather are an initial approximation of the temporal dimension of the landslide hazard in the area. Further satellite observations are necessary to prolong the period covered by the multi-temporal landslide inventory in order to make more reliable statements on landslide frequency in the study area. Such an extended landslide susceptibility assessment with elements of temporal analysis can be a valid alternative for regions like southern Kyrgyzstan where landslide triggering factors exert continuous rather than event-based influence on the landslide-prone slopes.

5.2 Relevance of Acquired Results for Study Area

The results of automated landslide detection (Behling et al., 2014b,a, 2016) are the single most comprehensive and systematic record of landslide activity for southern Kyrgyzstan. With over 1,500 landslides with their precise spatial extents and failure dates (periods), the quality and completeness of these data is unprecendented for the study area. As the acquisition of high-resolution optical satellite data continues, the dataset resulting from automated landslide detection can be extended in time and provide an even more realistic representation of the landslide activity in the region.

The combination of these data with the other information sources in a multi-source landslide inventory summarizes the available spatial landslide data for the region and makes it usable in a GIS. The inclusion of the other sources of landslide information compensates for the relatively short 30-year period covered by the results of automated landslide detection so far. Furthermore, the compilation of the multi-source inventory included transferring the verbal descriptions of landslides and sometimes oral knowledge of the local experts into digital spatial data, which can

potentially facilitate the further use of the archive landslide data in the region. This is important considering that the landslide investigations by the local authorities had been carried out at a larger scale before 1991.

The systematization of all the landslide data within a common spatial reference, which has been performed in this study, is the basis for providing access to it in the future. A prototype that can facilitate this task has been developed as a part of this thesis. It has been implemented as the Landslide Tools plugin for QGIS. It is an example of how GIS tools can be customized for reseach questions dealing with landslide inventories and landslide hazard assessment. The choice of the open-source software QGIS implies no license fees need to be paid, and the relatively easy user interface of QGIS (as compared e.g. to ArcGIS) is beneficial for people who are new to GIS. Depending on the needs of the authorities and other stakeholders working with the data, a customized interface for data queries and relevant tools for spatial analyses can be further implemented. An example of such tools are the scripts for the derivation of geometric landslide attributes that are part of the plugin.

The attributes that were derived in the course of this research project can be useful for people who study landslides in the region. The Central-Asian Institute for Applied Geosciences (CAIAG) in Bishkek is currently undertaking an effort to map landslides (as points) and their attributes in selected administrative districts of southern Kyrgyzstan. It would be interesting to compare the attribute distributions in their inventory to the ones obtained in the course of this study.

Because the results of automated landslide detection are available over the whole study area independently of the proximity to settlements or roads, landslide-prone slopes were identified that had not previously been reported by the local authorities. This reflected on the results of the susceptibility mapping. An example is the area of the Kurbu-Tash landslide shown in Fig. 4.10.

5.3 Transferability to Other Regions

Much of the landslide research that established the methodology for the various stages of landslide hazard and risk assessment was conducted in countries like Italy, Belgium, Austria, etc. These are countries with high population density, a long landslide record and considerable funding involved in the landslide research. E.g. the landslide inventory in Italy (Italian Landslide Inventory (IFFI) Project, 2017) contains over 600,000 landslides covering the territory of 23,000 km^2, which represents 7.5% of the national territory. Another example is the landslide inventory in Austria with over 13,000 landslides mapped from LiDAR data with the spatial resolution of 1x1 m (Petschko et al., 2016).

The situation in Kyrgyzstan is quite different. Due to the limited funding, the relatively young age of the permanent settlements in the area and discontinuities in landslide monitoring and data archiving due to the breakup of the Soviet Union, the data available without the use of remote sensing are very scarce. At the same time, this tectonically active region produces very large and dangerous landslides. The benefits of landslide observation based on remotely sensed data are particularly notable in such settings.

This situation is not exceptional. A lot of countries face the same or harsher problems; at the same time they are located in the regions with the highest landslide activity and face the majority of fatalities due to landsliding. An example is the very large landslide in Afghanistan in Argo district of Badakhshan province in May 2014 with, according to different estimates, 300–2700 (Petley, 2017d) fatalities. The approach presented in this study is especially suitable for regions like this, with a limited landslide record and general data scarcity.

The proposed approach does not rely on any assumptions that are specific for southern Kyrgyzstan only. E.g. a totally different set of factors can be included in the susceptibility model, without the requirement of a certain measurement scale (nominal, ordinal, etc.) or linearity. Because the automated detection relies on the change of NDVI values in time, it is suitable for regions where green vegetation is available at least in one of the seasons (and the cloud cover in that season enables observations from space). Landslide locations then exhibit a spectral contrast compared to unaffected terrain and can thus be differentiated. In regions without sufficient vegetation or with frequent cloud coverage, SAR methods are an alternative.

A good knowledge of the study area in question is always desirable, but the availability of an expert in geology (or other disciplines) of a particular region is not a must if the approach for automated landslide detection from satellite imagery is used. I.e. regions can be investigated for which little expert knowledge is available.

5.4 Methodological Contribution

Although the work presented here focuses on the study area in southern Kyrgyzstan, many findings address methodological aspects of the different steps of landslide hazard assessment. The scenario of a large landslide inventory that has been derived from time series of satellite images and is updated regularly as new images are acquired will become more widespread in the future due to the growing availability of high-resolution imagery and of efficient methods for its processing. This scenario requires the derivation of the attributes for the new landslides, updates of the susceptibility and hazard maps, etc. The automated approach proposed in this thesis makes it possible to carry out these tasks efficiently and in an objective manner.

The compilation of the multi-source inventory described in chapter 2 shows an approach on how remote sensing and GIS can be used to collect any heterogeneous data available for a data-scarce area and make it usable in a single system. In the case of data with very varying spatial precision, the present study suggests the use of appropriate mapping units (e.g. terrain units that represent slopes) as a way to accommodate the imprecisions and possible errors in the landslide data by transferring the analysis to a higher spatial level. Because landslides tend to have runout zones that may be located far away from the initiation zone, approximating the initiation zone as the highest part of the landslide polygon has been suggested and used to assign the lanslides to mapping units.

Chapter 3 of this study addresses the automated derivation of landslide attributes, which has received less attention within the framework of landslide hazard assessment. An approach has been suggested to calculate the landslide length and

width by combining vector landslide data and a DEM. Even though these attributes have been defined (IAEG Commission on Landslides, 2017) and are commonly used, it is difficult to apply their definitions in case of complex landslide geometries and long runout areas. Automated attribute derivation allows for more reproducibility compared to manual methods. It was found that if a landslide inventory is acquired from remote sensing images and the landslides preserve the zigzag-like boundaries that are typical for automated raster-to-vector conversions, then using the landslide perimeter to calculate any geometrical attributes will be biased and should be avoided.

The study of the influence of the landslide inventory properties on the results of susceptibility assessment has shown that this infleunce is quite substantial and should be considered when performing susceptibility assessment. The interpretation of a susceptibility map is only meaningful if it is clear what the obtained results represent: the likelihood of the area in question to initiate a landslide, to be hit by a landslide, etc.; and to which type of landslide activity the results apply (e.g. recent or historical).

Overall, the methodological framework for quantitative data-driven landslide hazard assessment (Guzzetti et al., 2005; Corominas et al., 2014) as shown in Fig. 1.3 can be regarded not as a sequence of operations where each result only serves as input data for the next step, but rather as a toolbox where tools can be applied and combined depending on the study objectives and data availability and their results used to assess various aspects of the landslide hazard. This is even more true for data-scarce regions.

5.5 Outlook

This study presented an approach for landslide hazard assessment in data-scarce regions that relies on the use of remote sensing and GIS. This approach resulted in a substantial improvement of the quality, systematicity and objectivity of the analyses. As the quality and availability of remotely sensed data increases in the future, the automated methods for landslide detection, attribute derivation and susceptibility analysis will be gaining in importance. The recent launch of the Sentinel-2A and -2B satellite missions that will be delivering optical data with the spatial resolution of up to 10 m and the revisit time of 5 days (ESA Sentinel Online, 2017) implies that it will be possible to document the landslide processes with greater detail and better investigate the link between the variations of the landslide predisposing and triggering factors and the landslide activity.

The continuation of observations beyond the 30-year record available so far will make it possible to analyze the temporal aspect of the landslide hazard more comprehensively and hopefully document the years with peak landslide activity much more fully. One of such peaks in 2003-2004 was documented reasonably well (Behling et al., 2016). However, during the even stronger peak of 1994 a lot of landslides were omitted from the inventory due to the long gap between the available images of 1990 and 1997/1998 and a coarser spatial resolution of the early imagery. The year 2017 has been one of such intensive years with a manifold increase in landslide numbers and sizes. It will probably be the best documented record of peak landslide

activity so far, in terms of both spatial and temporal resolution.

If the slope failures are dated more precisely (i.e. the period between the before and after images is short), it will be interesting to analyze to which degree slope failures can be traced back to changes in the triggering factors (e.g. start of the snowmelt, intensive precipitation or an earthquake) shortly beforehand. It is also possible that the link between the two is quite complex, e.g. if there is a substantial delay between rainfall and the response in the form of landsliding due to the infiltration of water into the ground, etc. It remains to be investigated to what extent the conditions under which landslides occur are altered due to the effects of climate change, e.g. in the patterns of snow accumulation and ground water levels.

For a better quality of the landslide hazard assessment, not only the landslide data needs to improve, but also the factor data. In this study, 30-meter digital elevation models were used. If a DEM with higher spatial resolution becomes available for the region, further predisposing factors (e.g. various types of curvature) could be derived that are not reasonable with the 30-meter DEM used in this thesis.

The research carried out in the framework of this thesis took place in a scientific institution in Germany. Therefore, the question arises about how to bridge the gap between the two countries and between the scientific community and the people who study landslides for a practical purpose in the region. This question includes the issue on how the results of these and similar analyses can be comminucated to the decision-makers and local residents. The data and the customized GIS tools produced in the course of this study could be shared with the local landslide researchers or new tools may be developed that correspond to their needs. Because of the abundance of landslides in the region, a large portion of the potential living space is potentially affected. Furthermore, the high speed and the energy of loess landslide failures and their sudden onset make timely evacuation difficult. Therefore, it is important to study the possible scenarios that result in active landsliding in the region, inform the local residens when such conditions occur and educate them about how the possible consequences of a slope failures. Moreover, raising awareness of the local residents about the landslide processes may help obtain information about the development of the landslide-prone slopes in time. Developing a tool (perhaps a smartphone application) to obtain warnings from the residents about the state of the slopes they observe and inform them about the current level of landslide hazard may benefit all parties.

Futher methodological research that elaborates on the best practices for landslide hazard assessment should be conducted. E.g. the establishment of best practices for the derivation of landslide attributes is a step towards standardizaton in order to facilitate the exchange of knowledge and data on landslides and to compile large regional inventories. Because landslides are such a diverse phenomenon that occurs in a discrete and localized manner, they are more difficult to observe and document systematically than more continuous and/or area-wide processes. Yet the better access to aerial and satellital data with sufficient spatial resolution will continue to improve the state of knowledge on landslides worldwide. Attempts at a unification of knowledge and at facilitating its exchange would benefit the community of landslide researchers worldwide, like it has happened with other natural hazards, e.g. earthquakes, floods, etc.

References

AKIpress (2017). Massive landslide in Osh region, Kyrgyzstan May 2017. https://akipress.com/video:651/. Accessed: 2017-05-27.

ALOS DEM World - 30m (2017). http://www.eorc.jaxa.jp/ALOS/en/aw3d30/. Accessed: 2017-07-30.

ArcGIS Help (2016). How proximity tools calculate distance. http://pro.arcgis.com/en/pro-app/tool-reference/analysis/how-near-analysis-works.htm. Accessed: 2016-09-14.

ASTER GDEM Version 2 (2011). http://gdem.ersdac.jspacesystems.or.jp/. Accessed: 2015-10-12.

Bedoui, S. E., Guglielmi, Y., Lebourg, T., and Pérez, J.-L. (2009). Deep-seated faillure propagation in a fractured rock slope over 10,000 years: The La Clapiére slope, the south-eastern French Alps. *Geomorphology*, 105:232–238.

Begueria, S. (2006). Validation and Evaluation of Predictive Models in Hazard Assessment and Risk Management. *Nat Hazards*, 37:315–329.

Behling, R. (2016). *Derivation of Spatiotemporal Landslide Activity for Large Areas Using Long-Term Multi-Sensor Satellite Time Series Data*. PhD thesis, Technical University of Berlin, https://depositonce.tu-berlin.de/handle/11303/6277.

Behling, R. and Roessner, S. (2017). Spatiotemporal Landslide Mapper for Large Areas Using Optical Satellite Time Series Data. In Mikos, M., Arbanas, Z., Yin, Y., and Sassa, K., editors, *Advancing Culture of Living with Landslides*. Springer International Publishing, Cham.

Behling, R., Roessner, S., Golovko, D., and Kleinschmit, B. (2016). Derivation of long-term spatiotemporal landslide activity âĂŤ A multi-sensor time series approach. *Remote Sensing of Environment*, 186:88–104.

Behling, R., Roessner, S., Kaufmann, H., and Kleinschmit, B. (2014a). Automated Spatiotemporal Landslide Mapping over Large Areas Using RapidEye Time Series Data. *Remote Sensing*, 6(9):8026–8055.

Behling, R., Roessner, S., Segl, K., Kleinschmit, B., and Kaufmann, H. (2014b). Robust Automated Image Co-Registration of Optical Multi-Sensor Time Series Data: Database Generation for Multi-Temporal Landslide Detection. *Remote Sensing*, 6(3):2572–2600.

Brenning, A. (2007). Spatial prediction models for landslide hazards: review, comparison and evaluation. *Nat. Hazards and Earth Syst. Sci*, 91:853–862.

Burger, W. and Burge, M. J. (2009). *Principles of Digital Image Processing: Core Algorithms*. Springer, London.

CAIAG Geonode (2017). Landslide Hazard. http://geonode.caiag.kg/layers/geonode:landslide. Accessed: 2017-11-12.

Calvello, M., Cascini, L., and Mastroianni, S. (2013). Landslide zoning over large areas from a simple inventory by means of scale-dependent terrain units. *Geomorphology*, 182:33–48.

Chung, C.-J. and Fabbri, A. G. (2008). Predicting landslides for risk analysis – Spatial models tested by a cross-validation technique. *Geomorphology*, 3-4:438–452.

Corominas, J. and Moya, J. (2008). A review of assessing landslide frequency for hazard zoning purposes. *Engineering Geology*, 102:193–213.

Corominas, J., van Westen, C., Frattini, P., Cascini, L., Malet, J.-P., Fotopoulou, S., Catani, F., Van Den Eeckhaut, M., Mavrouli, O., Agliardi, F., Pitilakis, K., Winter, M. G., Pastor, M., Ferlisi, S., Tofani, V., HervÃąs, J., and Smith, J. T. (2014). Recommendations for the quantitative analysis of landslide risk. *Bull Eng Geol Environ*, 73(2):209–263.

Costanzo, D., Rotigliano, E., Irigaray, C., Jiménez-Perálvarez, J. D., and Chacón, J. (2012). Factors selection in landslide susceptibility modelling on large scale following the gis matrix method: application to the river Beiro basin (Spain). *Nat. Hazards and Earth Syst. Sci.*, 12:327–340.

Cruden, D. M. and Varnes, D. J. (1996). Landslide types and processes. In Turner, A. K. and Schuster, R. L., editors, *Landslides, Investigation and Mitigation, Special Report 247*, pages 36–75. Transportation Research Board, Washington, D.C., USA.

Danneels, G., Bordeau, C., Torgoev, I., and Havenith, H.-B. (2008). Geophysical investigation and dynamic modelling of unstable slopes: case-study of Kainama (Kyrgyzstan). *Geophys. J. Int.*, 175:17–34.

Erener, A. and Düzgün (2012). Landslide susceptibility assessment: what are the effects of mapping unit and mapping method? *Environ. Earth Sci.*, 66:859–877.

ESA Sentinel Online (2017). Sentinel-2. https://sentinels.copernicus.eu/web/sentinel/missions/sentinel-2. Accessed: 2017-11-07.

Feld, C., Haberland, C., Schurr, B., Sippl, C., Wetzel, H.-U., Roessner, S., Ickrath, M., Abdybachaev, U., and Orunbaev, S. (2015). Seismotectonic study of the Fergana Region (Southern Kyrgyzstan): distribution and kinematics of local seismicity. *Earth, Planets and Space*, 67(40):13p.

Fressard, M., Thiery, Y., and Marquaire, O. (2014). Which data for quantitative landslide susceptibility mapping at operational scale? Case study of the Pays dâĂŹAuge plateau hillslopes (Normandy, France). *Nat. Hazards Earth Syst. Sci.*, 14:569–588.

Galli, M., Ardizzone, F., Cardinali, M., Guzzetti, F., and Reichenbach, P. (2008). Comparing landslide inventory maps. *Geomorphology*, 94:268–289.

Ghosh, S., Carranza, E. J. M., van Westen, C. J., Jetten, V. G., and Bhattacharya, N. (2011). Selecting and weighting spatial predictors for empirical modeling of landslide susceptibility in the Darjeeling Himalayas (India). *Geomorphology*, 131:35–56.

Ghosh, S., Van Westen, C. J., Carranza, E. J. M., Jetten, V. G., Cardinali, M., Rossi, M., and Guzzetti, F. (2012). Generating event-based landslide maps in a data-scarce Himalayan environment for estimating temporal and magnitude probabilities. *Engineering Geology*, 128:49–62.

Golovko, D., Roessner, S., Behling, R., and Kleinschmit, B. (2017a). Automated derivation and spatio-temporal analysis of landslide properties in southern Kyrgyzstan. *Nat Hazards*, 85:1461–1488.

Golovko, D., Roessner, S., Behling, R., Wetzel, H.-U., and Kleinschmit, B. (2015). Development of Multi-Temporal Landslide Inventory Information System for Southern Kyrgyzstan Using GIS and Satellite Remote Sensing. *PFG Photogrammetrie, Fernerkundung, Geoinformation*, 2:157–172.

Golovko, D., Roessner, S., Behling, R., Wetzel, H.-U., and Kleinschmit, B. (2017b). Evaluation of Remote-Sensing-Based Landslide Inventories for Hazard Assessment in Southern Kyrgyzstan. *Remote Sensing*, 9:943.

Gorum, T., Fan, X., van Westen, C. J., Huang, R. Q., Xu, Q., Tang, C., and Wang, G. (2011). Distribution pattern of earthquake-induced landslides triggered by the 12 May 2008 Wenchuan earthquake. *Geomorphology*, 133:152–167.

Guzzetti, F., Carrara, A., Cardinali, M., and Reichenbach, P. (1999). Landslide hazard evaluation: a review of current techniques and their application in a multi-scale study, Central Italy. *Geomorphology*, 31:181–216.

Guzzetti, F., Mondini, A. C., Cardinali, M., and Fiorucci, F. (2012). Landslide inventory maps: New tools for an old problem. *Earth-Science Reviews*, 112:42–66.

Guzzetti, F., Reichenbach, P., Cardinali, M., Galli, M., and Ardizzone, F. (2005). Probabilistic landslide hazard assessment at basin scale. *Geomorphology*, 72:272–299.

Haberland, C., Abdybachaev, U., Schurr, B., Wetzel, H.-U., Roessner, S., Sargagoev, A., Orunbaev, S., and Janssen, C. (2011). Landslides in Southern Kyrgyzstan: Understanding Tectonic Controls. *Eos, Transactions, American Geophysical Union*, 92(20):169–176.

Havenith, H.-B., Kal'metjeva, Z. A., Mikolaychuk, A. V., Moldobekov, B. D., Meleshko, A. V., Zhantaev, M. M., and Zubovich, A. V., editors (2009). *Atlas of earthquakes in Kyrgyzstan*. CAIAG, Bishkek, Kyrgyzstan.

Havenith, H.-B., Torgoev, A., Schlögel, R., Braun, A., Torgoev, I., and Ischuk, A. (2015). Tien Shan Geohazards Database: Landslide susceptibility and analysis. *Geomorphology*, 249:32–43.

Hervas, J. (2013). Landslide inventory. In Bobrowsky, P. T., editor, *Encyclopedia of Natural Hazards*, pages 610–611.

Hovius, N., Meunier, P., Ching-Weei, Hongey, C., Yue-Gau, C., Dadson, S., Ming-Jame, H., and Lines, M. (2011). Prolonged seismically induced erosion and the mass balance of a large earthquake. *Earth and Planetary Science Letters*, 304:347–355.

IAEG Commission on Landslides (2017). Suggested Nomenclature for landslides. *Bulletin of the International Association of Engineering Geology*, 41:13–16.

Ibatulin, K. V. (2011). *Monitoring of Landslides in Kyrgyzstan*. Ministry of Emergency Situations of the Kyrgyz Republic, Bishkek, Kyrgyzstan. in Russian.

Intarawichian, N. and Dasananda, S. (2011). Frequency ratio model based landslide susceptibility mapping in lower Mae Chaem watershed, Northern Thailand. *Environ Earth Sci*, 64:2271–2285.

International Geotechnical Societies' UNESCO Working Party for World Landslide Inventory (1993). *Multilingual Landslide Glossary*. BiTech Publishers Ltd., Richmond, B.C., Canada.

Italian Landslide Inventory (IFFI) Project (2017). http://www.isprambiente.gov.it/en/projects/soil-and-territory/iffi-project. Accessed: 2017-11-05.

Jebur, M. N., Pradhan, B., and Tehrany, M. S. (2014). Optimization of landslide conditioning factors using very high-resolution airborne laser scanning (LiDAR) data at catchment scale. *Remote Sensing of Environment*, 152:150–165.

Kalmetyeva, Z. A., Mikolaychuk, A. V., Moldobekov, B. D., Meleshko, A. V., Zhantaev, M. M., and Zubovich, A. V. (2009). *Atlas of Earthquakes in Kyrgyzstan*. CAIAG, Bishkek, Kyrgyzstan.

Korzhenkov, A. M., Rogozhin, E. A., Xuhui, S., Qinjian, T., and Yueren, X. (2014). Strong paleoearthquakes along the Talas-Fergana Fault, Kyrgyzstan. *Geodesy and Geodynamics*, 5(1):11–19.

Lebourg, T., Zerathe, S., Fabre, R., Giuliano, J., and Vidal, M. (2014). A Late Holocene deep-seated landslide in the northern French Pyrenees. *Geomorphology*, 208:1–10.

Lee, S. and Talib, J. A. (2005). Probabilistic landslide susceptibility and factor effect analysis. *Environ Geol*, 47:982–990.

Legorreta Paulín, G., Pouget, S., Bursik, M., Aceves Quesada, F., and Contreras, T. (2016). Comparing landslide susceptibility models in the Río El Estado watershed on the SW flank of the Pico de Orizaba volcano, Mexico. *Nat Hazards*, 80:127–139.

Lemzin, I. N. (2005). *Faults of the Kyrgyz Part of the Tian-Shan*. Ilim, Bishkek, Kyrgyzstan. in Russian.

Li, P., Li, T., Lu, Z., and Li, J. (2017). Study on Dynamic Response of Novel Masonry Structures Impacted by Debris Flow. *Sustainability*, 9(7):22p.

Longoni, L., Papini, M., Arosio, D., Zanzi, L., and Brambilla, D. (2014). A new geological model for Spriana landslide. *Bull Eng Geol Environ*, 73:959–970.

Malamud, B. D., Turcotte, D. L., Guzzetti, F., and Reichenbach, P. (2004). Landslide inventories and their statistical properties. *Earth Surf. Process. Landforms*, 29(6):687–711.

Mancini, F., Ceppi, C., and Ritrovato, G. (2010). GIS and statistical analysis for landslide susceptibility mapping in the Daunia area, Italy. *Nat. Hazards and Earth Syst. Sci.*, 10:1851–1864.

Marc, O. and Hovius, N. (2015). Amalgamation in landslide maps: effect and automatic detection. *Nat. Hazards and Earth Syst. Sci.*, 15:723–733.

Martha, T. R., van Westen, C. J., Kerle, N., Jetten, V., and Kumar, K. V. (2013). Landslide hazard and risk assessment using semi-automatically created landslide inventories. *Geomorphology*, 184:139–150.

Ministry of Emergency Situations of the Kyrgyz Republic (2017). Reasons for the Activization of Landsliding (in Russian). http://mes.kg/ru/news/full/9875.html. Accessed: 2017-05-27.

Mondini, A. C., Marchesini, I., Rosso, M., Chang, K.-T., and Pasquariello, G. Guzzetti, F. (2013). Bayesian framework for mapping and classifying shallow landslides exploiting remote sensing and topographic data. *Geomorphology*, 201:135–147.

Moore, I. D., Grayson, R. B., and Ladson, A. R. (1991). Digital terrain modelling: a review of hydrogical, geomorphological, and biological applications. *Hydrogical Processes*, 5(1):3–30.

Motagh, M., Wetzel, H.-U., Roessner, S., and Kaufmann, H. (2013). A TerraSAR-X InSAR study of landslides in southern Kyrgyzstan, Central Asia. *Remote Sensing Letters*, 4(7):657–666.

Nikulita, M. (2016). Automatic landslide length and width estimation based on the geometric processing of the bounding box and the geomorphometric analysis of DEMs. *Nat. Hazards Earth Syst. Sci.*, 16:2021–2030.

Osserman, R. (1978). The Isoperimetric Inequality. *Bulletin of the American Mathematical Society*, 84(6):1182–1238.

Ouyang, C., Zhao, W., He, S., Wang, D., Zhou, S., An, H. Wang, Z., and Cheng, D. (2017). Numerical modeling and dynamic analysis of the 2017 Xinmo landslide in Maoxian County, China. *Journal of Mountain Science*, 14(9):1701–1711.

Pellicani, R. and Spilotro, G. (2015). Evaluating the quality of landslide inventory maps: comparison between archive and surveyed inventories for the Daunia region (Apulia, Southern Italy). *Bull Eng Geol Environ*, 74:357–367.

Perkins, S. (2017). Death toll from landslides vastly underestimated. http://www.nature.com/news/death-toll-from-landslides-vastly-underestimated-1.11140. Accessed: 2017-11-09.

Petley, D. (2012). Global patterns of loss of life from landslides. *Geology*, 40(10):927–930.

Petley, D. (2017a). Ayu in Osh, Kyrgyzstan: a large landslide has killed 24 people, and another large flowslide in Uzgen region. http://blogs.agu.org/landslideblog/2017/05/02/ayu-1/. Accessed: 2017-05-27.

Petley, D. (2017b). Landslide weirdness: Sri Lanka. https://blogs.agu.org/landslideblog/2017/06/01/landslide-weirdness-sri-lanka/. Accessed: 2017-11-09.

Petley, D. (2017c). Regent landslide in Sierra Leone: the causes of the disaster. https://blogs.agu.org/landslideblog/2017/08/21/regent-landslide-2/. Accessed: 2017-11-09.

Petley, D. (2017d). The Ab Barak landslide in Afghanistan - a foreseeable event? http://blogs.agu.org/landslideblog/2014/05/05/ab-barak-1/. Accessed: 2017-11-05.

Petschko, H., Bell, R., and Glade, T. (2016). Effectiveness of visually analyzing LiDAR DTM derivatives for earth and debris slide inventory mapping for susceptibility modeling. *Landslides*, 13:857–872.

Popescu, M. E. (1994). A suggested method for reporting landslide causes. *Bulletin of the International Association of Engineering Geology*, 50:71–74.

Pourghasemi, H. R., Moradi, H. R., and Fatemi Aghda, S. M. (2013). Landslide susceptibility mapping by binary logistic regression, analytical hierarchy process, and statistical index models and assessment of their performances. *Nat Hazards*, 69(1):749–779.

Pradhan, B. (2013). A comparative study on the predictive ability of the decision tree, support vector machine and neuro-fuzzy models in landslide susceptibility mapping using gis. *Comput. Geosci.*, 51:350–365.

QGIS Development Team (2015). http://qgis.osgeo.org/. Accessed: 2015-10-09.

QGIS Plugin Landslide Tools (2017). https://github.com/daryagol/landslidetools. Accessed: 2017-05-05.

Rabus, B., Eineder, M., Roth, A., and Bamler, R. (2003). The shuttle radar topography mission âĂŞ a new class of digital elevation models acquired by spaceborne radar. *ISPRS Journal of Photogrammetry and Remote Sensing*, 57(4):241–262.

Remondo, J., González, A., Díaz de Terán, J., Cendrero, a., Fabbri, A., and Chung, C.-J. F. (2003). EValidation of Landslide Susceptibility Maps; Examples and Applications from a Case Study in Northern Spain. *Nat Hazards*, 30:437–449.

Roessner, S., Behling, R., Segl, K., Golovko, D., Wetzel, H.-U., and Kaufmann, H. (2014). Automated remote sensing based landslide detection for landslide inventories. In Sassa, K., Canuti, P., and Yin, Y., editors, *Landslide Science for a Safer Geoenvironment, Volume 2: Methods of Landslide Studies*. Springer International Publishing, Cham.

Roessner, S., Wetzel, H.-U., and Kaufmann, H. (2006). Satellite Remote Sensing and GIS for Analysis of Mass Movements with Potential for Dam Formation. *Italian Journal of Engineering Geology and Environment*, Special Issue 1:103–114.

Roessner, S., Wetzel, H.-U., Kaufmann, H., and Sarnagoev, A. (2005). Potential of Satellite Remote Sensing and GIS for Landslide Hazard Assessment in Southern Kyrgyzstan (Central Asia). *Nat Hazards*, 35(3):395–416.

Schlögel, R., Malet, J.-P., Reichenbach, P., Remaître, A., and Doubre, C. (2015). Analysis of a landslide multi-date inventory in a complex mountain landscape: the Ubaye valley case study. *Nat. Hazards and Earth Syst. Sci.*, 15:2369–2389.

Steger, S., Brenning, A., Bell, R., and Glade, T. (2016). The propagation of inventory-based positional errors into statistical landslide susceptibility models. *Nat. Hazards and Earth Syst. Sci.*, 16:2729–2745.

Steger, S., Brenning, A., Bell, R., Petschko, H., and Glade, T. (2017). Exploring discrepancies between quantitative validation results and the geomorphic plausibility of statistical landslide susceptibility maps. *Geomorphology*, 262:8–23.

Su, C., Wang, L., Wang, X., Huang, Z., and Zhang, X. (2015). Mapping of rainfall-induced landslide susceptibility in Wencheng, China, using support vector machine. *Nat Hazards*, 76:1759–1779.

Süzen, M. L. and Doyuran, V. (2004). Data driven bivariate landslide susceptibility assessment using geographical information systems: a method and application to Asarsuyu catchment, Turkey. *Engineering Geology*, 71:303–321.

Tang, C., van Westen, C. J., Tanyas, H., and Jetten, V. G. (2016). Analysing post-earthquake landslide activity using multi-temporal landslide inventories near the epicentral area of the 2008 Wenchuan earthquake. *Nat. Hazards Earth Syst. Sci. Discuss.*, 193:959–970.

Teshebaeva, K., Roessner, S., Echtler, H., Motagh, M., Wetzel, H.-U., and Moldobekov, B. (2015). ALOS/PALSAR InSAR Time-Series Analysis for Detecting Very Slow-Moving Landslides in Southern Kyrgyzstan. *Remote Sensing*, 7(7):8973–8994.

Torgoev, I. A., Aleshin, Y. G., Meleshko, A., and Havenith, H.-B. (2010). Landslide hazard in the Kyrgyz Tien Shan. In Glade, T., Casagli, N., and Malet, J. P., editors, *Proc. of the Mountain Risks conference*.

Trigila, A., Iadanza, C., and Spizzichino, D. (2010). Quality assessment of the Italian Landslide Inventory using GIS processing. *Landslides*, 7:455–470.

USGS (2004). Landslide Types and Processes. https://pubs.usgs.gov/fs/2004/3072/pdf/fs2004-3072.pdf. Accessed: 2017-11-10.

USGS (2017). Earthquake Hazards Program. https://earthquake.usgs.gov/. Accessed: 2017-11-12.

Van Den Eeckhaut, M. and Hervás, J. (2012). State of the art of national landslide databases in Europe and their potential for assessing susceptibility, hazard and risk. *Geomorphology*, 139-140:545–558.

Van Den Eeckhaut, M., Reichenbach, P., Guzzetti, F., Rossi, M., and Poesen, J. (2009). Combined landslide inventory and susceptibility assessment based on different mapping units: and example from the Flemish Ardennes, Belgium. *Nat. Hazards and Earth Syst. Sci.*, 9:507–521.

Van Westen, C. J., Castellanos, E., and Kuriakose, S. L. (2008). Spatial data for landslide susceptibility, hazard, and vulnerability assessment: An overview. *Engineering Geology*, 102:112–131.

Van Westen, C. J., van Asch, T. W. J., and Soeters, R. (2006). Landslide hazard and risk zonation – why is it still so difficult? *Bull Eng Geol Environ*, 65:167–184.

Varnes, D. (1978). Slope Movement Types and Processes. In Schuster, R. and Krizek, R., editors, *Landslides: Analysis and Control*. National Academy of Sciences, Washington, D.C.

Wang, Q., Wang, D., Huang, Y., Wang, Z., Zhang, L., Guo, Q., Chen, W., Chen, W., and Sang, M. (2015). Landslide Susceptibility Mapping Based on Selected Optimal Combination of Landslide Predisposing Factors in a Large Catchment. *Sustainability*, 7:16653–16669.

Wasowski, J. and Bovenga, F. (2014). Investigating landslides and unstable slopes with satellite Multi Temporal Interferometry: Current issues and future perspectives. *Engineering Geology*, 174:103–138.

Wetzel, H.-U., Roessner, S., and Sarnagoev, A. (2000). Remote sensing and GIS based geological mapping for assessment of landslide hazard in Southern Kyrgyzstan (Central Asia). In Brebbia, C. A. and Pascolo, P., editors, *Management Information Systems 2000 – GIS and Remote Sensing*, pages 337–342. WIT-Press, Southampton, UK.

Wieczorek, G. F. (1984). Preparing a Detailed Landslide-Inventory Map for Hazard Evaluation and Reduction. *Bulletin of the Association of Engineering Geologists*, XXI(3):337–342.

Xu, C. (2014). Preparation of earthquake-triggered landslide inventory maps using remote sensing and GIS technologies: Principles and case studies. *Geoscience Frontierts*, 5.

Yerokhin, S. A. (1999). *Investigation of Landslide Occurrence in Osh and Dzhalal-Abad Provinces of the Kyrgyz Republic*. Bishkek, Kyrgyzstan. in Russian.

Yilmaz, I. (2009). Landslide susceptibility mapping using frequency ratio, logistic regression, artificial neural networks and their comparison: A case study from Kat landslides (Tokat – Turkey). *Computers and Geosciences*, 35:1125–1138.

Zerathe, S. and Lebourg, T. (2012). Evolution stages of large deep-seated landslides at the front of a subalpine meridional chain (Maritime-Alps, France). *Geomorphology*, 138:390–403.